Monotonicity-based methods for inverse parameter identification problems in partial differential equations

Von der Fakultät Mathematik und Physik
und dem Stuttgart Research Centre for Simulation Technology
der Universität Stuttgart
zur Erlangung der Würde eines
Doktors der Naturwissenschaften (Dr. rer. nat.)
genehmigte Abhandlung

Vorgelegt von

Marcel Ullrich

aus Mainz

Hauptberichter:	Prof. Dr. Bastian von Harrach
Mitberichter:	Prof. Nuutti Hyvönen
	Prof. Dr. Andreas Kirsch
Tag der mündlichen Prüfung:	21.07.2015

Institut für Mathematische Methoden in den Ingenieurwissenschaften,
Numerik und geometrische Modellierung

2015

Das Thema stellte Herr Prof. Dr. Bastian von Harrach.

Der deutsche Titel der Arbeit lautet:

Monotoniemethoden für
inverse Parameteridentifikationsprobleme
partieller Differentialgleichungen

Contents

Abstract **VII**

Zusammenfassung **IX**

Danksagung **XI**

Introduction **1**

1 Monotonicity-based shape reconstruction in EIT **9**
1.1 Introduction 9
1.2 Basic notations and support definitions 12
1.2.1 Basic notations and the mathematical setting 12
1.2.2 Inner and outer support 13
1.3 Monotonicity and localized potentials 15
1.3.1 A monotonicity relation 15
1.3.2 Localized potentials 17
1.4 Monotonicity-based shape reconstruction 21
1.4.1 The definite case 21
1.4.2 The indefinite case 24
1.4.3 Remarks and extensions 29
1.5 Excursion - Numerical results 29
1.6 Appendix - Local definiteness of piecewise analytic functions 34

2 Resolution guarantees in EIT **39**
2.1 Introduction 39
2.2 The setting 41
2.3 Monotonicity 44
2.4 Resolution guarantees 46
2.4.1 Verification of resolution guarantees 47
2.4.2 Fast linearized verification of resolution guarantees 49
2.4.3 Verification for less conductive inclusions 51
2.5 Numerical results 52
2.5.1 Results for academic examples 52
2.5.2 Results using physiologically relevant parameters 54
2.5.3 Reconstruction guarantees in a region of interest 55
2.6 Conclusion and discussion 56

3 Combining frequency-difference and ultrasound-modulated EIT 59
3.1 Introduction . . . 59
3.2 Continuous boundary data . . . 61
3.2.1 The setting . . . 61
3.2.2 Monotonicity results for the continuum model . . . 62
3.2.3 Detecting inclusions in the continuous case . . . 63
3.2.4 Proof of the main results for the continuum model . . . 65
3.3 Electrode measurements . . . 71
3.3.1 The setting . . . 71
3.3.2 Monotonicity results for the shunt model . . . 73
3.3.3 Detecting inclusions from electrode measurements . . . 74
3.3.4 Proof of the main results for electrode measurements . . . 75
3.4 Numerical results . . . 77
3.4.1 Basic notations and assumptions . . . 77
3.4.2 Basic monotonicity tests . . . 77
3.4.3 Shape reconstruction of conductivity anomalies . . . 81
3.5 Conclusion and discussion . . . 85

4 Local uniqueness for an inverse BVP with partial data 87
4.1 Introduction . . . 87
4.2 Proof of the main result . . . 89
4.3 Monotonicity for Neumann-to-Dirichlet maps . . . 90
4.4 Unique continuation properties . . . 91
4.5 Localized potentials . . . 95

Bibliography 101

Abstract

This work, which is subdivided into four self-contained chapters, is concerned with monotonicity-based methods for inverse parameter reconstruction problems in partial differential equations. The first three chapters address the anomaly detection problem of electrical impedance tomography. While electrical impedance tomography aims on reconstructing the interior conductivity distribution of a conductive subject from boundary data, the goal of the specific anomaly detection problem is the reconstruction of areas inside a conductive subject where the conductivity differs from an expected reference conductivity. The considered boundary data can be understood as an operator that describes current-voltage measurements. In the final chapter we prove a novel uniqueness result for the inverse potential problem of the Schrödinger equation with partial data.

For the development of anomaly detection methods, both known and novel variants of a monotonicity relation are used. Roughly speaking, these monotonicity relations show that a pointwise decrease of the conductivity leads to larger boundary data (in sense of operator definiteness). At first glance, it is not obvious at all whether the converse of this implication holds also true, i.e., it is not clear whether larger boundary data could also result from a local decrease of the conductivity in some parts and a local increase in other parts. Assuming a local definiteness condition for the conductivity change, which is always fulfilled for piecewise analytic conductivities, we prove a partial converse of the monotonicity implication that holds for the case in which the measurements are modeled with the idealized continuum model. The proof of this result is essentially based on combining a monotonicity inequality with a known result on the existence of so-called *localized potentials*.

In the first chapter we develop novel anomaly detection methods for measurement data modeled with the continuum model. Moreover, fast linearized variants are presented that only require the computation of reference measurements for one homogeneous conductivity parameter. We prove that all presented methods are capable of reconstructing the exact outer shape of conductivity anomalies, even in the general indefinite case where the conductivity inside the anomaly region differs in both directions (lager and smaller) from the reference conductivity. Merely a local definiteness condition has to be fulfilled for the indefinite case.

In realistic electrical impedance tomography settings in which measurement data is collected on a finite number of electrodes, the reconstruction of the exact outer shape of anomalies cannot be guaranteed anymore. On top of that, systematic errors resulting from imprecise knowledge of the setting parameters as well as additional

random measurement errors need to be taken into account. In the second chapter we show that nevertheless (under certain conditions) resolution guarantees are principally possible for such settings. To model the measurements, we use the complete electrode model. We introduce the following concept of a resolution guarantee. For a resolution given by a partition of the imaging subject, a suitable method should be able to detect all partition elements that are covered by an anomaly and to mark no false positive partition elements in the anomaly-free case. Based on the idea of testing worst-case scenarios using an extended monotonicity relation, we derive simple test criteria that allow to decide whether a desired resolution guarantee is possible.

In the third chapter we develop a novel hybrid method that does not require the simulation of reference data but merely a natural contrast condition. We apply an idealized model for ultrasound modulation that alters the conductivity uniformly in a test region and we develop a test criterion to check whether the test region is located inside an anomaly. The test criterion consists of a monotonicity-based comparison of ultrasound modulated and weighted frequency-difference measurements. For measurement data modeled with the continuum model, we prove that it can be checked whether the ultrasound induced test anomaly is located inside the true anomaly or outside its outer boundary. For the shunt model, we show that the monotonicity test correctly identifies test anomalies located inside the true anomaly. The reliability of the test to avoid false positive test anomalies essentially depends on the realization of the shunt model, e.g., on the number and shape of the used electrodes.

Finally, in the fourth chapter, a local uniqueness result for the inverse potential problem of the Schrödinger equation with partial boundary data on a Lipschitz domain is shown. More precisely, we show that positive-valued bounded potentials that do not completely coincide in a neighborhood of a potentially arbitrarily small part of the boundary can be distinguished from Cauchy data on this boundary part provided that a local definiteness condition is fulfilled. The proof is based on combining a monotonicity inequality and a novel particular result on the existence of localized potentials.

Zusammenfassung

Die vorliegende Arbeit, welche in vier in sich geschlossene Kapitel unterteilt ist, behandelt Monotoniemethoden für inverse Parameteridentifikationsprobleme partieller Differentialgleichungen. Die ersten drei Kapitel befassen sich mit dem Detektionsproblem von Leitfähigkeitsanomalien innerhalb der elektrischen Impedanztomographie. Während die elektrische Impedanztomographie die Rekonstruktion der inneren Leitfähigkeitsverteilung eines leitenden Subjekts aus Randdaten zum Ziel hat, geht es bei dem speziellen Anomaliedetektionsproblem um die Rekonstruktion von Gebieten innerhalb eines leitenden Subjekts in denen die Leitfähigkeit von einer erwarteten Referenzleitfähigkeit abweicht. Die betrachteten Randdaten können dabei als ein Operator verstanden werden, welcher Strom-zu-Spannungsmessungen beschreibt. Im finalen Kapitel beweisen wir ein neues Eindeutigkeitsresultat für das inverse Potentialproblem der Schrödingergleichung mit partiellen Randdaten.

Für die Entwicklung von Methoden zur Anomaliedetektion verwenden wir sowohl bekannte als auch neue Varianten einer Monotonierelation. Anschaulich formuliert, besagen diese Monotonierelationen, dass eine punktweise Verringerung der Leitfähigkeit zu größeren Randdaten (im Sinne einer Definitheitsrelation für Operatoren) führt. Auf den ersten Blick ist überhaupt nicht ersichtlich, ob die umgekehrte Implikation ebenfalls gilt. Das heißt, es ist nicht klar, ob größere Randdaten auch aus einer lokalen Verringerung der Leitfähigkeit in einem Bereich und einer lokalen Erhöhung in einem anderen Bereich resultieren könnten. Unter Voraussetzung einer lokale Definitheitsbedingung für die Leitfähigkeitsänderung, welche für stückweise analytische Leitfähigkeiten immer erfüllt ist, beweisen wir eine partielle Umkehrung zur Implikation der Monotonierelation, die für Randdaten entsprechend dem *Continuum-Model* gilt. Der Beweis basiert im Wesentlichen auf der Kombination einer Monotonieungleichung und einem bekannten Resultat über die Existenz sogenannter *lokalisierter Potentiale*.

Im ersten Kapitel entwickeln wir neuartige Methoden zur Anomaliedetektion für Randdaten entsprechend dem *Continuum-Model*. Zudem präsentieren wir schnelle linearisierte Varianten, welche nur die Berechnung von Referenzdaten für einen einzigen homogenen Leitfähigkeitsparameter benötigen. Wir beweisen, dass alle präsentierten Methoden die exakte äußere Form von Anomalien rekonstruieren. Dies gilt selbst für den allgemeinen indefiniten Fall, bei dem die Leitfähigkeit innerhalb einer Anomalie nach oben und unten von der Referenzleitfähigkeit abweicht. In diesem Fall muss lediglich eine lokale Definitheitsbedingung erfüllt sein.

Betrachtet man die elektrische Impedanztomographie in einem realistischen Setting,

in dem Messdaten auf einer endlichen Anzahl von Elektroden gesammelt werden, so lässt sich die Rekonstruktion der exakten äußeren Form von Anomalien natürlich nicht mehr garantieren. Erschwerend kommt hinzu, dass systematische Fehler, resultierend aus ungenauer Kenntnis von Settingparametern, sowie zufällige Messfehler berücksichtigt werden müssen. Im zweiten Kapitel zeigen wir, dass Auflösungsgarantien (unter gewissen Voraussetzungen) dennoch auch für solche Settings prinzipiell möglich sind. Zur Modellierung der Messungen verwenden wir dabei das *Complete-Electrode-Model*. Wir führen das folgende Konzept einer Auflösungsgarantie ein: Für eine gegebene Auflösungspartition des Untersuchungsobjekts soll ein geeignetes Verfahren in der Lage sein, alle von einer Anomalie überdeckten Partitionselemente zu identifizieren und im anomaliefreien Fall keine Partitionselemente falsch-positiv zu markieren. Basierend auf der Idee Worst-Case-Szenarien mithilfe einer erweiterten Monotonierelation zu testen, entwickeln wir ein einfaches Testkriterium, welches es uns erlaubt, die Möglichkeit einer erwünschten Auflösungsgarantie zu prüfen.

Im dritten Kapitel entwickeln wir eine neuartige Hybridmethode, die nicht die Simulation von Referenzdaten benötigt, stattdessen muss lediglich eine natürliche Kontrastbedingung erfüllt sein. Wir verwenden ein idealisiertes Modell zur Ultraschallmodulation, das die Leitfähigkeit gleichmäßig in einer Testregion erhöht. Zudem entwickeln wir ein Testkriterium, das aus einem monotoniebasierten Vergleich von Ultraschall-modulierten und gewichteten Frequenz-Differenz-Messungen besteht. Für mit dem *Continuum-Model* modellierte Messdaten beweisen wir, dass sich sicher prüfen lässt, ob eine Ultraschall-induzierte Testanomalie innerhalb der echten Anomalie oder außerhalb ihres äußeren Randes liegt. Für das *Shunt-Model* zeigen wir, dass der Monotonietest Testanomalien korrekt identifiziert, falls diese innerhalb der wahren Anomalie liegen. Die Zuverlässigkeit des Tests falsch-positive Testanomalien zu vermeiden, hängt im Wesentlichen von der Umsetzung des *Shunt-Models* ab, wie z. B. von der Anzahl und der Form der verwendeten Elektroden.

Abschließend wird im vierten Kapitel ein lokales Eindeutigkeitsresultat für das inverse Potentialproblem der Schrödingergleichung mit partiellen Randdaten auf einem Lipschitz-Gebiet bewiesen. Genauer gesagt zeigen wir, dass sich positivwertige beschränkte Potentiale, die in einer Umgebung eines Randstücks nicht komplett übereinstimmen, anhand von Cauchy-Daten auf diesem Randstück unterscheiden lassen, vorausgesetzt eine lokale Definitheitsbedingung ist erfüllt. Der Beweis basiert auf der Kombination einer Monotonieungleichung mit einem neuen speziellen Resultat über die Existenz lokalisierter Potentiale.

Danksagung

An dieser Stelle möchte ich mich bei allen herzlich bedanken, die zum Gelingen dieser Arbeit beigetragen haben.

An erster Stelle gilt dieser Dank meinem Doktorvater Prof. Dr. Bastian von Harrach, der bereits meine Diplomarbeit betreute und mich schon damals für das Gebiet der inversen Probleme und insbesondere das inverse Problem der elektrischen Impedanztomographie begeisterte. Ich danke ihm insbesondere für die Themenstellung, den Freiraum das Thema auszufüllen, seine zeitintensive Betreuung, spannende Diskussionen und seine großartige Unterstützung.

Des Weiteren gilt mein Dank der Deutschen Forschungsgemeinschaft (DFG) für ihre finanzielle Unterstützung innerhalb des Exzellenzculsters Simulation Technology (EXC 310/1) an der Universität Stuttgart.

Zudem möchte ich meiner Familie sowie meinen Freunden/Kollegen danken, die mich während meiner Arbeit mit vielen hilfreichen Ratschlägen, dem Korrekturlesen des Manuskripts sowie einem angemessen Maß an Ablenkung unterstützt haben.

Ein ganz besonderer Dank gilt meiner Frau Melina, die mich immer bei all meinen Zielen mit viel Liebe, Verständnis und wertvollem Rat unterstützt.

Introduction

Partial differential equations are commonly used for describing physical phenomena such as, e.g., electrical charge distribution, wave or diffuse light propagation. When all parameters that describe a physical system by a partial differential equation are known, the behavior of the system can be described from the knowledge of the solutions of the equation. Conversely, the question arises: can we determine the parameter of the system by observing its behavior? In many practical applications the reconstruction of the parameters of a system is a fundamentally important problem and belongs, in mathematical terms, to the field of *inverse problems*.

Hadamard took the view that a mathematical model describing a physical phenomenon should have the following properties (see [Had23]). A solution should exist, the solution should be unique for given input data and the solution should depend continuously on the input data. When these conditions are satisfied, the mathematical problem is called *well-posed*, otherwise it is called *ill-posed*. Since there are a many ill-posed inverse problems that are of considerable practical use, these problems cannot just be ignored as was suggested by Hadamard. Regarding inverse parameter reconstruction, there are two major goals. Finding a parameter space such that unique existence of a solution can be shown and applying so-called *regularization strategies* to handle noisy data that dramatically affect the inverse parameter reconstruction in cases where the solution does not depend continuously on the input data.

This work deals with two severely ill-posed inverse parameter reconstruction problems in partial differential equations. These are the inverse problem of electrical impedance tomography (aka inverse conductivity problem) and the inverse potential problem of the elliptic Schrödinger equation.

Electrical impedance tomography (EIT)

Originally, EIT refers to a medical imaging technique. In this work we will also use this name to consolidate methods for the inverse conductivity problem not necessarily in a medical context.

The inverse problem of EIT is to reconstruct the conductivity distribution of a conductive subject from current-voltage measurements taken on its boundary. Let Ω be the conductive subject and σ be the spatial conductivity distribution. Then

$$\operatorname{div}(\sigma \nabla u) = 0 \quad \text{in } \Omega \tag{0.1}$$

models (in conjunction with boundary conditions modeling electric current injection appropriately) the spatial distribution of the electrical potential u in Ω.

The corresponding forward problem is to compute the mapping that models the current-voltage measurements. These measurements have been described in the literature by several different models. In the so-called *continuum model* (CM) the boundary data is given by the Neumann-to-Dirichlet operator that models the current-to-voltage mapping continuously on the whole boundary. While the CM is appealing for a theoretical point of view, for practical applications, the current-voltage measurements should be described by an electrode model that models the measurements on a finite number of electrodes attached to the boundary of the subject. For this purpose, in addition to the CM, we use the so-called *shunt model* (SM) and *complete electrode model* (CEM) in this work. The latter seems to be the most established model predicting measurements up to a high precision (see [SCI92] for a comparison of the SM and CEM).

In the context of medical imaging, EIT has some potential advantages compared to other techniques. The conductivity, which one wants to image, is of high physiological specificity and the method is both non-invasive and harmless as the patient is not exposed to radiation such that the method is potentially suitable for long-time monitoring. Furthermore, the required equipment is comparably cheap and easily portable. For a broad overview of the EIT and its practical medical or industrial applications, see, e.g., [HW78, BB84, BS$^+$87, WFN85, NGI88, MBSB96, CIN99, Bor02, Bor03, Bro03, Lio04, Hol05, Bay06, CKI$^+$07, HHP08, MAF$^+$10, AGL11, GM08, NJTM12].

The inverse potential problem of the Schrödinger equation

The inverse potential problem of the Schrödinger equation that aims on reconstructing the potential parameter q of

$$-\Delta v + qv = 0 \quad \text{in } \Omega \tag{0.2}$$

from the knowledge of the Neumann-to-Dirichlet operator (or Cauchy data) is closely related to the inverse conductivity problem. For conductivities $\sigma \in C^2\left(\overline{\Omega}\right)$, there is a well-known substitution that reduces the inverse conductivity problem to the inverse potential problem (see, e.g., [NS10]).

The anomaly detection problem of the EIT

A particular problem in EIT is the detection of anomalies (aka inclusions), which has attracted growing attention since it has firstly been considered by Friedmann and Isakov in [Fri87, FI89]. The goal of anomaly detection is the reconstruction of areas inside a conductive subject wherein the conductivity differs from a given

reference conductivity. Applications are, e.g., the detection of pathological areas or material faults in the field of medical imaging or non-destructive material testing, respectively.

In the following we comment on related work and give a brief classification of the results presented in this work.

Several reconstruction methods have been designed for the task of anomaly detection. Essentially, these methods can be classified to the class of iterative or the class of non-iterative (direct) methods. Typically, iterative methods are in some way based on a shape evolution strategy (see, e.g., Rahmati et al. [RSP+12] for an iterative level set-based approach). Due to the fundamental ill-posedness of EIT, regularization strategies and a high number of iterations are required. Non-iterative methods have attracted growing attention over the last 3 decades (see [Pot06] for a overview). To give a brief overview we will list two of the most prominent methods. These are the factorization method and the enclosure method.

The factorization method was introduced by Kirsch [Kir98, Kir00] for inverse scattering problems and extended to EIT by Brühl and Hanke [BH00, Brü01]. Since then remarkably further developments have been done (see [Har13] for a recent review). Within the CM the factorization method reconstructs the outer shape of anomalies while two major problems have not been entirely solved so far: the method relies on a range test for which there is no known convergent implementation and the method has only been justified for the so-called *definite case* in which the anomaly conductivity differs only in one direction from the reference conductivity (or cases in which the conductive subject can be split into two a-priori known regions with the definiteness property, cf. [Sch09, Har13]).

The enclosure method was introduced by Ikehata [Ike99, Ike00]. Further extensions have been worked out in [BH00, IS00, Ike02, IS04, IIN+07, UW08, IINS10]. The method yields a stable testing criterion (based on the construction of special probe functions) and does not require the definiteness assumption (see [IIN+07]), but it reconstructs only the convex hull of anomalies (plus some non-convex features depending on the probe functions).

Regarding the question whether two conductivities can be distinguished by idealized noise-free measurements within the CM (*Calderón-Problem* [Cal80, Cal06]), great progress has been made, see, e.g., the overview [Uhl08]. Nevertheless, in realistic settings including modeling or measurement errors the reliability of anomaly detection suffers from the intrinsic ill-posedness of the EIT. Let us list some results that deal with this challenging issue. The distinguishability of conductivities from finite precision data has been studied in [SYB84, SB85, Isa86, GIN87, GIN90, PLP93, GKI94]. Results that show strategies to deal with uncertainties in the setting parameters as the shape of the subject and the contact impedances of the electrodes are presented in [KLO08, NKK11]. Moreover, there is a recent result on *optimal resolutions* of Winkler and Rieder [WR14] and the work of Tamburrino et al. [TVR10] where the

concept of *visible voxels* is introduced.

In this work we develop novel monotonicity-based methods for anomaly detection. These methods are based on definiteness tests that are non-iterative and stable implementable. Monotonicity-based methods have been firstly developed and numerically tested by Taburrino and Rubinacci [TR02, Tam06]. The underlying monotonicity property on which these methods are based is given by the intuitive and well-known relation that increasing the conductivity of a subject leads to smaller voltage measurements on its boundary. More precisely, increasing the conductivity distribution pointwise leads to smaller measurement operators in the sense of operator definiteness. Tamburrino and Rubinacci showed that their methods are able to reconstruct an upper and a lower bound for the anomaly region.

Using Harrach's concept of *localized potentials* [Geb08], we derive a partly converse of the monotonicity relation. This partly converse shows that locally increasing the conductivity in some part and decreasing it in another part cannot lead to a smaller measurement operator provided that a local definiteness condition is satisfied (which is the case for, e.g., piecewise analytic conductivity distributions). Using this result, we develop novel monotonicity methods that are able to reconstruct the exact outer shape of inclusions within the CM. Furthermore, we present linearized variants of our methods that still reconstruct the outer shape of anomalies. At first glance, this seems to be counterintuitive and surprising, but in fact the linearized methods implement the result of Harrach and Seo [HS10] that shows that the linearized inverse conductivity problem does not lose any information on the shape of the anomaly regions.

Obviously, the reconstruction of the exact outer shape of conductivity anomalies cannot be achieved within a realistically modeled measurement setting including systematic modeling and random measurement errors. For such a setting modeled by the CEM, we introduce a (basic) concept of a rigorous resolution guarantee for anomaly detection. Using monotonicity-based ideas to test worst-case scenarios, we show that it is principally possible to rigorously guarantee a certain resolution even for settings including general (e.g., measurement) errors and in which the reference conductivity as well as the contact impedances of the electrodes are known only approximately. To our knowledge the possibility to verify comparable rigorous resolution guarantees has not been shown before. Moreover, we derive a validation criterion to evaluate whether a desired resolution can be guaranteed and we also describe simple reconstruction algorithms that implement a resolution guarantee if the validation criterion is satisfied.

In addition, in this work we develop a novel hybrid method which basically uses a monotonicity-based comparison of weighted frequency-difference EIT (fdEIT) and ultrasound-modulated EIT (UMEIT) measurements. Weighted fdEIT has been introduced in order to improve the reconstruction stability with respect to modeling errors in settings in which no reference (anomaly-free) data is available, see [SLZ$^+$08, HS09, HSW10]. The hybrid tomography technique UMEIT was introduced

in [ABC+08]. The additional information that is available in UMEIT eliminates the major cause of ill-posedness in the reconstruction process, which could greatly increase the image resolution (cf. the related idea of Impedance-Acoustic Tomography [GS08]). Nevertheless, UMEIT requires information on the measurement geometry. We show that our method unifies some advantages of weighted fdEIT and UMEIT. In particular, it does not require the computation of reference measurements and thus it does not require information on the measurement geometry. At this point, it has to be noted that we use an idealized model for the ultrasound modulation in which ultrasound waves can be focused uniformly to certain regions.

Uniqueness of the inverse potential problem with partial data

The final Chapter of this work is devoted to the challenging problem of showing uniqueness of the inverse potential problem with partial data. We will show that two different potentials can be distinguished from partial Cauchy data on a possibly arbitrarily small subset of the boundary provided that a local definiteness condition is satisfied.

In the following we comment on related work and give a brief classification of the results presented in this work.

While the uniqueness of the inverse potential problem and the uniqueness of the related inverse conductivity problem have been extensively studied in the last 30 years (see, e.g., the seminal works [KV84, KV85, SU87, Nac96, AP06, BB08, HT+13]), the uniqueness problem from partial boundary data has attracted growing attention over the last years. For the two-dimensional euclidean space and sufficiently smooth potentials, we refer to the work of Imanuvilov et al. [IUY10]. This work shows uniqueness from Cauchy data on an arbitrary relatively open boundary part. For the three-dimensional euclidean space and bounded potentials, we list some recent work (see also the review of Kenig and Salo [KS14]). We refer to the work of Kenig et al. [KSU07] for a proof of uniqueness from Cauchy data with Dirichlet and Neumann data that is supported and measured on different boundary parts, respectively. These boundary parts are required to be front and back faces in some sense (see also the constructive proof of Nachman and Street [NS10]). In [Isa07] Isakov proved uniqueness from Cauchy data on a possibly arbitrarily small boundary part while the remaining boundary part has to be contained in a plane or a sphere. In [KS12] Kenig and Salo presented a result that unifies and improves the approaches of [KSU07] and [Isa07]. In particular, they reduced the assumptions regarding the boundary parts on which the Cauchy data is collected and the remaining boundary part (if there is such a remaining part).

In this work we prove uniqueness from Cauchy data on an arbitrary relatively open boundary part for positive-valued potentials. Except the assumption that Ω has to be a Lipschitz domain, there are no further assumptions to the boundary required: neither to the boundary part where the Cauchy data is given nor to the remaining

boundary part. Instead, a local definiteness condition has to be satisfied.

Overview

In Chapter 1 we derive four variants of a non-iterative monotonicity-based anomaly detection method for EIT where the boundary data is modeled by the CM. We will treat the following cases separately: the definite case where the conductivity inside the anomaly region differs only in one direction (smaller or lager) from the background and the general indefinite case where the conductivity inside the anomaly region possibly differs in both directions. For each of these cases, a non-linearized and a "fast" linearized method will be presented. We show that all four monotonicity methods are able to reconstruct the exact outer shape of anomalies.

Chapter 2 deals with the anomaly detection problem of EIT for boundary data modeled by the CEM. We introduce a rigorous concept of a resolution guarantee for realistically modeled settings including systematic and random errors and we show that rigorous resolution guarantees are principle possible. We derive simple test criteria that allow to decide whether a resolution guarantee (for a desired resolution) is possible. Moreover, monotonicity methods (linearized and non-linearized) will be developed which do achieve the resolution guarantee provided that this guarantee can be verified with our test criterion.

In Chapter 3 we develop a hybrid anomaly detection method for EIT that makes use of a monotonicity-based comparison of ultrasound-modulated and weighted frequency-difference measurements. This method does not require the simulation of reference measurements. In particular, it does not require information on the position of the electrodes or the shape of the probed subject. Merely a natural contrast condition has to be satisfied. Furthermore, we use an idealized model for ultrasound modulation that alters the conductivity uniformly in a test region and we present novel monotonicity relations that are used to test whether the test region is located inside an anomaly. We show that the monotonicity tests are exact for the CM and we present a heuristic justification for the SM.

In Chapter 4 we study the question whether the potential parameter of the Schrödinger equation on a three-dimensional Lipschitz domain is uniquely determined by partial Cauchy data on an arbitrarily small open boundary part. We prove an uniqueness result for positive potentials that fulfill a local definiteness condition. For this purpose, we combine the monotonicity approach and a novel variant of the concept of localized potentials.

Published results

All results included in this work have been published, accepted for publication or have been recently submitted for publication. All these publications are joint work with my supervisor Prof. Dr. Bastian von Harrach. Moreover, the results of Chapter 3 (in addition) are joint work with Eunjung Lee (Associate Professor, Department of Computational Science and Engineering, Yonsei University, Korea). Her contribution to this work has been her ideas for designing and testing sample settings in Subsection 3.4.2 as well as her assistance with proof reading parts of the paper.

The results of Chapter 1 and parts of the introduction have been published in the SIAM Journal on Mathematical Analysis under the title "Monotonicity-Based Shape Reconstruction in Electrical Impedance Tomography" [HU].

The results of Chapter 2 and parts of the introduction have been published in the journal IEEE transactions of medical imaging under the title "Resolution Guarantees in Electrical Impedance Tomography" [HU15a].

The results of Chapter 3 and parts of the introduction have been published in the journal Inverse Problems under the title "Combining frequency-difference and ultrasound-modulated EIT" [HEU15].

The results of Chapter 4 and parts of the introduction are submitted for publication to the Proceedings of the American Mathematical Society under the title "Local uniqueness for an inverse boundary value problem with partial data" [HU15b]. The decision about the acceptance is still open.

Chapter 1

Monotonicity-based shape reconstruction in EIT

The Sections 1.1 - 1.4 and 1.6 are the Sections 1-5 of the paper [HU] up to minor changes. © SIAM. Unauthorized reproduction is prohibited.

1.1 Introduction

We consider the shape reconstruction (aka inclusion or anomaly detection) problem in electrical impedance tomography (EIT).[1] Let Ω describe an electrically conducting object which contains inclusions in which the conductivity $\sigma(x)$ differs from an otherwise known background conductivity. Our aim is to detect these inclusions from current-voltage measurements on the boundary $\partial\Omega$.

We assume that $\Omega \subset \mathbb{R}^n$, $n \geq 2$, is a domain with smooth boundary $\partial\Omega$ and outer normal vector ν. For ease of presentation, we also assume that Ω is bounded, that the background conductivity is equal to 1 and that we are given measurements on the complete boundary $\partial\Omega$. Our results easily extend to inhomogeneous (but known) backgrounds and partial boundary measurements, cf. Section 1.4.3.

With these assumptions, our goal is to determine the shape of the inclusions, i.e., the set $\operatorname{supp}(\sigma - 1)$, from knowledge of the Neumann-to-Dirichlet (NtD) operator

$$\Lambda(\sigma) : \; g \mapsto u_\sigma^{(g)}|_{\partial\Omega},$$

where $u_\sigma^{(g)}$ is the solution of

$$\nabla \cdot \sigma \nabla u_\sigma^{(g)} = 0 \text{ in } \Omega, \quad \sigma \partial_\nu u_\sigma^{(g)}|_{\partial\Omega} = g \text{ on } \partial\Omega,$$

cf. Section 1.2.1 for the precise mathematical setting.

In this chapter we show that $\operatorname{supp}(\sigma - 1)$ can be reconstructed by so-called *monotonicity tests*, which simply compare $\Lambda(\sigma)$ (in the sense of operator definiteness) to

[1] In an applied context, as in the Chapters 2 and 3, we preferentially use the name *anomaly detection*.

NtD operators $\Lambda(\tau)$ of test conductivities τ. To be more precise, the support of $\sigma-1$ can be reconstructed under the assumption that $\operatorname{supp}(\sigma-1) \subset \Omega$ has connected complement. Otherwise, what we can reconstruct is essentially the support together with all holes that have no connection to the boundary $\partial\Omega$.

Moreover, we show that the test NtD operators $\Lambda(\tau)$ can be replaced (without losing any information) by their linear approximations using the Fréchet derivative $\Lambda'(1)$ of $\Lambda(\sigma)$ around the background conductivity. Let us stress that the linearized tests still exactly recover the inclusion, which is in accordance with the general principle that the linearized EIT problem still contains the exact shape information, cf. [HS10].

The term *monotonicity tests* is used because our test criteria are motivated and partly follow from the simple and well-known monotonicity relation

$$\sigma \leq \tau \quad \text{implies} \quad \Lambda(\sigma) \geq \Lambda(\tau). \tag{1.1}$$

It seems quite natural and intuitive to probe the domain with test inclusions using the implication (1.1). This idea has been worked out and numerically tested in the works of Tamburrino and Rubinacci [TR02, Tam06]. The main new part that we present in this chapter is to rigorously justify this natural idea by proving a non-trivial converse of the implication (1.1). Our proofs are based on the theory of localized potentials [Geb08].

For a quick impression of our result, let us state it for two frequently considered special cases (see Examples 1.4.2, 1.4.4, 1.4.8 and 1.4.10). (Note that throughout this chapter we use the relation symbol "$\subset$" instead of "$\subseteq$", if non-equality of the two related sets is obvious.)

(a) Let $\sigma = 1 + \chi_D$, where D is open and $\overline{D} \subset \Omega$ has a connected complement. Then for every open ball $B \subseteq \Omega$

$$\begin{aligned} B \subseteq D \quad & \text{if and only if} \quad \Lambda(1+\chi_B) \geq \Lambda(\sigma) \\ & \text{if and only if} \quad \Lambda(1) + \tfrac{1}{2}\Lambda'(1)\chi_B \geq \Lambda(\sigma). \end{aligned}$$

(b) Let $\sigma = 1 + \chi_{D^+} - \frac{1}{2}\chi_{D^-}$, where $D^+, D^- \subseteq \Omega$ are open, $\overline{D^+} \cap \overline{D^-} = \emptyset$ and $\overline{D^+} \cup \overline{D^-} \subset \Omega$ has a connected complement. Then for every closed $C \subset \Omega$ with a connected complement

$$\begin{aligned} D^+ \cup D^- \subseteq C \quad & \text{if and only if} \quad \Lambda(1+\chi_C) \leq \Lambda(\sigma) \leq \Lambda(1-\tfrac{1}{2}\chi_C) \\ & \text{if and only if} \quad \Lambda(1) + \Lambda'(1)\chi_C \leq \Lambda(\sigma) \leq \Lambda(1) - \Lambda'(1)\chi_C. \end{aligned}$$

(a) is a special case of the *definite case* in which either all inclusions have a higher conductivity or all inclusions have a lower conductivity than the background. (a) shows how to test whether a small ball B lies inside the inclusion or not. The inclusion can thus be obtained as the union of all balls that fulfill the test. (b) is a special case of the more general *indefinite case* in which the conductivity may differ

in both directions from the background. Using the result in (b), we can test whether a large set C contains the inclusions or not. The inclusions can thus be obtained as the intersection of all these large sets.

Our results show that (under quite general assumptions) monotonicity tests determine $\operatorname{supp}(\sigma - 1)$ up to holes that have no connection to the boundary $\partial\Omega$.

Several reconstruction methods have been designed for the task of inclusion detection. There are iterative methods (see, e.g., Rahmati et al. [RSP$^+$12] for an iterative level set-based approach) and non-iterative methods. In this chapter we introduce monotonicity-based methods that can be classified as belonging to the class of non-iterative methods for shape reconstruction problems. Non-iterative shape reconstruction methods have been studied intensively in the last 3 decades, cf., e.g., the overview of Potthast [Pot06]. In the context of EIT the inclusion detection problem was first considered by Friedmann and Isakov [Fri87, FI89]. For the following brief overview, we restrict ourselves to the two most prominent and elaborated methods for detecting inclusions of unknown conductivity from the full Neumann-to-Dirichlet (or Dirichlet-to-Neumann) operator on all or part of the boundary: the factorization method and the enclosure method.

The factorization method was introduced by Kirsch [Kir98, Kir00] for inverse scattering problems and extended to impedance tomography by Brühl and Hanke [BH00, Brü01]. For its further developments in the context of EIT, see [HB03, Hyv04, Kir05, Geb06, GH07, HHP07, NPT07, Geb08, HS08, KG08, LHH08, HH09, HS09, Sch09, HSW10, AGL11, SK11] and the recent review [Har13]. The factorization method reconstructs the shape of inclusions (up to holes that have no connection to the boundary), but two major problems have not been solved so far. First of all, the method relies on a range test (or infinity test) for which there is no known convergent implementation (see, however, Lechleiter [Lec06] for a first step in this direction). Second, the method has only been justified for the *definite case* (or cases in which the domain can be split into two a-priori known regions with the definiteness property, cf. Schmitt [Sch09] and the review [Har13]).

The enclosure method was introduced by Ikehata [Ike99, Ike00]. Further extensions including the use of the Sylvester-Uhlmann complex geometrical optics solutions have been worked out in [BH00, IS00, Ike02, IS04, IIN$^+$07, UW08, IINS10]. The method yields a stable testing criterion and it does not require the definiteness assumption (see [IIN$^+$07]). However, it does require the construction of special, strongly oscillating probe functions and only reconstructs the convex hull of the inclusions (plus some non-convex features depending on the probe functions).

The monotonicity tests presented in this chapter seem to be a particularly simple and intuitively appealing solution to the long-studied inclusion detection problem. They characterize the outer shape of the inclusions and not just the convex hull. They work for the general indefinite case (though the implementation is simpler in the definite case). Also, they allow a stable implementation (see Remark 1.3.5) and

their linearized versions do not require solving inhomogeneous forward problems.

The chapter is organized as follows. Section 1.2 introduces the mathematical setting and the concept of inner and outer support. In Section 1.3 we derive the main theoretical tools for our proofs: monotonicity estimates and localized potentials. Section 1.4 then contains our main results: the characterization of inclusions by simple and stable monotonicity tests. Section 1.5 consists of a brief numerical excursion presenting a simple implementation of a monotonicity-based method for the definite case.

1.2 Basic notations and support definitions

1.2.1 Basic notations and the mathematical setting

Let $\Omega \subset \mathbb{R}^n$, $n \geq 2$, be a bounded domain with smooth boundary $\partial\Omega$ and outer normal vector ν. $L^\infty_+(\Omega)$ denotes the subset of $L^\infty(\Omega)$-functions with positive essential infima. $H^1_\diamond(\Omega)$ and $L^2_\diamond(\partial\Omega)$ denote the spaces of $H^1(\Omega)$- and $L^2(\partial\Omega)$-functions with vanishing integral mean on $\partial\Omega$.

The $L^2_\diamond(\partial\Omega)$-inner product is denoted by $\langle\cdot,\cdot\rangle$. For two bounded self-adjoint operators $A, B:\ L^2_\diamond(\partial\Omega) \to L^2_\diamond(\partial\Omega)$, we write

$$A \geq B$$

if it holds in the sense of quadratic forms, i.e.,

$$\langle g, (A-B)g\rangle \geq 0, \quad \text{for all } g \in L^2_\diamond(\partial\Omega).$$

For $\sigma_1, \sigma_2 \in L^\infty(\Omega)$, we write $\sigma_1 \geq \sigma_2$ if it holds pointwise (a.e.) on Ω.

For $\sigma \in L^\infty_+(\Omega)$, the Neumann-to-Dirichlet (NtD) operator $\Lambda(\sigma)$ is defined by

$$\Lambda(\sigma):\ L^2_\diamond(\partial\Omega) \to L^2_\diamond(\partial\Omega), \quad g \mapsto u^{(g)}_\sigma|_{\partial\Omega},$$

where $u^{(g)}_\sigma \in H^1_\diamond(\Omega)$ is the unique solution of

$$\nabla\cdot\sigma\nabla u^{(g)}_\sigma = 0 \text{ in } \Omega, \quad \sigma\partial_\nu u^{(g)}_\sigma|_{\partial\Omega} = g \text{ on } \partial\Omega, \tag{1.2}$$

which is equivalent to

$$\int_\Omega \sigma\nabla u^{(g)}_\sigma\cdot\nabla v\,\mathrm{d}x = \int_{\partial\Omega} gv|_{\partial\Omega}\,\mathrm{d}s \quad \text{for all } v \in H^1_\diamond(\Omega). \tag{1.3}$$

The existence of an unique solution is a consequence of the Lax-Milgram theorem. Furthermore, it is well known that $\Lambda(\sigma)$ is a self-adjoint compact linear operator and that the associated bilinear form is given by

$$\langle g, \Lambda(\sigma)h\rangle = \int_\Omega \sigma\nabla u^{(g)}_\sigma\cdot\nabla u^{(h)}_\sigma\,\mathrm{d}x.$$

Λ is Fréchet-differentiable, cf., e.g. Lechleiter and Rieder [LR08] for a recent proof that uses only the abstract variational formulation (see also [Ike90] for similar results). Given some direction $\kappa \in L^\infty(\Omega)$, the derivative

$$\Lambda'(\sigma)\kappa : \; L^2_\diamond(\partial\Omega) \to L^2_\diamond(\partial\Omega)$$

is the self-adjoint compact linear operator associated to the bilinear form

$$\langle (\Lambda'(\sigma)\kappa)\, g, h\rangle = -\int_\Omega \kappa \nabla u_\sigma^{(g)} \cdot \nabla u_\sigma^{(h)} \,\mathrm{d}x.$$

Note that for $\kappa_1, \kappa_2 \in L^\infty(\Omega)$, we obviously have that

$$\kappa_1 \le \kappa_2 \quad \text{implies} \quad \Lambda'(\sigma)\kappa_1 \ge \Lambda'(\sigma)\kappa_2. \tag{1.4}$$

The terms piecewise continuous and piecewise analytic are to be understood in the following sense.

Definition 1.2.1. (a) A subset $\Gamma \subseteq \partial O$ of the boundary of an open set $O \subseteq \mathbb{R}^n$ is called a *smooth boundary piece* if it is locally a C^∞-surface and O lies on one side of it, i.e., if for each $z \in \Gamma$ there exists a ball $B_\epsilon(z)$ and a function $\gamma \in C^\infty(\mathbb{R}^{n-1}, \mathbb{R})$ such that upon relabeling and reorienting

$$B_\epsilon(z) \cap \Gamma = \partial O \cap B_\epsilon(z) = \{x \in B_\epsilon(z) \mid x_n = \gamma(x_1, \ldots, x_{n-1})\},$$
$$O \cap B_\epsilon(z) = \{x \in B_\epsilon(z) \mid x_n > \gamma(x_1, \ldots, x_{n-1})\}.$$

(b) O is said to have *smooth boundary* if ∂O is a smooth boundary piece. O is said to have *piecewise smooth boundary* if ∂O is a countable union of the closures of smooth boundary pieces.

(c) A function $\kappa \in L^\infty(\Omega)$ is called *piecewise analytic* if there exist finitely many pairwise disjoint subdomains $O_1, \ldots, O_M \subset \Omega$ with piecewise smooth boundaries, such that $\overline{\Omega} = \overline{O_1 \cup \ldots \cup O_M}$, and $\kappa|_{O_m}$ has an extension which is (real) analytic in a neighborhood of $\overline{O_m}$, $m = 1, \ldots, M$.

(d) A function $\kappa \in L^\infty(\Omega)$ is called *piecewise continuous* if κ is continuous on an open set $O \subset \Omega$ and $\Omega \setminus O$ is a set of zero measure.

1.2.2 Inner and outer support

We will show that our method reconstructs $\operatorname{supp}(\sigma - 1)$ (the *inclusion*) up to holes that cannot be connected to the boundary $\partial\Omega$ without crossing the support. For the precise formulation, we will now introduce the concept of the *inner* and the *outer support* of a measurable function. For the frequently considered case that the inclusion has a connected complement and the conductivity is piecewise continuous, the inner and the outer support differ only by the boundary of the support, cf. Corollary 1.2.5. The following has been inspired by the use of the infinity support of Kusiak and Sylvester [KS03], cf. also [GH08, HS10].

Definition 1.2.2. A relatively open set $U \subseteq \overline{\Omega}$ is called *connected to* $\partial\Omega$ if $U \cap \Omega$ is connected and $U \cap \partial\Omega \neq \emptyset$.

Definition 1.2.3. For a measurable function $\kappa : \Omega \to \mathbb{R}$, we define

(a) the *support* $\operatorname{supp}\kappa$ as the complement (in $\overline{\Omega}$) of the union of those relatively open $U \subseteq \overline{\Omega}$, for which $\kappa|_U \equiv 0$;

(b) the *inner support* $\operatorname{inn}\operatorname{supp}\kappa$ as the union of those open sets $U \subseteq \Omega$, for which $\operatorname{ess\,inf}_{x\in U}|\kappa(x)| > 0$;

(c) the *outer support* $\operatorname{out}_{\partial\Omega}\operatorname{supp}\kappa$ as the complement (in $\overline{\Omega}$) of the union of those relatively open $U \subseteq \overline{\Omega}$ that are connected to $\partial\Omega$ and for which $\kappa|_U \equiv 0$.

The interior of a set $M \subseteq \Omega$ is denoted by $\operatorname{int} M$ and its closure (with respect to $\mathbb{R}^n$) by $\overline{M}$. If M is measurable, we also define

(d) $\operatorname{out}_{\partial\Omega} M = \operatorname{out}_{\partial\Omega}\operatorname{supp}\chi_M$,

where χ_M is the characteristic function of M.

Lemma 1.2.4. *For every measurable function $\kappa : \Omega \to \mathbb{R}$ and every measurable set M, the following properties hold.*

(a) $\operatorname{supp}\kappa, \operatorname{out}_{\partial\Omega}\operatorname{supp}\kappa, \operatorname{out}_{\partial\Omega} M \subseteq \overline{\Omega}$ *are closed.*

(b) $\operatorname{inn}\operatorname{supp}\kappa \subseteq \Omega$ *is open.*

(c) $\operatorname{inn}\operatorname{supp}\kappa \subseteq \operatorname{supp}\kappa \subseteq \operatorname{out}_{\partial\Omega}\operatorname{supp}\kappa$.

(d) $\operatorname{out}_{\partial\Omega}(\operatorname{supp}\kappa) = \operatorname{out}_{\partial\Omega}\operatorname{supp}\kappa$.

(e) If $\operatorname{supp}\kappa \subseteq \Omega$ *and* $\Omega \setminus \operatorname{supp}\kappa$ *is connected then* $\operatorname{supp}\kappa = \operatorname{out}_{\partial\Omega}\operatorname{supp}\kappa$.

(f) If κ is piecewise continuous then $\operatorname{supp}\kappa = \overline{\operatorname{inn}\operatorname{supp}\kappa}$.

Proof.

(a) and (b) immediately follow from Definition 1.2.3.

(c) If $\kappa = 0$ (a.e.) on a relatively open set $U \subset \overline{\Omega}$, then $\kappa = 0$ (a.e.) on the open set $U \cap \operatorname{inn}\operatorname{supp}\kappa$. From the definition of the inner support, it follows that $U \cap \operatorname{inn}\operatorname{supp}\kappa = \emptyset$. This shows the first inclusion in (c). The second inclusion is obvious.

(d) follows from the fact that for every relatively open set $U \subseteq \overline{\Omega}$ we have

$$\begin{aligned} \kappa = 0 \text{ (a.e.) on } U \quad &\text{if and only if} \quad U \subseteq \overline{\Omega} \setminus \operatorname{supp}\kappa \\ &\text{if and only if} \quad \chi_{\operatorname{supp}\kappa} = 0 \text{ (a.e.) on } U. \end{aligned}$$

(e) Since $\operatorname{supp}\kappa \subseteq \Omega$ implies that $\overline{\Omega} \setminus \operatorname{supp}\kappa$ contains $\partial\Omega$, (e) immediately follows from (c) and Definition 1.2.3.

(f) Let κ be continuous on an open set $O \subset \Omega$, where $\Omega \setminus O$ has zero measure.

The assertion follows from (a) and (c) if we can show that for every $x \in \overline{\Omega}$

$$x \notin \overline{\operatorname{inn}\operatorname{supp}\kappa} \quad \text{implies} \quad x \notin \operatorname{supp}\kappa.$$

Let $x \notin \overline{\operatorname{inn}\operatorname{supp}\kappa}$. Then there exists a relatively open set $B \subset \overline{\Omega}$ with $x \in B$ and $B \cap \overline{\operatorname{inn}\operatorname{supp}\kappa} = \emptyset$. Obviously, $\{\xi \in O : \kappa(\xi) \neq 0\} \subseteq \operatorname{inn}\operatorname{supp}\kappa$ so that $\kappa = 0$ on $O \cap B$. Since $\Omega \setminus O$ has zero measure, we have that $\kappa = 0$ (a.e.) on B and thus $B \cap \operatorname{supp}\kappa = \emptyset$, which shows the assertion.

□

As a consequence of Lemma 1.2.4 (e) and (f), we obtain the following corollary.

Corollary 1.2.5. *If κ is piecewise continuous, $\operatorname{supp}\kappa \subseteq \Omega$ and $\Omega \setminus \operatorname{supp}\kappa$ is connected, then*

$$\overline{\operatorname{inn}\operatorname{supp}\kappa} = \operatorname{supp}\kappa = \operatorname{out}_{\partial\Omega}\operatorname{supp}\kappa.$$

1.3 Monotonicity and localized potentials

1.3.1 A monotonicity relation

Our main theoretical tools are a monotonicity estimate and the theory of localized potentials. The following estimate goes back to Ikehata, Kang, Seo, and Sheen [KSS97, Ike98], cf., also the similar results in Ide et al. [IIN+07], Kirsch [Kir05], and in [HS09, HS10]. For the convenience of the reader, we state the estimate together with a short proof that we copy from [HS10, Lemma 2.1].

Lemma 1.3.1. *Let $\sigma_1, \sigma_2 \in L^\infty_+(\Omega)$ be two conductivities, $g \in L^2_\diamond(\Omega)$ be an applied boundary current and $u_2 := u^{(g)}_{\sigma_2} \in H^1_\diamond(\Omega)$. Then*

$$\int_\Omega (\sigma_1 - \sigma_2)|\nabla u_2|^2 \,\mathrm{d}x \geq \langle g, (\Lambda(\sigma_2) - \Lambda(\sigma_1))\, g\rangle \geq \int_\Omega \frac{\sigma_2}{\sigma_1}(\sigma_1 - \sigma_2)|\nabla u_2|^2 \,\mathrm{d}x. \quad (1.5)$$

Proof. Let $u_1 := u^{(g)}_{\sigma_1} \in H^1_\diamond(\Omega)$. From (1.3) we deduce

$$\int_\Omega \sigma_1 \nabla u_1 \cdot \nabla u_2 \,\mathrm{d}x = \langle g, \Lambda(\sigma_2) g\rangle = \int_\Omega \sigma_2 \nabla u_2 \cdot \nabla u_2 \,\mathrm{d}x$$

and thus

$$\begin{aligned}\int_\Omega \sigma_1 |\nabla(u_1 - u_2)|^2 \,\mathrm{d}x &= \int_\Omega \sigma_1 |\nabla u_1|^2 \,\mathrm{d}x - 2\int_\Omega \sigma_2 |\nabla u_2|^2 \,\mathrm{d}x + \int_\Omega \sigma_1 |\nabla u_2|^2 \,\mathrm{d}x \\ &= \langle g, \Lambda(\sigma_1) g\rangle - \langle g, \Lambda(\sigma_2) g\rangle + \int_\Omega (\sigma_1 - \sigma_2)|\nabla u_2|^2 \,\mathrm{d}x.\end{aligned}$$

Since the left-hand side is non-negative, the first asserted inequality follows.

Interchanging σ_1 and σ_2, we obtain

$$\begin{aligned}
&\langle g, (\Lambda(\sigma_2) - \Lambda(\sigma_1))\, g\rangle \\
&= \int_\Omega (\sigma_1 - \sigma_2)|\nabla u_1|^2 \,\mathrm{d}x + \int_\Omega \sigma_2 |\nabla(u_2 - u_1)|^2 \,\mathrm{d}x \\
&= \int_\Omega \left(\sigma_1|\nabla u_1|^2 + \sigma_2|\nabla u_2|^2 - 2\sigma_2 \nabla u_1 \cdot \nabla u_2\right) \mathrm{d}x \\
&= \int_\Omega \sigma_1 \left|\nabla u_1 - \frac{\sigma_2}{\sigma_1}\nabla u_2\right|^2 \mathrm{d}x + \int_\Omega \left(\sigma_2 - \frac{{\sigma_2}^2}{\sigma_1}\right)|\nabla u_2|^2 \,\mathrm{d}x.
\end{aligned}$$

Since the first integral on the right-hand side is non-negative, the second asserted inequality follows. □

We call Lemma 1.3.1 a *monotonicity estimate* because of the following corollary.

Corollary 1.3.2. *For two conductivities $\sigma_1, \sigma_2 \in L^\infty_+(\Omega)$,*

$$\sigma_1 \leq \sigma_2 \quad \textit{implies} \quad \Lambda(\sigma_1) \geq \Lambda(\sigma_2). \tag{1.6}$$

Remark 1.3.3. Corollary 1.3.2 already yields a simple monotonicity-based reconstruction algorithm. Assume that the conductivity in the investigated object is $\sigma = 1 + \chi_D$, where the measurable set $D \subseteq \Omega$ describes the unknown inclusion. Then for all other measurable sets $B \subseteq \Omega$,

$$B \subseteq D \quad \text{implies} \quad \Lambda(1 + \chi_B) \geq \Lambda(\sigma), \tag{1.7}$$

so that the set

$$R := \bigcup \{B \subseteq \Omega \,:\, B \text{ measurable and } \Lambda(1 + \chi_B) \geq \Lambda(\sigma)\}$$

is an upper bound of D.

A numerical approximation of (this upper bound of) D can be calculated by choosing a number of small balls $B = B_\epsilon(z) \subseteq \Omega$ (with center $z \in \Omega$ and radius $\epsilon > 0$) and marking all balls where the *monotonicity test* $\Lambda(1 + \chi_B) \geq \Lambda(\sigma)$ holds true. Algorithms based on this idea have been worked out and numerically tested in the works of Tamburrino and Rubinacci [TR02, Tam06].

Also, Lemma 1.3.1 gives an estimate for the Fréchet derivative of Λ that will be the basis for linearizing our monotonicity tests without losing shape information (cf. [HS10] for the origin of this idea).

Corollary 1.3.4. *Let $\sigma \in L^\infty_+(\Omega)$. Let $\Lambda(1)$ be the NtD operator corresponding to the background conductivity 1 and let $\Lambda'(1)$ be its Fréchet derivative (see Subsection 1.2.1). Then*

$$\Lambda'(1)(1-\sigma) \geq \Lambda(1) - \Lambda(\sigma) \geq \Lambda'(1)\left(\frac{1}{\sigma}(1-\sigma)\right).$$

Of course, in practical EIT applications, it is not possible to measure boundary data with infinite precision. Moreover, with a limited number of electrodes on the boundary of an imaging subject and limited accuracy, we can only obtain a finite-dimensional approximation to the true NtD operator. Also, we can only calculate finite-dimensional approximations of the NtD operator for test conductivities (and their linearized counterparts). Hence, let us comment on the stability of monotonicity tests with respect to such errors.

Remark 1.3.5. Monotonicity/definiteness tests can be stably implemented in the following sense. Let $A \in \mathcal{L}(H)$ be a self-adjoint compact operator on a Hilbert space H and let $(A^\delta)_{\delta>0} \subseteq \mathcal{L}(H)$ be a family of compact (e.g. finite-dimensional) approximations with

$$\|A^\delta - A\|_{\mathcal{L}(\mathcal{H})} < \delta.$$

Possibly replacing A^δ by its symmetric part, we can assume that A^δ is self-adjoint.

For $\alpha > 0$, we define the regularized definiteness test

$$R_\alpha(A^\delta) := \begin{cases} 1 & \text{if } \langle A^\delta g, g\rangle \geq -\alpha \|g\|^2 \text{ for all } g \in H, \\ 0 & \text{otherwise,} \end{cases}$$

which is equivalent to checking whether the smallest eigenvalue of A^δ is not below $-\alpha$.

If $A \geq 0$, then $\langle A^\delta g, g\rangle \geq -\delta \|g\|^2$ for all $g \in H$. If $A \ngeq 0$, then A has a negative eigenvalue $\lambda < 0$ so that $\langle A^\delta g, g\rangle \geq -\delta \|g\|^2$ cannot hold for all $g \in H$ for $\delta < |\lambda|/2$. Hence,

$$R_\delta(A^\delta) = \begin{cases} 1 & \text{if } A \geq 0, \\ 0 & \text{if } A \ngeq 0 \text{ and } \delta \text{ is sufficiently small.} \end{cases}$$

1.3.2 Localized potentials

For each of the monotonicity relations (1.6) and (1.7), we will show that a certain converse holds true. The main theoretical tool for this result is to use the theory of localized potentials by Harrach [Geb08] to control the energy terms $|\nabla u|^2$ in the monotonicity estimate in Lemma 1.3.1.

Roughly speaking, [Geb08] shows that there exist electric potentials which have arbitrarily large energy $|\nabla u|^2$ in some region and arbitrarily small energy in another

region, as long as the high-energy region can be reached from the boundary without crossing the low-energy region.

We will make use of the following variant of the result in [Geb08].

Theorem 1.3.6. *Let $D_1, D_2 \subseteq \overline{\Omega}$ be two measurable sets with*

$$\operatorname{int} D_1 \not\subseteq \operatorname{out}_{\partial\Omega} D_2.$$

Furthermore, let $\sigma \in L^\infty_+(\Omega)$ be piecewise analytic.

Then there exists $(g_m)_{m\in\mathbb{N}} \subset L^2_\diamond(\partial\Omega)$ such that the solutions $(u_m)_{m\in\mathbb{N}} \subset H^1_\diamond(\Omega)$ with $u_m := u_\sigma^{(g_m)}$ of (1.2) fulfill

$$\lim_{m\to\infty} \int_{D_1} |\nabla u_m|^2 \,\mathrm{d}x = \infty \quad \textit{and} \quad \lim_{m\to\infty} \int_{D_2} |\nabla u_m|^2 \,\mathrm{d}x = 0.$$

Proof. The proof is a slight adaptation of the one in [Geb08, Sect. 2.2], see also [Har12] for the general approach.

(a) *Reformulation as range (non-)inclusion:*

We define the *virtual measurement* operators L_j $(j = 1, 2)$ by

$$L_j : \; L^2(D_j)^n \to L^2_\diamond(\partial\Omega), \qquad F \mapsto v|_{\partial\Omega},$$

where $v \in H^1_\diamond(\Omega)$ solves

$$\int_\Omega \sigma\nabla v \cdot \nabla w \,\mathrm{d}x = \int_{D_j} F \cdot \nabla w \,\mathrm{d}x \quad \text{for all } w \in H^1_\diamond(\Omega).$$

Note that this implies $\nabla \cdot \sigma\nabla v = 0$ in $\Omega \setminus \overline{D}_j$ and if $\overline{D}_j \subseteq \Omega$, then it also implies the homogeneous Neumann boundary condition $\sigma\partial_\nu v|_{\partial\Omega} = 0$.

It is easily checked that the adjoint operators

$$L_j^* : \; L^2_\diamond(\partial\Omega) \to L^2(D_j)^n, \quad j = 1, 2$$

are given by $L_j^* g = \nabla u|_{D_j}$, where $u = u_\sigma^{(g)} \in H^1_\diamond(B)$ solves (1.2).

Now the assertion is equivalent to the statement

$$\nexists C > 0 \;:\; \|L_1^* g\| \le C \|L_2^* g\| \quad \text{for all } g \in L^2_\diamond(\partial\Omega),$$

which is (see, e.g., [Geb08, Lemma 2.5]) equivalent to the range (non-)inclusion

$$\mathcal{R}(L_1) \not\subseteq \mathcal{R}(L_2). \tag{1.8}$$

(b) *Proof of the range (non-)inclusion* (1.8)*:*

Since $\operatorname{int} D_1 \not\subseteq \operatorname{out}_{\partial\Omega} D_2$, the set $\operatorname{int} D_1$ must intersect one of the sets U in the definition of the outer support of χ_{D_2}. Hence, there exists a set $U \subset \overline{\Omega} \setminus \operatorname{out}_{\partial\Omega} D_2$ with U (relatively) open in $\overline{\Omega}$, U connected to $\partial\Omega$ and $U \cap D_1$ contains an open ball B. Possibly shrinking the ball, we can assume that $\overline{B} \subset \Omega$ and that $(U \cap \Omega) \setminus \overline{B}$ is connected.

Let L_B denote the virtual measurement operator corresponding to the ball B. Obviously, $B \subseteq D_1$ implies $\mathcal{R}(L_B) \subseteq \mathcal{R}(L_1)$ so that it suffices to prove that

$$\mathcal{R}(L_B) \not\subseteq \mathcal{R}(L_2). \tag{1.9}$$

To that end let $\varphi \in \mathcal{R}(L_B) \cap \mathcal{R}(L_2)$. Then there exist $v_B, v_2 \in H^1_\diamond(\Omega)$ with $v_B|_{\partial\Omega} = \varphi = v_2|_{\partial\Omega}$, $\sigma\partial_\nu v_B|_{U\cap\partial\Omega} = 0 = \sigma\partial_\nu v_2|_{U\cap\partial\Omega}$ and

$$\begin{aligned} \nabla\cdot\sigma\nabla v_B &= 0 \quad \text{in } \Omega\setminus\overline{B}, \\ \nabla\cdot\sigma\nabla v_2 &= 0 \quad \text{in } U. \end{aligned}$$

By unique continuation, it follows that $v_B = v_2$ in $U \setminus \overline{B}$. Hence,

$$u := \begin{cases} v_B & \text{in } \Omega\setminus\overline{B}, \\ v_2 & \text{in } \overline{B} \end{cases}$$

defines a function $u \in H^1_\diamond(\Omega)$ with $u = u^{(0)}_\sigma$, i.e., $\nabla\cdot\sigma\nabla u = 0$ in Ω and homogeneous Neumann boundary data $\sigma\partial_\nu u|_{\partial\Omega} = 0$. It follows that $\varphi = u|_{\partial\Omega} = 0$ and thus we have shown that $\mathcal{R}(L_B) \cap \mathcal{R}(L_2) = \{0\}$.

Finally, using unique continuation again, we obtain that L_B^* is injective so that $\mathcal{R}(L_B)$ is dense in $L^2_\diamond(\partial\Omega)$. A fortiori, $\mathcal{R}(L_B) \neq \{0\}$, which, together with $\mathcal{R}(L_B) \cap \mathcal{R}(L_2) = \{0\}$, proves (1.9) and thus the assertion.

□

Note that Theorem 1.3.6 also holds for less regular conductivities as long as a unique continuation property is fulfilled and that localized potentials can be constructed by solving regularized operator equations, cf. [Geb08].

We now show that (regardless of regularity) the properties of the localized potentials do not depend on the conductivity in the low-energy region.

Lemma 1.3.7. *Let $D_1, D_2 \subseteq \overline{\Omega}$ be two measurable sets. Let $\sigma, \tau \in L^\infty_+(\Omega)$ and $u^{(g_m)}_\sigma, u^{(g_m)}_\tau \in H^1_\diamond(\Omega)$ denote the corresponding solutions of* (1.2) *for a sequence of boundary currents $(g_m)_{m\in\mathbb{N}} \subset L^2_\diamond(\partial\Omega)$.*

If $\operatorname{supp}(\sigma - \tau) \subseteq D_2$*, then*

$$\lim_{m\to\infty} \int_{D_1} \left|\nabla u^{(g_m)}_\sigma\right|^2 \mathrm{d}x = \infty \quad \textit{and} \quad \lim_{m\to\infty} \int_{D_2} \left|\nabla u^{(g_m)}_\sigma\right|^2 \mathrm{d}x = 0$$

holds if and only if

$$\lim_{m\to\infty}\int_{D_1}\left|\nabla u_\tau^{(g_m)}\right|^2\,\mathrm{d}x=\infty\quad\textit{and}\quad\lim_{m\to\infty}\int_{D_2}\left|\nabla u_\tau^{(g_m)}\right|^2\,\mathrm{d}x=0.$$

Proof. For both conductivities σ and τ, we define the virtual measurement operators

$$L_{2,\sigma}, L_{2,\tau}:\ L^2(D_2)^n\to L^2_\diamond(\partial\Omega),$$

as in the proof of Theorem 1.3.6. If $v_\sigma|_{\partial\Omega}=L_{2,\sigma}F$ with $F\in L^2(D_2)^n$ and a solution $v_\sigma\in H^1_\diamond(\Omega)$ of

$$\int_\Omega\sigma\nabla v_\sigma\cdot\nabla w\,\mathrm{d}x=\int_{D_2}F\cdot\nabla w\,\mathrm{d}x\quad\text{for all } w\in H^1_\diamond(\Omega),$$

then v_σ also solves

$$\int_\Omega\tau\nabla v_\sigma\cdot\nabla w\,\mathrm{d}x=\int_{D_2}(F+(\tau-\sigma)\nabla v_\sigma)\cdot\nabla w\,\mathrm{d}x\quad\text{for all } w\in H^1_\diamond(\Omega).$$

This shows that $\mathcal{R}(L_{2,\sigma})\subseteq\mathcal{R}(L_{2,\tau})$. As in the proof of Theorem 1.3.6, this implies that

$$\exists C>0:\ \int_{D_2}\left|\nabla u_\sigma^{(g_m)}\right|^2\mathrm{d}x\le C\int_{D_2}\left|\nabla u_\tau^{(g_m)}\right|^2\,\mathrm{d}x\quad\text{for all } m\in\mathbb{N}.$$

By interchanging σ and τ, we obtain that

$$\lim_{m\to\infty}\int_{D_2}\left|\nabla u_\sigma^{(g_m)}\right|^2\,\mathrm{d}x=0\quad\text{if and only if}\quad\lim_{m\to\infty}\int_{D_2}\left|\nabla u_\tau^{(g_m)}\right|^2\,\mathrm{d}x=0.$$

Using the same argument on $D_1\cup D_2$, it follows that also

$$\lim_{m\to\infty}\int_{D_1\cup D_2}\left|\nabla u_\sigma^{(g_m)}\right|^2\,\mathrm{d}x=\infty\quad\text{if and only if}\quad\lim_{m\to\infty}\int_{D_1\cup D_2}\left|\nabla u_\tau^{(g_m)}\right|^2\,\mathrm{d}x=\infty$$

so that the assertion follows. □

Remark 1.3.8. Localized potentials can be numerically constructed by solving regularized operator equations (see [Geb08]) and they can be used to probe for an unknown inclusion in the spirit of the probe or needle method, cf., e.g., [Ike05, Ike07]. We briefly sketch the idea on a simple test example. Let us assume that the conductivity is $\sigma=1+\chi_D$ and that $(g_m)_{m\in\mathbb{N}}$ is a sequence such that the solutions $(u_m)_{m\in\mathbb{N}}\subset H^1_\diamond(\Omega)$ of $\Delta u_m=0$ and $\partial_\nu u_m|_{\partial\Omega}=g_m$ (i.e., $u_m=u_1^{(g_m)}$) fulfill

$$\lim_{m\to\infty}\int_{D_1}|\nabla u_m|^2\,\mathrm{d}x=\infty\quad\text{and}\quad\lim_{m\to\infty}\int_{D_2}|\nabla u_m|^2\,\mathrm{d}x=0.$$

Then the monotonicity estimate in Lemma 1.3.1 yields that

$$\begin{aligned}D\subseteq D_2\quad&\text{implies}\quad|\langle g_m,(\Lambda(1)-\Lambda(\sigma))g_m\rangle|\to 0,\\ D_1\subseteq D\quad&\text{implies}\quad|\langle g_m,(\Lambda(1)-\Lambda(\sigma))g_m\rangle|\to\infty.\end{aligned}$$

Choosing D_2 to cover most of Ω and D_1 to be, e.g., a small ball inside $\Omega \setminus D_2$, one may thus estimate the shape of D by slowly shrinking D_2.

Such an algorithm would however suffer from high computational cost (to construct a high number of localized potentials) and it is not clear how to check the limit of $\langle g_m, (\Lambda(1) - \Lambda(\sigma))g_m \rangle$ in a numerically stable way. Furthermore, the choice of the sets D_1 and D_2 would certainly impose some geometrical restrictions on the shapes of inclusions that can be recovered.

In the following we take a different approach. The monotonicity methods derived in the next section do not require the numerical construction of localized potentials. We will require only the above abstract existence results for localized potentials in order to show that simple monotonicity tests recover the true (outer) shape of an inclusion.

1.4 Monotonicity-based shape reconstruction

1.4.1 The definite case

We will now show how the shape reconstruction problem can be solved via simple monotonicity tests. We start with the definite case, in which the conductivity of the inclusions is everywhere higher or everywhere lower than the background. We treat this case separately since it allows a particularly simple reconstruction strategy. Given a small ball, the following theorems show how to check whether the ball belongs to the inclusion or not. The proofs of the theorems are postponed until the end of this subsection. The main idea of this subsection has previously been summarized in the extended conference abstract [HU10].

Theorem 1.4.1. *Let $\sigma \in L^\infty_+(\Omega)$ and $\sigma \geq 1$.*

For every open ball $B := B_\epsilon(z)$ and every $\alpha > 0$,

$$\begin{aligned} \alpha\chi_B \leq \sigma - 1 \qquad &\text{implies} \quad \Lambda(1 + \alpha\chi_B) \geq \Lambda(\sigma), \\ B \nsubseteq \operatorname{out}_{\partial\Omega} \operatorname{supp}(\sigma - 1) \qquad &\text{implies} \quad \Lambda(1 + \alpha\chi_B) \ngeq \Lambda(\sigma). \end{aligned}$$

Hence, the set

$$R := \bigcup_{\alpha > 0} \{B = B_\epsilon(z) \subseteq \Omega \ : \ \Lambda(1 + \alpha\chi_B) \geq \Lambda(\sigma)\}$$

fulfills

$$\operatorname{inn} \operatorname{supp}(\sigma - 1) \subseteq R \subseteq \operatorname{out}_{\partial\Omega} \operatorname{supp}(\sigma - 1).$$

Example 1.4.2. *Let $\sigma = 1 + \chi_D$, where the inclusion D is open and $\overline{D} \subset \Omega$ has a connected complement. Then for every open ball $B \subseteq \Omega$,*

$$B \subseteq D \quad \text{if and only if} \quad \Lambda(1 + \chi_B) \geq \Lambda(\sigma).$$

Note that implementing the monotonicity tests in Theorem 1.4.1 or Example 1.4.2 would be computationally expensive since for each ball B (and possibly also for each test level α), we would have to solve the EIT equation with a new inhomogeneous conductivity in order to calculate $\Lambda(1+\alpha\chi_B)$. The following theorem shows that we can replace the tests by linearized versions that do not require such inhomogeneous forward solutions. Since this is a bit counterintuitive, let us stress that the following result is not affected by the linearization error, no matter how large that may be. The linearized inverse problem in EIT still contains the exact shape information, cf. [HS10].

Theorem 1.4.3. *Let $\sigma \in L^\infty_+(\Omega)$ and $\sigma \geq 1$.*

For every open ball $B := B_\epsilon(z)$ and every $\alpha > 0$,

$$\begin{aligned} \alpha\chi_B \leq \frac{1}{\sigma}(\sigma - 1) \qquad & \textit{implies} \quad \Lambda(1) + \alpha\Lambda'(1)\chi_B \geq \Lambda(\sigma), \\ B \nsubseteq \operatorname{out}_{\partial\Omega} \operatorname{supp}(\sigma - 1) \qquad & \textit{implies} \quad \Lambda(1) + \alpha\Lambda'(1)\chi_B \ngeq \Lambda(\sigma). \end{aligned}$$

Hence, the set

$$R := \bigcup_{\alpha>0} \{B = B_\epsilon(z) \subseteq \Omega \,:\, \Lambda(1) + \alpha\Lambda'(1)\chi_B \geq \Lambda(\sigma)\}$$

fulfills

$$\operatorname{inn} \operatorname{supp}(\sigma - 1) \subseteq R \subseteq \operatorname{out}_{\partial\Omega} \operatorname{supp}(\sigma - 1).$$

Example 1.4.4. *Let $\sigma = 1 + \chi_D$, where the inclusion D is open and $\overline{D} \subset \Omega$ has a connected complement. Then for every ball $B = B_\epsilon(z)$,*

$$B \subseteq D \quad \textit{if and only if} \quad \Lambda(1) + \tfrac{1}{2}\Lambda'(1)\chi_B \geq \Lambda(\sigma).$$

Proof of Theorem 1.4.1. Let $\sigma \in L^\infty_+(\Omega)$, $\sigma \geq 1$. Let $B = B_\epsilon(z)$ and $\alpha > 0$. Corollary 1.3.2 yields that

$$\alpha\chi_B \leq \sigma - 1 \quad \text{implies} \quad \Lambda(1 + \alpha\chi_B) \geq \Lambda(\sigma).$$

It remains to show that

$$B \nsubseteq \operatorname{out}_{\partial\Omega} \operatorname{supp}(\sigma - 1) \quad \text{implies} \quad \Lambda(1 + \alpha\chi_B) \ngeq \Lambda(\sigma).$$

Let $B \nsubseteq \operatorname{out}_{\partial\Omega} \operatorname{supp}(\sigma - 1)$. Corollary 1.3.2 yields that shrinking the ball B only makes $\Lambda(1 + \alpha\chi_B)$ larger so that we can assume w.l.o.g. that

$$B \subseteq \Omega \setminus \operatorname{out}_{\partial\Omega} \operatorname{supp}(\sigma - 1).$$

We have that $1 + \alpha\chi_B$ is piecewise analytic,

$$B = \operatorname{int} B \quad \text{and} \quad \operatorname{out}_{\partial\Omega} \operatorname{supp}(\sigma - 1) = \operatorname{out}_{\partial\Omega}(\operatorname{supp}(\sigma - 1))$$

(see Lemma 1.2.4 (d)). Hence, we can apply Theorem 1.3.6 and obtain a sequence of currents $(g_m)_{m\in\mathbb{N}} \subset L^2_\diamond(\partial\Omega)$ so that the solutions $(u_m)_{m\in\mathbb{N}} \subset H^1_\diamond(\Omega)$ of

$$\nabla \cdot (1+\alpha\chi_B)\nabla u_m = 0 \quad \text{in } \Omega, \qquad (1+\alpha\chi_B)\partial_\nu u_m|_{\partial\Omega} = g_m,$$

fulfill

$$\lim_{m\to\infty} \int_B |\nabla u_m|^2 \,\mathrm{d}x = \infty \quad \text{and} \quad \lim_{m\to\infty} \int_{\operatorname{supp}(\sigma-1)} |\nabla u_m|^2 \,\mathrm{d}x = 0.$$

From Lemma 1.3.1 it follows that

$$\begin{aligned}\langle g_m, (\Lambda(1+\alpha\chi_B) - \Lambda(\sigma))\, g_m\rangle &\le \int_\Omega (\sigma - 1 - \alpha\chi_B)|\nabla u_m|^2 \,\mathrm{d}x \\ &= -\alpha \int_B |\nabla u_m|^2 \,\mathrm{d}x + \int_{\operatorname{supp}(\sigma-1)} (\sigma-1)|\nabla u_m|^2 \,\mathrm{d}x \\ &\to -\infty,\end{aligned}$$

and hence $\Lambda(1+\alpha\chi_B) \not\geq \Lambda(\sigma)$. □

Proof of Theorem 1.4.3. Let $\sigma \in L^\infty_+(\Omega)$, $\sigma \ge 1$. Let $B = B_\epsilon(z)$ and $\alpha > 0$. For every $g \in L^2_\diamond(\partial\Omega)$ and solution $u \in H^1_\diamond(\Omega)$ of

$$\Delta u = 0 \quad \text{in } \Omega, \qquad \partial_\nu u|_{\partial\Omega} = g,$$

we obtain from Lemma 1.3.1

$$\langle g, (\Lambda(1) + \alpha\Lambda'(1)\chi_B - \Lambda(\sigma))\, g\rangle \ge \int_\Omega \left(\frac{1}{\sigma}(\sigma-1) - \alpha\chi_B\right) |\nabla u|^2 \,\mathrm{d}x.$$

This shows that

$$\alpha\chi_B \le \frac{1}{\sigma}(\sigma-1) \quad \text{implies} \quad \Lambda(1) + \alpha\Lambda'(1)\chi_B \ge \Lambda(\sigma).$$

It remains to show that

$$B \not\subseteq \operatorname{out}_{\partial\Omega} \operatorname{supp}(\sigma-1) \quad \text{implies} \quad \Lambda(1) + \alpha\Lambda'(1)\chi_B \not\geq \Lambda(\sigma).$$

To show this let $B \not\subseteq \operatorname{out}_{\partial\Omega} \operatorname{supp}(\sigma-1)$. The linearized monotonicity relation (1.4) yields that shrinking the ball B only makes $\Lambda(1) + \alpha\Lambda'(1)\chi_B$ larger so that we can assume w.l.o.g. that $B \subseteq \Omega \setminus \operatorname{out}_{\partial\Omega} \operatorname{supp}(\sigma-1)$. Then

$$\begin{aligned}&\langle g, (\Lambda(1) + \alpha\Lambda'(1)\chi_B - \Lambda(\sigma))\, g\rangle \\ &\le \int_\Omega (\sigma - 1 - \alpha\chi_B)\,|\nabla u|^2 \,\mathrm{d}x = -\alpha \int_B |\nabla u|^2 \,\mathrm{d}x + \int_{\operatorname{supp}(\sigma-1)} (\sigma-1)|\nabla u|^2 \,\mathrm{d}x\end{aligned}$$

so that the assertion follows using localized potentials for the background conductivity 1 and the same sets as in Theorem 1.3.6. □

Remark 1.4.5. If $\sigma \in L^\infty_+(\Omega)$ and $\sigma \leq 1$, then we obtain with the same arguments that for every open ball $B \subseteq \Omega$ and every $0 < \alpha < 1$,

$$\begin{aligned} \alpha\chi_B \leq 1 - \sigma \quad &\text{implies} \quad \Lambda(1 - \alpha\chi_B) \leq \Lambda(\sigma), \\ B \not\subseteq \operatorname{out}_{\partial\Omega} \operatorname{supp}(\sigma - 1) \quad &\text{implies} \quad \Lambda(1 - \alpha\chi_B) \not\leq \Lambda(\sigma), \end{aligned}$$

and for every open ball $B \subseteq \Omega$ and every $\alpha > 0$,

$$\begin{aligned} \alpha\chi_B \leq 1 - \sigma \quad &\text{implies} \quad \Lambda(1) - \alpha\Lambda'(1)\chi_B \leq \Lambda(\sigma), \\ B \not\subseteq \operatorname{out}_{\partial\Omega} \operatorname{supp}(\sigma - 1) \quad &\text{implies} \quad \Lambda(1) - \alpha\Lambda'(1)\chi_B \not\leq \Lambda(\sigma). \end{aligned}$$

Remark 1.4.6. An inspection of the proofs shows that the balls can be replaced by arbitrary measurable sets B with non-empty interior in Theorem 1.4.3 (and the second part of Remark 1.4.5). For Theorem 1.4.1 (and the first part of Remark 1.4.5), the sets B must additionally possess a piecewise smooth boundary (so that $1 + \alpha\chi_B$ remains piecewise analytic). We comment on further generalizations in Section 1.4.3.

1.4.2 The indefinite case

We now consider the general indefinite case, where σ is no longer required to be everywhere larger or everywhere smaller than the background conductivity 1. Instead of testing whether a small test region is part of the unknown inclusions, we will now test whether a large test region contains the unknown inclusions.

The main idea is the following. Consider a large test region C with connected complement. If C overlaps the inclusions, a large enough or small enough test conductivity on C will make the corresponding test NtD operator smaller or larger than the measured NtD operator, respectively. Hence, if C covers the inclusions, two monotonicity tests (one with a large and one with a small test level on C) hold true. On the other hand, if C does not cover the inclusions, we can connect the non-covered part with the boundary and construct a localized potential with large energy in the non-covered part and small energy in C. Depending on whether the conductivity of the inclusions is either larger or smaller than the background in the non-covered part, this localized potential shows that one of the monotonicity tests cannot hold true.

However, for this argument we need a *local definiteness property*. If a conductivity differs from the background, there must either be a neighborhood of the boundary where it differs from the background in the positive direction or a neighborhood where it differs in the negative direction. Note that even C^∞-conductivities might oscillate infinitely and thus violate this property. This property holds, however, if the conductivity is either piecewise analytic or if the higher-conductivity and lower-conductivity parts have some distance from each other, and the inner support does not deviate too much from the true support (which already holds, e.g., for piecewise continuous functions, see Corollary 1.2.5).

More precisely, we assume that $\sigma \in L^\infty_+(\Omega)$ is either piecewise-analytic or

$$\operatorname{supp}(\sigma-1)^+ \cap \operatorname{supp}(\sigma-1)^- = \emptyset, \quad \overline{\operatorname{inn}\operatorname{supp}(\sigma-1)} = \operatorname{supp}(\sigma-1), \tag{1.10}$$

where $(\sigma-1)^+ := \max\{\sigma-1,0\}$, $(\sigma-1)^- := \min\{\sigma-1,0\}$.

Theorem 1.4.7. *Let $\sigma \in L^\infty_+(\Omega)$ either be piecewise-analytic or fulfill* (1.10)*. Then for every set $C \subseteq \overline{\Omega}$ with $C = \operatorname{out}_{\partial\Omega} C$ and every $\alpha > 1$,*

$$\begin{aligned} 1 - \tfrac{\alpha-1}{\alpha}\chi_C \le \sigma \quad &\text{implies} \quad \Lambda\left(1 - \tfrac{\alpha-1}{\alpha}\chi_C\right) \ge \Lambda(\sigma), \\ 1 + \alpha\chi_C \ge \sigma \quad &\text{implies} \quad \Lambda\left(1 + \alpha\chi_C\right) \le \Lambda(\sigma) \end{aligned}$$

and

$$\Lambda\left(1+\alpha\chi_C\right) \le \Lambda(\sigma) \le \Lambda\left(1-\tfrac{\alpha-1}{\alpha}\chi_C\right) \quad \text{implies} \quad \operatorname{out}_{\partial\Omega}\operatorname{supp}(\sigma-1) \subseteq C.$$

Hence,

$$R := \bigcap \left\{ C = \operatorname{out}_{\partial\Omega} C \subseteq \overline{\Omega},\ \exists \alpha > 1 :\ \Lambda(1+\alpha\chi_C) \le \Lambda(\sigma) \le \Lambda\left(1-\tfrac{\alpha-1}{\alpha}\chi_C\right) \right\}$$

fulfills $R = \operatorname{out}_{\partial\Omega}\operatorname{supp}(\sigma-1)$.

We postpone the proof until the end of this subsection and first give an example and formulate the linearized version.

Example 1.4.8. *Let $\sigma = 1 + \chi_{D^+} - \frac{1}{2}\chi_{D^-}$, where $D^+, D^- \subseteq \Omega$ are open sets with $\overline{D^+} \cap \overline{D^-} = \emptyset$ and $\overline{D^+} \cup \overline{D^-} \subset \Omega$ has a connected complement.*

Then for every closed set $C \subset \Omega$ with connected complement $\Omega \setminus C$,

$$D^+ \cup D^- \subseteq C \quad \text{if and only if} \quad \Lambda(1+\chi_C) \le \Lambda(\sigma) \le \Lambda(1-\tfrac{1}{2}\chi_C).$$

Theorem 1.4.9. *Under the assumptions of Theorem 1.4.7 we have that for every set $C \subseteq \overline{\Omega}$ with $C = \operatorname{out}_{\partial\Omega} C$ and every $\alpha > 0$,*

$$\begin{aligned} 1 - \alpha\chi_C \le 2 - \tfrac{1}{\sigma} \quad &\text{implies} \quad \Lambda(1) - \alpha\Lambda'(1)\chi_C \ge \Lambda(\sigma), \\ 1 + \alpha\chi_C \ge \sigma \quad &\text{implies} \quad \Lambda(1) + \alpha\Lambda'(1)\chi_C \le \Lambda(\sigma) \end{aligned}$$

and

$$\Lambda(1) + \alpha\Lambda'(1)\chi_C \le \Lambda(\sigma) \le \Lambda(1) - \alpha\Lambda'(1)\chi_C \quad \text{implies} \quad \operatorname{out}_{\partial\Omega}\operatorname{supp}(\sigma-1) \subseteq C.$$

Hence,

$$\begin{aligned} R := \bigcap \big\{ C = \operatorname{out}_{\partial\Omega} C \subseteq \overline{\Omega},\ \exists \alpha > 0 :\ & \\ \Lambda(1) + \alpha\Lambda'(1)\chi_C \le \Lambda(\sigma) \le \Lambda(1) - \alpha\Lambda'(1)\chi_C \big\} & \end{aligned}$$

fulfills $R = \operatorname{out}_{\partial\Omega}\operatorname{supp}(\sigma-1)$.

Example 1.4.10. *Let $\sigma = 1 + \chi_{D^+} - \frac{1}{2}\chi_{D^-}$, where $D^+, D^- \subseteq \Omega$ are open sets with $\overline{D^+} \cap \overline{D^-} = \emptyset$ and $\overline{D^+} \cup \overline{D^-} \subset \Omega$ has a connected complement.*

Then for every closed set $C \subset \Omega$ with connected complement $\Omega \setminus C$,

$$D^+ \cup D^- \subseteq C \quad \text{if and only if} \quad \Lambda(1) + \Lambda'(1)\chi_C \leq \Lambda(\sigma) \leq \Lambda(1) - \Lambda'(1)\chi_C.$$

Proof of Theorem 1.4.7. Let $\alpha > 1$ and $C = \operatorname{out}_{\partial\Omega} C \subseteq \overline{\Omega}$. Then C is closed and thus measurable so that $1 - \frac{\alpha-1}{\alpha}\chi_C, 1 + \alpha\chi_C \in L^\infty_+(\Omega)$.

Corollary 1.3.2 yields the first two assertions

$$\begin{aligned} 1 - \tfrac{\alpha-1}{\alpha}\chi_C \leq \sigma \quad &\text{implies} \quad \Lambda\left(1 - \tfrac{\alpha-1}{\alpha}\chi_C\right) \geq \Lambda(\sigma), \\ 1 + \alpha\chi_C \geq \sigma \quad &\text{implies} \quad \Lambda(1 + \alpha\chi_C) \leq \Lambda(\sigma). \end{aligned}$$

It remains to show that $\operatorname{out}_{\partial\Omega} \operatorname{supp}(\sigma - 1) \nsubseteq C$ implies that either

$$\Lambda\left(1 - \tfrac{\alpha-1}{\alpha}\chi_C\right) \ngeq \Lambda(\sigma) \quad \text{or} \quad \Lambda(1 + \alpha\chi_C) \nleq \Lambda(\sigma).$$

Let $\operatorname{out}_{\partial\Omega} \operatorname{supp}(\sigma - 1) \nsubseteq C = \operatorname{out}_{\partial\Omega} C$. Then there exists a relatively open set $U \subseteq \overline{\Omega}$ that is connected to $\partial\Omega$ where $\sigma|_U \not\equiv 1$ and $C \cap U = \emptyset$.

We first prove the assertion for the case that σ is piecewise analytic. Using the local definiteness property derived in Corollary 1.6.2 in the appendix (Section 1.6), we can choose (note that $\Omega \setminus D_2 \subseteq U$ implies $C \subseteq D_2$)

$$D_1, D_2 \subseteq \overline{\Omega}, \quad \text{with} \quad D_1 = \operatorname{int} D_1 \nsubseteq \operatorname{out}_{\partial\Omega} D_2 = D_2, \quad C \subseteq D_2$$

so that either

(a) $\sigma \geq 1$ on $\Omega \setminus D_2$, $\quad \sigma - 1 \in L^\infty_+(D_1)$, or

(b) $\sigma \leq 1$ on $\Omega \setminus D_2$, $\quad 1 - \sigma \in L^\infty_+(D_1)$.

Replacing D_1 with $D_1 \setminus \operatorname{out}_{\partial\Omega} D_2$, we can also assume that $D_1 \cap D_2 = \emptyset$.

Then for the homogeneous conductivity $\tau = 1$, we use Theorem 1.3.6 and obtain a sequence $(g_m)_{m\in\mathbb{N}} \subset L^2_\diamond(\partial\Omega)$ so that the solutions $(u_\tau^{(g_m)})_{m\in\mathbb{N}} \subseteq H^1_\diamond(\Omega)$ of (1.2) fulfill

$$\lim_{m\to\infty} \int_{D_1} \left|\nabla u_\tau^{(g_m)}\right|^2 \mathrm{d}x = \infty \quad \text{and} \quad \lim_{m\to\infty} \int_{D_2} \left|\nabla u_\tau^{(g_m)}\right|^2 \mathrm{d}x = 0.$$

Since $C \subseteq D_2$, it follows from Lemma 1.3.7 that the solutions $u_\tau^{(g_m)}$ for the conductivities $\tau = 1 - \frac{\alpha-1}{\alpha}\chi_C$ and $\tau = 1 + \alpha\chi_C$ have the same property.

Hence, in case (a) we apply Lemma 1.3.1 with $\tau = 1 + \alpha\chi_C$ and obtain (using that

$\sigma \geq 1$ on $\Omega \setminus (D_1 \cup D_2)$, $D_1 \cap D_2 = \emptyset$ and $C \subseteq D_2$)

$$
\begin{aligned}
&\langle g_m, (\Lambda(1+\alpha\chi_C) - \Lambda(\sigma))\, g_m \rangle \\
&\geq \int_\Omega \frac{1+\alpha\chi_C}{\sigma}(\sigma - (1+\alpha\chi_C)) \left|\nabla u_\tau^{(g_m)}\right|^2 \,\mathrm{d}x \\
&= \int_{\Omega\setminus(D_1\cup D_2)} \frac{\sigma-1}{\sigma} \left|\nabla u_\tau^{(g_m)}\right|^2 \,\mathrm{d}x + \int_{D_1} \frac{\sigma-1}{\sigma} \left|\nabla u_\tau^{(g_m)}\right|^2 \,\mathrm{d}x \\
&\qquad + \int_{D_2} \frac{1+\alpha\chi_C}{\sigma}(\sigma - (1+\alpha\chi_C)) \left|\nabla u_\tau^{(g_m)}\right|^2 \,\mathrm{d}x \\
&\geq \int_{D_1} \frac{\sigma-1}{\sigma} \left|\nabla u_\tau^{(g_m)}\right|^2 \,\mathrm{d}x + \int_{D_2} \frac{1+\alpha\chi_C}{\sigma}(\sigma - (1+\alpha\chi_C)) \left|\nabla u_\tau^{(g_m)}\right|^2 \,\mathrm{d}x \to \infty.
\end{aligned}
$$

In case (b) we apply Lemma 1.3.1 with $\tau = 1 - \frac{\alpha-1}{\alpha}\chi_C$ and obtain (using that $\sigma \leq 1$ on $\Omega \setminus (D_1 \cup D_2)$ and that $C \subseteq D_2$)

$$
\begin{aligned}
&\left\langle g_m, \left(\Lambda\left(1 - \tfrac{\alpha-1}{\alpha}\chi_C\right) - \Lambda(\sigma)\right) g_m \right\rangle \\
&\leq \int_\Omega \left(\sigma - \left(1 - \tfrac{\alpha-1}{\alpha}\chi_C\right)\right) \left|\nabla u_\tau^{(g_m)}\right|^2 \,\mathrm{d}x \\
&= \int_{\Omega\setminus(D_1\cup D_2)} (\sigma-1) \left|\nabla u_\tau^{(g_m)}\right|^2 \,\mathrm{d}x + \int_{D_1} (\sigma-1) \left|\nabla u_\tau^{(g_m)}\right|^2 \,\mathrm{d}x \\
&\qquad + \int_{D_2} \left(\sigma - \left(1 - \tfrac{\alpha-1}{\alpha}\chi_C\right)\right) \left|\nabla u_\tau^{(g_m)}\right|^2 \,\mathrm{d}x \\
&\leq \int_{D_1} (\sigma-1) \left|\nabla u_\tau^{(g_m)}\right|^2 \,\mathrm{d}x + \int_{D_2} \left(\sigma - \left(1 - \tfrac{\alpha-1}{\alpha}\chi_C\right)\right) \left|\nabla u_\tau^{(g_m)}\right|^2 \,\mathrm{d}x \to -\infty,
\end{aligned}
$$

which proves the assertion for piecewise analytic conductivities.

Now we prove that the assertion also holds for (not necessary piecewise analytic) conductivities fulfilling (1.10). It suffices to show that also in this case there exist

$$
D_1, D_2 \subseteq \overline{\Omega}, \quad \text{with} \quad D_1 = \operatorname{int} D_1 \not\subseteq \operatorname{out}_{\partial\Omega} D_2 = D_2, \quad C \subseteq D_2,
$$

such that either (a) or (b) from above holds.

First note that if $\operatorname{supp}(\sigma-1)^+$ and $\operatorname{supp}(\sigma-1)^-$ are disjoint compact sets, then

$$
\delta := \operatorname{dist}\left(\operatorname{supp}(\sigma-1)^+, \operatorname{supp}(\sigma-1)^-\right) > 0.
$$

$\sigma|_U \not\equiv 1$ implies that there exists a point $y \in U \cap \operatorname{supp}(\sigma-1)$. Let $x \in \partial\Omega \cap U$. Since $\partial\Omega$ is a smooth boundary and $U \cap \Omega$ is open and connected, we can connect x and y with a continuous path

$$
\gamma:\ [0,1] \to U, \quad \gamma(0) = x,\ \gamma(1) = y.
$$

Using that U is relatively open, there exists for each $t \in [0,1]$ a ball $B_t := B_{\epsilon(t)}(\gamma(t))$ with radius $\epsilon(t) < \delta/2$ and $B_t \cap \overline{\Omega} \subseteq U$.

By compactness of $\gamma([0,1])$, we can choose a finite number $0 \leq t_1 < \ldots < t_N \leq 1$ so that

$$\gamma([0,1]) \subset (B_{t_1} \cup \ldots \cup B_{t_N}) \cap \overline{\Omega}.$$

Since $\gamma(1) = y \in \operatorname{supp}(\sigma - 1)$, there exists a smallest index J for which

$$B_{t_J} \cap \overline{\operatorname{inn}\operatorname{supp}(\sigma - 1)} = B_{t_J} \cap \operatorname{supp}(\sigma - 1) \neq \emptyset$$

so that there exists an open set $D_1 \subseteq B_{t_J}$ with $|\sigma - 1| \in L^\infty_+(D_1)$.

We define $D_2 := \Omega \setminus (B_{t_1} \cup \ldots \cup B_{t_J})$. Then

$$D_1, D_2 \subseteq \overline{\Omega}, \quad \text{with} \quad D_1 = \operatorname{int} D_1 \not\subseteq \operatorname{out}_{\partial\Omega} D_2 = D_2, \quad C \subseteq D_2.$$

Furthermore, since B_{t_J} has diameter less than δ, it cannot intersect both $\operatorname{supp}(\sigma - 1)^+$ and $\operatorname{supp}(\sigma - 1)^-$ so that either

(a) $\sigma \geq 1$ on $\Omega \setminus D_2$, $\quad \sigma - 1 \in L^\infty_+(D_1)$, or

(b) $\sigma \leq 1$ on $\Omega \setminus D_2$, $\quad 1 - \sigma \in L^\infty_+(D_1)$,

which finishes the proof. □

Proof of Theorem 1.4.9.

If $1 - \alpha\chi_C \leq 2 - \frac{1}{\sigma}$, then $\alpha\chi_C \geq \frac{1}{\sigma}(1 - \sigma)$ so that (1.4) and Corollary 1.3.4 imply that

$$\Lambda(\sigma) \leq \Lambda(1) - \Lambda'(1)\left(\frac{1}{\sigma}(1 - \sigma)\right) \leq \Lambda(1) - \alpha\Lambda'(1)\chi_C.$$

Likewise, if $1 + \alpha\chi_C \geq \sigma$, then (1.4) and Corollary 1.3.4 imply that

$$\Lambda(\sigma) \geq \Lambda(1) - \Lambda'(1)(1 - \sigma) \geq \Lambda(1) + \alpha\Lambda'(1)\chi_C.$$

This shows the first two assertions.

Moreover, Lemma 1.3.1 yields that for all $\alpha \in \mathbb{R}$,

$$\langle(\Lambda(1) + \alpha\Lambda'(1)\chi_C - \Lambda(\sigma))g, g\rangle \geq \int_\Omega \left(\frac{1}{\sigma}(\sigma - 1) - \alpha\chi_C\right)|\nabla u^{(g)}|^2 \,\mathrm{d}x$$

and

$$\langle(\Lambda(1) - \alpha\Lambda'(1)\chi_C - \Lambda(\sigma))g, g\rangle \leq \int_\Omega (\sigma - 1 + \alpha\chi_C)|\nabla u^{(g)}|^2 \,\mathrm{d}x,$$

where $u^{(g)} \in H^1_\diamond(\Omega)$ solves $\Delta u^{(g)} = 0$ and $\partial_\nu u^{(g)}|_{\partial\Omega} = g$. Hence, the third assertion follows by using localized potentials for the homogeneous conductivity and the same sets D_1, D_2 as in Theorem 1.4.7. □

1.4.3 Remarks and extensions

Let us comment on some extensions and generalizations of our results. Our assumption that the background conductivity is equal to 1 and that we are given measurements on the complete boundary $\partial\Omega$ have been merely for the ease of presentation. All our results and proofs remain valid if $\partial\Omega$ is replaced by an arbitrarily small open piece $\Gamma \subset \partial\Omega$ and we are given the partial NtD operator

$$\Lambda_\Gamma(\sigma) : \ L^2_\diamond(\Gamma) \to L^2_\diamond(\Gamma), \quad g \mapsto u_\sigma^{(g)}|_\Gamma,$$

where $u_\sigma^{(g)} \in H^1_\diamond(\Omega)$ is the unique solution of

$$\nabla \cdot \sigma \nabla u_\sigma^{(g)} = 0 \text{ in } \Omega, \quad \sigma \partial_\nu u_\sigma^{(g)}|_{\partial\Omega} = \begin{cases} g & \text{on } \Gamma, \\ 0 & \text{on } \partial\Omega \setminus \Gamma. \end{cases}$$

In addition, all of our results still hold true when the background conductivity 1 is replaced by a known piecewise analytic function.

Let us also note that our results require piecewise analyticity for only two purposes: the existence of localized potentials and the local definiteness property. Localized potentials exist for less regular conductivities, it only requires that the solutions of the corresponding elliptic EIT equations satisfy a unique continuation property, cf. [Geb08]. Local definiteness can hold for quite general functions if additional assumption are made (e.g., that positive and negative part are separated as in (1.10)). However, we are not aware of any natural function classes beyond piecewise analytic functions in which a property in the spirit of Theorem 1.6.1 holds without further assumptions.

1.5 Excursion - Numerical results

Here (and in Chapter 3) the real and imaginary part of a function $f : \mathbb{R}^n \to \mathbb{C}$ are denoted by $\Re(f)$ and $\Im(f)$, respectively.

In this brief excursion we will present some numerical results (for the definite case) that are based on a simplified and discretized version of the linearized reconstruction method of Theorem 1.4.3. The implementation of monotonicity-based methods in realistically modeled electrode settings is considered in Chapter 2 and 3.

The numerical results in this section are generated with MATLAB® and the commercial FEM-software COMSOL®.

Below, we present some reconstructions where $\Omega \subseteq \mathbb{R}^3$ is given by the unit ball and $\sigma = 1 + \chi_D$ with an inclusion $D \subseteq \Omega$. For the numerical implementation of our method, we have to discretize the NtD operators. To this end, let

$$S := \{g_1, g_2, \ldots, g_N\}$$

be an orthogonal system in $L^2_\diamond(\partial\Omega)$ and let

$$\overline{A} := (\langle g_i, Ag_j\rangle)_{i,j=1}^N \in \mathbb{R}^{N\times N}$$

denotes the discretized operator corresponding to $A \in \mathcal{L}(L^2_\diamond(\partial\Omega))$.

For the reconstructions in this section, we choose an orthonormal system given by

$$S := \{Y_n^0, \sqrt{2}\,\Re(Y_n^m), \sqrt{2}\,\Im(Y_n^m) \,:\, n = 1, 2, \ldots, 7,\ m = 1, 2, \ldots, n\},$$

where

$$Y_n^m := \sqrt{\frac{2n+1}{4\pi}\cdot\frac{(n-|m|)!}{(n+|m|)!}}P_n^{|m|}(\cos(\theta))\exp(im\varphi)$$

are the spherical harmonics with azimuthal and polar angles

$$\varphi = \varphi(x, y, z) \quad \text{and} \quad \theta = \theta(x, y, z)$$

and the associated Legendre polynomials

$$P_n^m(x) := (1-x^2)^{\frac{m}{2}}\frac{\mathrm{d}^m}{\mathrm{d}x^m}P_n(x)$$

with

$$P_n(x) := \frac{1}{2^n n}\left(\frac{\mathrm{d}^n}{\mathrm{d}x^n}\left(x^2-1\right)^n\right).$$

Motivated by Theorem 1.4.3 and Example 1.4.4, we check for each element of a collection of cubic test inclusions $B_1, B_2, \ldots, B_M \subseteq \Omega$ filling-out Ω, whether all eigenvalues of

$$\overline{\Lambda(1)} - \overline{\Lambda(\sigma)} + \tfrac{1}{2}\overline{\Lambda'(1)\chi_{B_m}}, \quad m \in \{1, 2, \ldots, M\}$$

are lager than a regularization parameter $\alpha < 0$ (cf. Remark 1.3.5). Then the reconstruction is given by the union of all test inclusions that fulfill this test. To speed up the evaluation of the test criterion, the integrals required for the calculation of the Fréchet derivatives $\Lambda'(1)\chi_{B_m}$, $m = 1, 2, \ldots, M$, are evaluated with the midpoint rule. Furthermore, as in [GH07, Section 3], to increase the precision of the evaluation of the test criterion, we directly compute the difference

$$v|_{\partial\Omega} := (\Lambda(1) - \Lambda(\sigma))\, g_k$$

for $g_k \in S$ by solving

$$\nabla \cdot (\sigma \nabla v) = \nabla \cdot (\chi_D \nabla u_1^{(g_k)}), \quad \sigma \partial_\nu v|_{\partial\Omega} = 0$$

where

$$u_1^{(g_k)} = \frac{r^n}{n} g_k \quad \text{with} \quad r(x,y,z) = \|(x,y,z)\|$$

is the exact solution of (1.2), i.e.,

$$\Delta u_1^{(g_k)} = 0, \quad \partial_\nu u_1^{(g_k)}|_{\partial\Omega} = g_k.$$

In addition to reconstructions for noise-free data, as in [GH07, Section 3], we present reconstructions after adding 0.1% noise on the difference data, i.e.,

$$\overline{\Lambda(1)} - \overline{\Lambda(\sigma)}$$

is replaced by

$$\left(\overline{\Lambda(1)} - \overline{\Lambda(\sigma)}\right)_{\text{noisy}} = \overline{\Lambda(1)} - \overline{\Lambda(\sigma)} + 10^{-3} \|\overline{\Lambda(1)} - \overline{\Lambda(\sigma)}\| \frac{E}{\|E\|},$$

where $E \in \mathbb{R}^{N \times N}$ contains randomly distributed entries between -1 and 1.

In accordance with Remark 1.3.5, the regularization parameter α is set to 0 and $-10^{-3}\|\overline{\Lambda(1)} - \overline{\Lambda(\sigma)}\|$ for the reconstructions with and without noisy data, respectively. In addition, we present reconstructions with a heuristically chosen regularization parameter.

Remark 1.5.1. For the discretized monotonicity test, only the forward implication of the monotonicity relation remains valid, i.e., a test inclusion will fulfill the test criterion if it is completely covered by the inclusion. The converse of this implication is only valid for the non-discretized test, where the existence of localized potentials follows from Theorem 1.3.6. Nevertheless, Theorem 1.3.6 motivates that the larger the orthogonal system S, the better the discretized reconstruction. Moreover, as it can be seen in Figure 1.1 and 1.2, the larger a test inclusion, the better it can be correctly excluded from the reconstruction, cf. the result of Rubinacci, Tamburrino and Ventre [RTV06] where the authors propose to test overlapping test inclusions to increase the resolution of the reconstruction for a monotonicity-based method in the field of eddy current imaging.

Example 1.5.2. *The inclusion area is*

$$D = \{(x, y, z) \in \mathbb{R}^3 \,:\, (0.5 - \|(x, y, 0)\|)^2 + (z - 0.6)^2 \leq 0.1^2\}.$$

Some reconstructions are illustrated in Figure 1.1 and 1.3 (a). In Figure 1.1 the regularization parameter α is chosen in accordance with Remark 1.3.5. In Figure 1.3 (a) α is heuristically chosen.

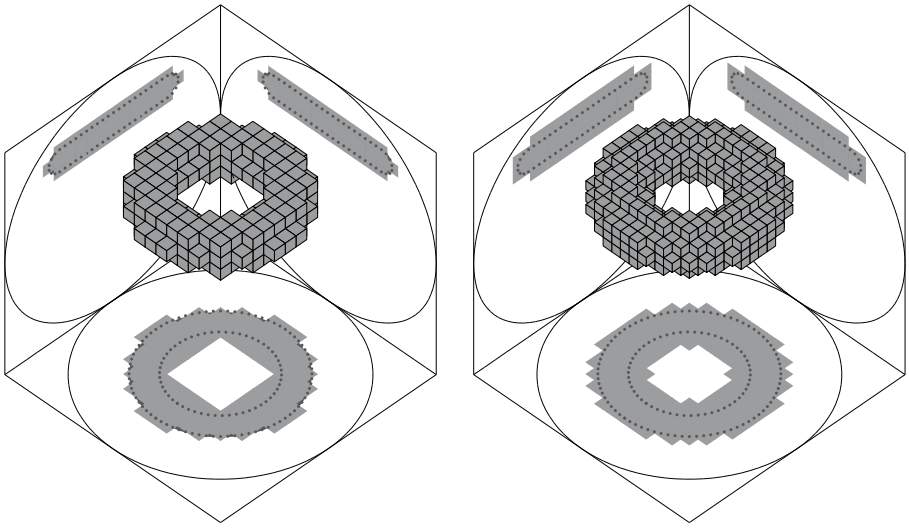

(a) Noise-free case with $h = 0.1$.

(b) Noise-free case with $h = 0.08$.

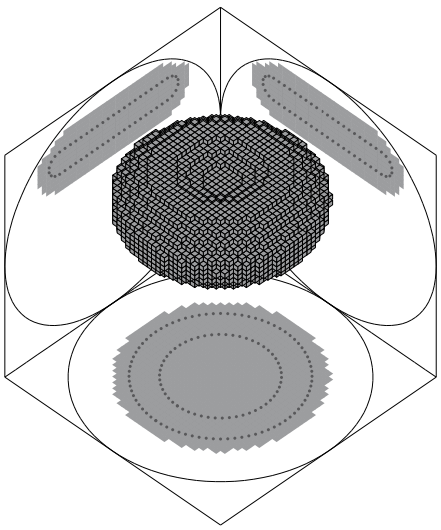

(c) Noise-free case with $h = 0.04$.

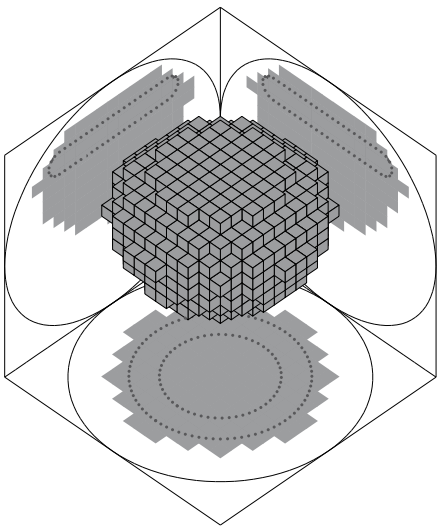

(d) Noisy data (0.1%) with $h = 0.1$.

Figure 1.1: Reconstructions (bright gray) of a torus-shaped inclusion (dark gray and dotted lines), where h denotes the edge size of the cubic test inclusions.

Example 1.5.3. *The inclusion area is* $D = D_1 \cup D_2$ *with*

$$D_1 = \{(x, y, z) \in \mathbb{R}^3 \,:\, (x - 0.4)^2 + (y + 0.4)^2 + (z + 0.5)^2) \leq 0.2^2\},$$
$$D_2 = \{(x, y, z) \in \mathbb{R}^3 \,:\, (x + 0.4)^2 + (y - 0.4)^2 + (z - 0.5)^2) \leq 0.15^2\}.$$

Some reconstructions are illustrated in Figure 1.2 and 1.3 (b). In Figure 1.2 the regularization parameter α *is chosen in accordance with Remark 1.3.5. In Figure 1.3 (b)* α *is heuristically chosen.*

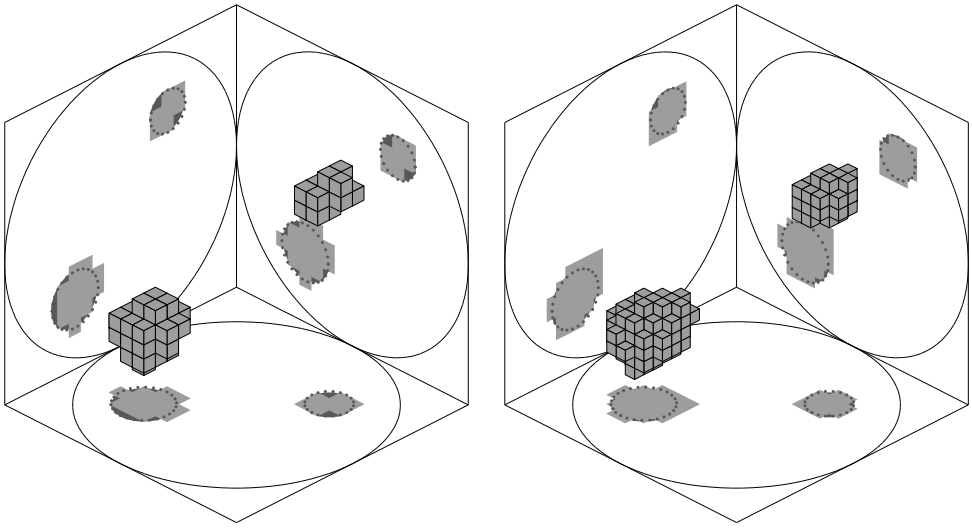

(a) Noise-free case with $h = 0.1$.

(b) Noise-free case with $h = 0.08$.

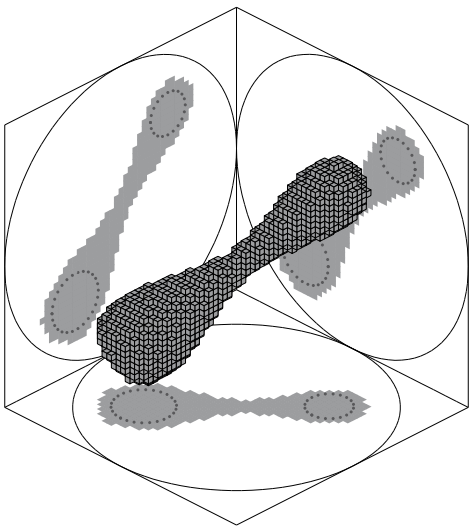

(c) Noise-free case with $h = 0.04$.

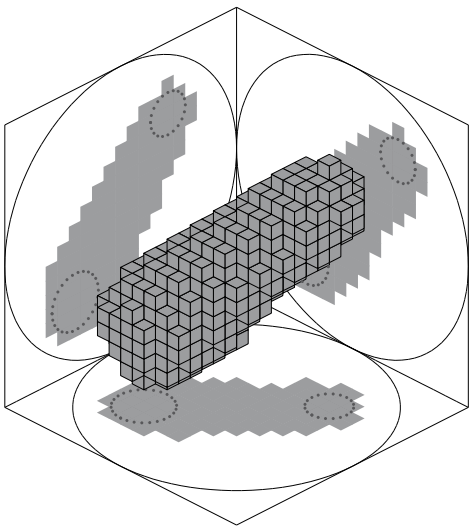

(d) Noisy data (0.1%) with $h = 0.1$.

Figure 1.2: Reconstructions (bright gray) of two ball-shaped inclusions (dark gray and dotted lines), where h denotes the edge size of the cubic test inclusions.

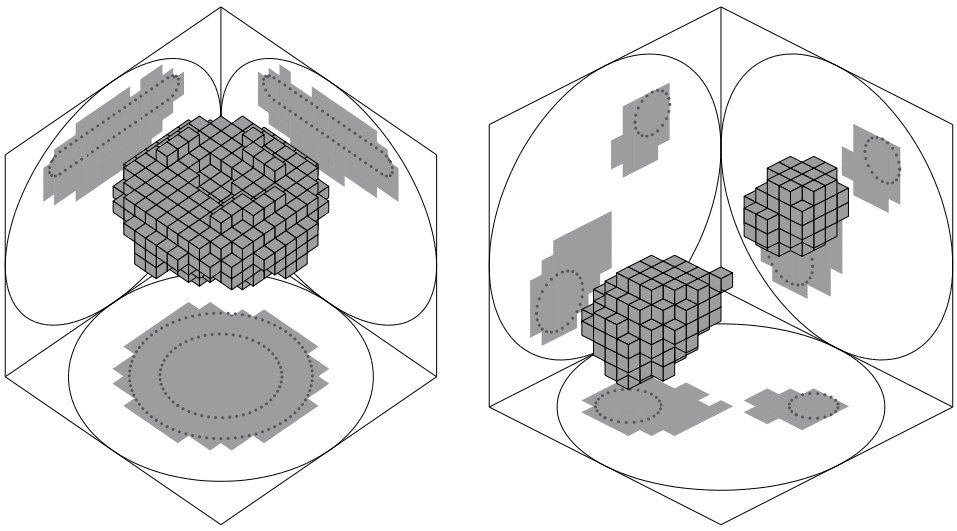

(a) Noisy data (0.1%) with $h = 0.1$ and $\alpha = -10^{-5}$.

(b) Noisy data (0.1%) with $h = 0.1$ and $\alpha = -10^{-5}$.

Figure 1.3: Reconstructions for noisy data with heuristically chosen parameter α.

1.6 Appendix - Local definiteness of piecewise analytic functions

In this appendix we show that piecewise analytic functions have a *local definiteness property*. If they do not vanish identically, then there is either a neighborhood of the boundary where they differ from zero in the positive direction or a neighborhood where they differ in the negative direction.

The property follows from the arguments used in the proofs of [Har09, Theorem 4.2] and [HS10, Lemma 3.7]. However, some subtle and not entirely trivial topological details were omitted in [Har09, HS10], which is why we give the proof here in full detail.

Theorem 1.6.1. *Let $\Omega \subset \mathbb{R}^n$, $n \geq 2$, be a smoothly bounded domain and let $\sigma \in L^\infty(\Omega)$ be piecewise analytic. Let $U \subseteq \overline{\Omega}$ be relatively open and connected to $\partial\Omega$ and let $\sigma|_U \not\equiv 0$.*

Then we can find a subset $V \subseteq U$ with the same properties on which σ has no change of sign, i.e.,

(a) $V \subseteq \overline{\Omega}$ is relatively open, V is connected to $\partial\Omega$, $V \subseteq U$,

(b) $\sigma|_V \not\equiv 0$ and either $\sigma|_V \geq 0$ or $\sigma|_V \leq 0$.

Obviously, if a piecewise analytic function is not identically zero, we can find a neighborhood where it is bounded away from zero. Hence, choosing $D_2 := \Omega \setminus V$,

we obtain the following corollary.

Corollary 1.6.2. *Under the assumptions of Theorem 1.6.1, we can choose*

$$D_1, D_2 \subseteq \overline{\Omega}, \quad \text{with} \quad D_1 = \operatorname{int} D_1 \not\subseteq \operatorname{out}_{\partial\Omega} D_2 = D_2, \quad \Omega \setminus D_2 \subseteq U,$$

and either

$$\begin{aligned} &\sigma|_{\Omega\setminus D_2} \geq 0, \quad \sigma|_{D_1} \in L^\infty_+(D_1), \quad \text{or} \\ &\sigma|_{\Omega\setminus D_2} \leq 0, \quad -\sigma|_{D_1} \in L^\infty_+(D_1). \end{aligned}$$

In the following let $\Omega \subset \mathbb{R}^n$, $n \geq 2$, be a smoothly bounded domain and $\sigma \in L^\infty(\Omega)$ be piecewise analytic with respect to

$$\overline{\Omega} = \overline{O_1 \cup \ldots \cup O_M}, \quad \partial O_m = \bigcup_{k\in\mathbb{N}} \overline{\Gamma^k_m},$$

where, w.l.o.g., we assume that every ∂O_m consists of infinitely many pieces. Furthermore, let $U \subseteq \overline{\Omega}$ be relatively open and connected to $\partial\Omega$.

Lemma 1.6.3. *There exists an open ball $B \subseteq \mathbb{R}^n$ such that*

$$B \cap \overline{\Omega} \subseteq U \quad \text{and} \quad B \cap \overline{\Omega} \text{ is connected to } \partial\Omega,$$

and for one of the O_m and one of its smooth boundary pieces $\Gamma^k_m \subseteq \partial O_m$,

$$B \cap \Omega = B \cap O_m \quad \text{and} \quad B \cap \partial\Omega \subseteq \Gamma^k_m.$$

Proof. Since U is relatively open and $U \cap \partial\Omega \neq \emptyset$, there exists an open ball B' with $\emptyset \neq B' \cap \partial\Omega$ and $B' \cap \overline{\Omega} \subseteq U$. Furthermore, we can assume that B' is sufficiently small such that

$$\emptyset \neq S := \overline{B' \cap \partial\Omega} \subseteq \overline{B'} \cap \partial\Omega \subseteq U.$$

$\overline{\Omega} = \overline{O_1 \cup \ldots \cup O_M}$ implies that

$$\partial\Omega \subseteq \bigcup_{m=1}^{M} \partial O_m = \bigcup_{m=1}^{M} \bigcup_{k\in\mathbb{N}} \overline{\Gamma^k_m} \quad \text{and thus} \quad S = \bigcup_{m,k} \left(\overline{\Gamma^k_m} \cap S \right).$$

By Baire's theorem, one of the countably many closed sets $\overline{\Gamma^k_m} \cap S$ must have nonempty interior in S. Hence, for one of the $\overline{\Gamma^k_m}$, there exists an open subball $B'' \subseteq B'$ with

$$\emptyset \neq B'' \cap \partial\Omega \subseteq \overline{\Gamma^k_m} \cap U.$$

Moreover, $B'' \cap \partial\Omega$ must intersect Γ^k_m because of the following dimension theoretical argument, cf., e.g., the classical book of Hurewicz and Wallman [HW48, Ch. IV, §4].

$\Omega \cap B''$ is an open (neither empty nor dense) subset of the n-dimensional ball B''. As a subset of B'', the boundary of $\Omega \cap B''$ is $\partial\Omega \cap B''$, which shows that $\partial\Omega \cap B''$ is $(n-1)$-dimensional (and not of lower dimension). Γ_m^k is a (neither empty nor dense) open subset of a set that is homeomorphic to $\mathbb{R}^{n-1}$. Hence, Γ_m^k is $(n-1)$-dimensional and $\overline{\Gamma_m^k} \setminus \Gamma_m^k$ is $(n-2)$-dimensional. This shows that $B'' \cap \partial\Omega \not\subseteq \overline{\Gamma_m^k} \setminus \Gamma_m^k$ so that there exists an open subball $B''' \subseteq B''$ with

$$\emptyset \neq B''' \cap \partial\Omega = B''' \cap \Gamma_m^k.$$

Finally, we can shrink B''' such that we obtain an open subball B so that $B \cap \Omega = B \cap O_m$ and $B \cap \Omega$ is connected. □

Lemma 1.6.4. *Every open ball $B \subseteq \mathbb{R}^n$ that intersects a smooth boundary piece Γ_m^k contains an open subball $B' \subseteq B$ intersecting Γ_m^k where either*

$$\sigma|_{B' \cap O_m} \geq 0 \quad \text{or} \quad \sigma|_{B' \cap O_m} \leq 0.$$

Proof. We use an argument of Kohn and Vogelius [KV84]. If $\sigma|_{B \cap O_m} \equiv 0$, then the assumption is trivial. Otherwise, by analyticity, there must be a smallest $k \in \mathbb{N}$ so that the normal derivative $\partial_{\nu(z)}^k \sigma(z)$ is not identically zero for all $z \in \Gamma_m^k \cap B$. Hence, there is a neighborhood of a point $z \in \Gamma_m^k \cap B$ on which either $\sigma \geq 1$ or $\sigma \leq 1$. □

Now we are ready to prove the local definiteness property.

Proof of Theorem 1.6.1. From Lemma 1.6.3, we obtain an open ball $B \subseteq \mathbb{R}^n$ with

$$B \cap \overline{\Omega} \subseteq U, \quad B \cap \overline{\Omega} \text{ is connected to } \partial\Omega,$$

and (w.l.o.g.)

$$B \cap \Omega = B \cap O_1, \quad B \cap \partial\Omega \subseteq \Gamma_1^1.$$

If σ is not identically zero on O_1, then the assertion follows from Lemma 1.6.4.

Otherwise, $M > 1$ and the set $V := B \cap \overline{\Omega}$ has the following properties.

(i) V is a relatively open subset of $\overline{\Omega}$ that is connected to $\partial\Omega$,

(ii) V fulfills $B \cap \overline{\Omega} \subseteq V \subseteq U$,

(iii) $\sigma|_V \equiv 0$.

Obviously, these properties are closed under union so that we can choose V to be the maximal set fulfilling (i)–(iii).

Now we show that

$$\emptyset \neq \partial V \cap U \cap \Omega \subseteq \bigcup_{m=1}^{M} \partial O_m. \tag{1.11}$$

Since V is relatively open in Ω and $V \subseteq U$, it follows that $V \cap \Omega$ is relatively open in $U \cap \Omega$. If ∂V has no intersection with $U \cap \Omega$, then $V \cap \Omega$ is relatively closed in

$U \cap \Omega$ so that $U \cap \Omega = V \cap \Omega$, which contradicts $\sigma|_U \not\equiv 0$. Hence, we obtain that $\partial V \cap U \cap \Omega \neq \emptyset$. To show the second assertion in (1.11), assume that there exists an element $z \in \partial V \cap \Omega \cap U$ with $z \in O_m$ for one O_m. Then we can choose an open ball $B \subseteq O_m \cap U$ containing z. Since σ is analytic on B and $B \cap V$ has non-empty interior, it follows that $\sigma|_B \equiv 0$ and hence $V \cup B$ has the properties (i)–(iii). This contradicts the maximality of V so that also the second assertion in (1.11) must hold.

Because of (1.11) we can choose an open ball B' with $\overline{B'} \subseteq U \cap \Omega$ and

$$\emptyset \neq S := \overline{B' \cap \partial V} \subseteq \overline{B'} \cap \partial V \quad \text{with} \quad S = \bigcup_{m,k} \overline{\Gamma_m^k} \cap S. \tag{1.12}$$

Using the same arguments as in the proof of Lemma 1.6.3 it follows that there exists an open subball $B''' \subseteq B'$ such that

$$\emptyset \neq B''' \cap \partial V = B''' \cap \Gamma_m^k$$

with a smooth boundary piece Γ_m^k of one O_m.

Since $\partial O_m \subseteq \bigcup_{m' \neq m} \partial O_{m'} \cup \partial\Omega$, equation (1.12) still holds if we restrict the union to all $m' \in \{1, \ldots, M\} \setminus \{m\}$. By repeating the above argument (starting with B''' instead of B'), we obtain an open subball $B'''' \subseteq B'''$ with (upon possibly shrinking B'''' again)

$$\emptyset \neq \overline{B''''} \cap \partial V = \overline{B''''} \cap \left(\Gamma_m^k \cap \Gamma_{m'}^{k'} \right) \quad \text{and} \quad m' \neq m.$$

From the definition of smooth boundary pieces, it follows that (if we choose B'''' small enough)

$$B'''' \subseteq \overline{(B'''' \cap O_m) \cup B'''' \cap O_{m'}},$$

so that either $B'''' \cap O_m$ or $B'''' \cap O_{m'}$, but not both, intersects V. W.l.o.g., let $B'''' \cap O_m$ intersect V. Then $\sigma|_{O_m} \equiv 0$ and using Lemma 1.6.4 we can shrink B'''' so that $\sigma|_{B'''' \cap O_{m'}}$ is either non-negative or non-positive. Hence, $B'''' \cup V$ fulfills the above properties (i) and (ii) and it is a proper superset of U. Hence, σ cannot identically vanish on $B'''' \cup V$, which shows that $B'''' \cup V$ fulfills the assertion of Theorem 1.6.1. □

Chapter 2

Resolution guarantees in EIT

The Sections 2.1 - 2.6 are the Sections 1-6 of the paper [HU15a] up to minor changes. Furthermore, Section 2.1 is shortened and some parts are slightly reformulated to provide more mathematical details. © IEEE. Re-use with permission from B. Harrach and M. Ullrich, Resolution guarantees in EIT, 2015.

2.1 Introduction

We will focus on the anomaly (aka inclusion) detection problem of EIT for a realistically modeled electrode setting in this chapter. A major challenge is that the reconstruction process in EIT suffers from the fundamental ill-posedness of the underlying mathematical inverse problem which leads to an enormous sensitivity to modeling and measurement errors. Due to these inherent instability issues, high resolution EIT imaging remains an extremely challenging topic. However, several applications would already greatly benefit from low resolution EIT images, e.g. in the field of the detection of tumors or hemorrhages in surrounding homogeneous tissue that has a certain conductivity contrast. For these applications, fast and low-cost monitoring techniques have to be developed in order to decide which patients should undergo more extensive diagnosis. For this task, the main concern seems to be the reliability of EIT images.

In this chapter we show that it is principally possible to give rigorous resolution guarantees in EIT even in the presence of systematic and random measurement errors. We consider a measurement setting as in Figure 2.1 where voltage-current measurements are taken on a number of electrodes attached to the boundary of an imaging domain Ω. The aim is to detect whether the domain contains one or several anomalies where the conductivity differs from some normal background range.

We describe a desired *resolution* by a partition of Ω into disjoint subsets $\omega_1, \omega_2, \ldots \subseteq \Omega$. We say that a *resolution guarantee* holds if the measured data contains enough information to

(a) correctly mark every element ω_s that is completely covered by an anomaly,

(b) correctly mark no element if there is no anomaly at all.

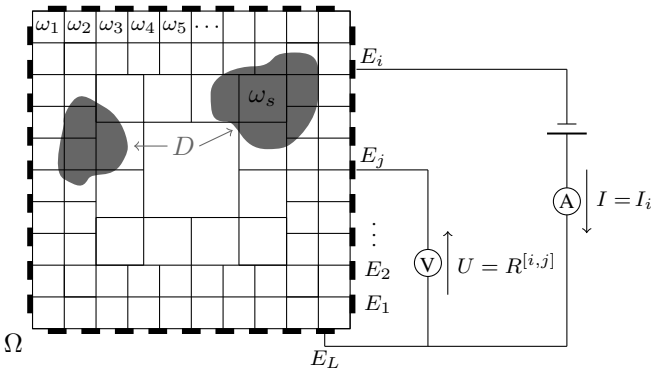

Figure 2.1: Measurement setting with inclusions D occupying a subset of a subject Ω, which is decomposed into a partition of subsets $\omega_1, \omega_2, \ldots \subseteq \Omega$. Driving a current through the i-th and the L-th electrode, we measure the corresponding voltage $R^{[i,j]}$ (in mV per applied mA) between the j-th and the L-th electrode. Repeating this for all i and j, we obtain the measurement matrix $R = (R^{[i,j]})_{i,j=1,\ldots,L-1} \in \mathbb{R}^{(L-1)\times(L-1)}$. © 2015 IEEE

In other words, a resolution guarantee ensures that no false positives are detected in the anomaly-free case, and no false negatives are detected in the case of inclusions over a certain size. Let us stress that in this chapter we aim to characterize the resolution up to which an anomaly can be detected. Assumptions (a) and (b) do not guarantee that the shape of a detected anomaly can be correctly determined up to a certain resolution. In that sense, the subject of this chapter might be called a (resolution-based) detection guarantee.

Whether a certain desired resolution can be guaranteed will depend on a number of facts, including the number and position of electrodes, the measurement pattern, the inclusion contrast, the modeling and measurement errors. The aim of this chapter is to derive a validation criterion to evaluate whether a desired resolution can be guaranteed. We also describe a simple reconstruction algorithm that implements (a) and (b) above.

Let us comment on the vast literature on identifiability in EIT. In the last decades, great theoretical progress has been made on the question whether two arbitrary conductivities can be distinguished by idealized noise-free and continuous measurements (the *Calderón-Problem* [Cal80, Cal06]). We refer to the seminal works [KV84, KV85, Nac96, AP06], the overview [Uhl08] and the recent breakthroughs for partial boundary data [IUY11, KS14]. The distinguishability of conductivities from finite precision data has been studied in the works of Bates, Gençer, Gisser, Ider, Isaacson, Kuzuoglu, Lionheart, Newell, Seagar, Paulson, Pidcock and Yeo [SYB84, SB85, Isa86, GIN87, GIN90, PLP93, GKI94]. Also, let us refer to a recent result of Winkler and Rieder [WR14] on optimal resolution meshes and to the works of Kolehmainen, Lassas, Nissinen, Ola and Kaipio [KLO08, NKK11] regarding uncertainties in the shape of the subject and the contact impedances of the electrodes.

See also the work of Tamburrino, Ventre and Rubinacci [TVR10] where the concept of *visible voxels* is introduced.

Several reconstruction methods have been proposed for anomaly (or inclusion) detection problems, cf., e.g., Potthast [Pot06] for an overview. Arguably, the most prominent inclusion detection method is the Factorization Method (FM) of Kirsch, Brühl and Hanke [Kir98, BH00, Brü01], see also the listing in Section 1.1 for further developments of the FM in the field of EIT. Notably, in the overview [Har13], the FM is formulated on the basis of monotonicity-based arguments and the recent result [HU] (presented in Chapter 1) indicates that, for EIT, the FM can be outperformed by monotonicity-based methods first formulated by Tamburrino and Rubinacci in [TR02, Tam06].

The main new idea presented in this chapter is to obtain rigorous resolution guarantees by treating worst-case scenarios with monotonicity-based ideas. To our knowledge, the results derived herein are the firsts to rigorously quantify the achievable resolution in the case of realistic electrode measurements in a setting with imprecisely known background conductivity, contact impedances and measurement noise. We believe that this will be useful for designing reliable EIT systems. Our results may be used to determine whether a desired resolution can be achieved and to quantify the required measurement accuracy. Moreover, our results could be the basis of optimization strategies regarding the resolution, the driving patterns or the number and the positions of the electrodes.

The chapter is organized as follows. The measurement setting including systematic and random errors is introduced in Section 2.2. Section 2.3 presents a monotonicity relation and motivates how this relation can be used to design inclusion detection methods. In Section 2.4 we introduce the concept of a rigorous resolution guarantee and show how to verify such guarantees by a simple test. We also derive fast linearized versions of our tests that allow faster verifications at the price of (possibly) underestimating the achievable resolution. Section 2.5 presents some numerical results for the verification of the resolution guarantees described in Section 2.4. Section 2.6 contains some concluding remarks.

2.2 The setting

The current-voltage measurements can be modeled by the *complete electrode model* (CEM) as follows (cf. [SCI92]). Let $\Omega \subseteq \mathbb{R}^n$ be a bounded domain with piecewise smooth boundary representing the conductive subject and let $\sigma \in L^\infty_+(\Omega)$ be the real valued conductivity distribution inside Ω, where $L^\infty_+(\Omega)$ denotes the subset of $L^\infty(\Omega)$-functions with positive essential infima.

Electrodes are attached to the boundary of the subject as shown in Figure 2.1. Their locations are well-separated domains $E_1, E_2, \ldots, E_L$ in $\partial\Omega$ and their contact

impedances are denoted by a vector with positive entries

$$z := \left(z^{[1]}, \ldots, z^{[L]}\right) \in \mathbb{R}_+^L.$$

The electrodes are assumed to be perfectly conducting.

For each $i \in \{1, 2, \ldots, L-1\}$, we drive a current I_i with strength 1 mA through the i-th electrode while keeping the L-th electrode grounded and all other electrodes insulated (so that the current flows through the grounded L-th electrode).

Then the potentials $u_i \in H^1(\Omega)$ and $U_i = \left(U_i^{[1]}, \ldots, U_i^{[L]}\right) \in \mathbb{R}^L$ inside Ω and the electrodes, respectively, can mathematically be modeled by the unique solution $(u_i, U_i) \in H$ of the corresponding variational formulation of the CEM

$$V^{[i]} = \int_\Omega \sigma \nabla u_i \cdot \nabla v \mathrm{d}x + \sum_{l=1}^{L} \frac{1}{z^{[l]}} \int_{E_l} \left(u_i - U_i^{[l]}\right)\left(v - V^{[l]}\right) \mathrm{d}s \quad \forall (v, V) \in H, \quad (2.1)$$

where

$$H := \{(v, V) \in H^1(\Omega) \times \mathbb{R}^L \,:\, V^{[L]} = 0\}. \quad (2.2)$$

For the existence of a unique solution of this variational formulation, cf., e.g., [SCI92, Hyv04]. Typically, one describes the CEM by the equations (2.3)-(2.6) below, which are more suitable to show the physical interpretation but have to be understood in an appropriate weak sense, cf., e.g., [SCI92, Hyv04]. In this formulation, the inner potentials u_i and the electrode potentials U_i fulfill

$$\nabla \cdot \sigma \nabla u_i = 0 \quad \text{in } \Omega, \quad (2.3)$$

with boundary conditions

$$\int_{E_l} \sigma \left(\nabla u_i\right) \cdot \nu \, \mathrm{d}S = \delta_{l,i} - \delta_{l,L}, \quad (2.4)$$

$$u_i|_{E_l} + z^{[l]} \sigma \left(\nabla u_i\right) \cdot \nu|_{E_l} = \text{const.} =: U_i^{[l]} \quad (2.5)$$

for $l \in \{1, 2, \ldots, L\}$,

$$\sigma \left(\nabla u_i\right) \cdot \nu = 0 \quad \text{on} \quad \partial\Omega \setminus \bigcup_{l=1}^{L} E_l, \quad (2.6)$$

and $U_i^{[L]} = 0$, where ν is the outer normal on the boundary of Ω. For a proof of the equivalence of the variational and equation-based formulation, see, e.g., [SCI92], where the conductivity is assumed to be sufficiently smooth. All results presented in this chapter are derived from the variational formulation of the CEM.

To collect measurement data, for each injected current, we measure the voltages on E_1,...,E_{L-1} against the grounded L-th electrode and thus collect a matrix of measurements

$$R(\sigma, z) := \left(R^{[i,j]}(\sigma, z)\right)_{i,j=1}^{L-1} := \left(U_i^{[j]}\right)_{i,j=1}^{L-1} \in \mathbb{R}^{(L-1)\times(L-1)}. \quad (2.7)$$

The matrix $R(\sigma, z)$ is easily shown to be symmetric.

For such measurements modeled with the CEM, we consider the anomaly detection problem (cf. Chapter 1), i.e., we try to detect regions (the so-called inclusions) in Ω where the conductivity differs from a normal background range.[1] To allow for modeling and measurement errors in this context, we make the following setting assumptions:

(a) **Conductivity distribution $\sigma(x)$:** The true conductivity distribution is given by an inclusion conductivity $\sigma_D(x) \in L^\infty_+(D)$ inside an inclusion $D \subseteq \Omega$ and by a background conductivity $\sigma_B(x) \in L^\infty_+(\Omega \setminus D)$ inside $\Omega \setminus D$, i.e.

$$\sigma(x) = \begin{cases} \sigma_D(x), & x \in D, \\ \sigma_B(x), & x \in \Omega \setminus D. \end{cases}$$

(b) **Background error $\epsilon \geq 0$:** The background conductivity approximately agrees with a known positive constant $\sigma_0 > 0$,

$$|\sigma_B(x) - \sigma_0| \leq \epsilon \quad \text{for all } x \in \Omega \setminus D.$$

(c) **Inclusion conductivity contrast $c > 0$:** We assume that we know a lower bound on the inclusion contrast, i.e., that we know $c > 0$ with either

(i) $\sigma_D(x) - \sigma_0 \geq c$ for all $x \in D$, or

(ii) $\sigma_0 - \sigma_D(x) \geq c$ for all $x \in D$.

(d) **Contact impedances error $\gamma \geq 0$:** We assume that we approximately know the vector of contact impedances $z \in \mathbb{R}^L_+$, i.e., that we know $z_0 \in \mathbb{R}^L_+$ with

$$\left| z^{[l]} - z_0^{[l]} \right| \leq \gamma \quad \text{for all } l \in \{1, 2, \ldots, L\}.$$

(e) **Measurement noise $\delta \geq 0$:** We assume that we can measure the voltages $R(\sigma, z)$ up to a noise level $\delta > 0$, i.e., that we are given $R_\delta \in \mathbb{R}^{(L-1)\times(L-1)}$ with

$$\|R(\sigma, z) - R_\delta\| \leq \delta.$$

Possibly replacing R_δ by its symmetric part, we can assume that R_δ is symmetric.

[1] We implicitly assume that all sets that we consider in this chapter (e.g., inclusions or test inclusions) are at least measurable sets.

2.3 Monotonicity

Our results are based on the following monotonicity relations that extend results of Gisser, Ikehata, Isaacson, Kang, Newell, Rubinacci, Seo, Sheen, and Tamburrino [GIN90, Ike98, KSS97, TR02]. Cf. also the monotonicity relations presented in Chapter 1 for measurements modeled with the *continuum model* (CM).

Theorem 2.3.1. *For $i \in \{1,2\}$, let $\sigma_i \in L^\infty_+(\Omega)$ be a conductivity distribution and $z_i \in \mathbb{R}^L_+$ be a contact impedances vector. Then*

$$\sigma_1 \leq \sigma_2, z_1 \geq z_2 \quad \text{implies} \quad R(\sigma_1, z_1) \geq R(\sigma_2, z_2). \tag{2.8}$$

The inequalities on the left-hand side of the implication are meant pointwise. The inequality on the right-hand side has to be understood in the sense of matrix definiteness.

Proof. This follows from the more general Theorem 2.3.2 below. □

Theorem 2.3.1 yields monotonicity-based inclusion detection methods, cf. [TR02]. To present the main idea, consider the simple example where $\sigma = 1 + \chi_D$, where χ_D is the characteristic function on D, and the vector of the contact impedances $z \in \mathbb{R}^L_+$ is known exactly.

For a small ball $B \subseteq \Omega$, we define a test conductivity $\tau_B = 1 + \chi_B$. From the monotonicity relation of Theorem 2.3.1 we have that

$$B \subseteq D \quad \text{implies} \quad R(\tau_B, z) \geq R(\sigma, z).$$

Hence, the union of all test balls B fulfilling $R(\tau_B, z) \geq R(\sigma, z)$ is an upper bound of the inclusion D.

In Chapter 1 (see [HU] for the published version) we showed that for continuous boundary data monotonicity methods are actually capable of reconstructing the exact shape D under rather general assumptions. Moreover, in Chapter 1 it is shown how to replace the monotonicity tests by fast linearized versions without losing shape information, see also [HS10].

We cannot expect exact shape reconstructions in settings with a finite number of electrodes and imprecisely known contact impedances and background conductivities. However, monotonicity-based arguments will allow us to characterize the achievable resolution in such settings. For this, we formulate a quantitative version of Theorem 2.3.1:

Theorem 2.3.2. *For $i \in \{1,2\}$, let $\sigma_i \in L^\infty_+(\Omega)$ be a conductivity distribution and $z_i \in \mathbb{R}^L_+$ be a contact impedances vector. Given $w \in \mathbb{R}^{L-1}$, let $(v_i, V_i) \in H$ be the corresponding potentials resulting from driving a current of w_i through the i-th electrode, respectively. (Note that this implies a current flux of $-\sum_{l=1}^L w_l$ through*

the grounded L-th electrode.) Then

$$\begin{aligned}
&\int_\Omega (\sigma_1 - \sigma_2) \left|\nabla v_2\right|^2 \mathrm{d}x \\
&+ \sum_{l=1}^{L} \left(\frac{1}{z_1^{[l]}} - \frac{1}{z_2^{[l]}} \right) \int_{E_l} \left(v_2 - V_2^{[l]} \right)^2 \mathrm{d}s \\
&\geq w^T \left(R\left(\sigma_2, z_2\right) - R\left(\sigma_1, z_1\right) \right) w \\
&\geq \int_\Omega \frac{\sigma_2}{\sigma_1} (\sigma_1 - \sigma_2) \left|\nabla v_2\right|^2 \mathrm{d}x \\
&\quad + \sum_{l=1}^{L} \frac{z_1^{[l]}}{z_2^{[l]}} \left(\frac{1}{z_1^{[l]}} - \frac{1}{z_2^{[l]}} \right) \int_{E_l} \left(v_2 - V_2^{[l]} \right)^2 \mathrm{d}s.
\end{aligned}$$

Proof. From the variational formulation of the CEM (2.1), we obtain for $i, j \in \{1, 2\}$,

$$\begin{aligned}
w^T V_j \;&=\; \int_\Omega \sigma_i \nabla v_i \cdot \nabla v_j \mathrm{d}x \\
&\quad + \sum_{l=1}^{L} \frac{1}{z_i^{[l]}} \int_{E_l} \left(v_i - V_i^{[l]} \right) \left(v_j - V_j^{[l]} \right) \mathrm{d}s \\
&=: B_i((v_i, V_i), (v_j, V_j))
\end{aligned}$$

and, by linearity, we have that

$$V_j = R(\sigma_j, z_j) w, \quad j \in \{1, 2\}.$$

Hence, it holds that

$$\begin{aligned}
&w^T \left(R\left(\sigma_2, z_2\right) - R\left(\sigma_1, z_1\right) \right) w \\
&= w^T \left(V_2 - V_1 \right) \\
&= 2B_1\left(\left(v_1, V_1\right), \left(v_2, V_2\right) \right) - B_2\left(\left(v_2, V_2\right), \left(v_2, V_2\right) \right) \\
&\quad - B_1\left(\left(v_1, V_1\right), \left(v_1, V_1\right) \right) \\
&= - \int_\Omega \sigma_1 \left|\nabla \left(v_1 - v_2\right)\right|^2 \mathrm{d}x \\
&\quad - \sum_{l=1}^{L} \frac{1}{z_1^{[l]}} \int_{E_l} \left(\left(v_1 - V_1^{[l]} \right) - \left(v_2 - V_2^{[l]} \right) \right)^2 \mathrm{d}s \\
&\quad + \int_\Omega (\sigma_1 - \sigma_2) \left|\nabla v_2\right|^2 \mathrm{d}x \\
&\quad + \sum_{l=1}^{L} \left(\frac{1}{z_1^{[l]}} - \frac{1}{z_2^{[l]}} \right) \int_{E_l} \left(v_2 - V_2^{[l]} \right)^2 \mathrm{d}s.
\end{aligned}$$

Since the first two summands are non-negative, the first inequality of the theorem follows.

Interchanging the pairs (σ_1, z_1) and (σ_2, z_2) and applying

$$\begin{aligned}
&\sigma_2 \left|\nabla\left(v_2 - v_1\right)\right|^2 + \left(\sigma_1 - \sigma_2\right)\left|\nabla v_1\right|^2 \\
&= \sigma_1 \left|\nabla v_1 - \frac{\sigma_2}{\sigma_1}\nabla v_2\right|^2 + \frac{\sigma_2}{\sigma_1}\left(\sigma_1 - \sigma_2\right)\left|\nabla v_2\right|^2
\end{aligned}$$

as well as

$$\begin{aligned}
&\frac{1}{z_2^{[l]}}\left(\left(v_2 - V_2^{[l]}\right) - \left(v_1 - V_1^{[l]}\right)\right)^2 \\
&+ \left(\frac{1}{z_1^{[l]}} - \frac{1}{z_2^{[l]}}\right)\left(v_1 - V_1^{[l]}\right)^2 \\
&= \frac{1}{z_1^{[l]}}\left(\left(v_1 - V_1^{[l]}\right) - \frac{z_1^{[l]}}{z_2^{[l]}}\left(v_2 - V_2^{[l]}\right)\right)^2 \\
&\quad + \frac{z_1^{[l]}}{z_2^{[l]}}\left(\frac{1}{z_1^{[l]}} - \frac{1}{z_2^{[l]}}\right)\left(v_2 - V_2^{[l]}\right)^2,
\end{aligned}$$

yields

$$\begin{aligned}
&w^T\left(R\left(\sigma_2, z_2\right) - R\left(\sigma_1, z_1\right)\right)w \\
&= \int_\Omega \sigma_1 \left|\nabla v_1 - \frac{\sigma_2}{\sigma_1}\nabla v_2\right|^2 \mathrm{d}x + \int_\Omega \frac{\sigma_2}{\sigma_1}\left(\sigma_1 - \sigma_2\right)\left|\nabla v_2\right|^2 \mathrm{d}x \\
&\quad + \sum_{l=1}^{L} \int_{E_l} \frac{1}{z_1^{[l]}}\left(\left(v_1 - V_1^{[l]}\right) - \frac{z_1^{[l]}}{z_2^{[l]}}\left(v_2 - V_2^{[l]}\right)\right)^2 \mathrm{d}s \\
&\quad + \sum_{l=1}^{L} \int_{E_l} \frac{z_1^{[l]}}{z_2^{[l]}}\left(\frac{1}{z_1^{[l]}} - \frac{1}{z_2^{[l]}}\right)\left(v_2 - V_2^{[l]}\right)^2 \mathrm{d}s.
\end{aligned}$$

Since the last two summands are non-negative, the second inequality of the theorem is proven. □

2.4 Resolution guarantees

In this section we introduce the concept of rigorous resolution guarantees and show how to verify such guarantees by a simple test. We consider the setting described in Section 2.2, see also Figure 2.2. Let Id denotes the unit matrix in $\mathbb{R}^{(L-1)\times(L-1)}$.

Definition 2.4.1. An inclusion detection method that yields a reconstruction D_R to the true inclusion D is said to fulfill a **resolution guarantee** with respect to a partition $(\omega_s)_{s=1}^N \subseteq \Omega$ if

(i) $\omega_s \subseteq D$ implies $\omega_s \subseteq D_R$ for $s \in \{1, 2, \ldots, N\}$ (i.e., every element that is covered by the inclusion will correctly be marked in the reconstruction), and

(ii) $D = \emptyset$ implies $D_R = \emptyset$ (i.e., if there is no inclusion then no element will be marked in the reconstruction).

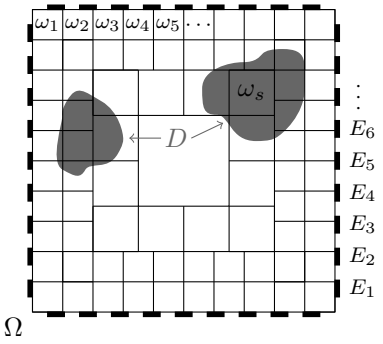

Figure 2.2: Setting with a sample inclusion and resolution. © 2015 IEEE

Hence, if a resolution guarantee holds true, then no false positives are detected in the anomaly-free case, and no false negatives are detected in the case of inclusions over a certain size.

Obviously, a resolution guarantee will not hold true for arbitrarily fine partitions. The achievable resolution will depend on the number of electrodes, the contrast of the inclusions, the background error, the contact impedances error, and the measurement noise, cf. Section 2.2 (a)-(e).

We will derive a simple test to verify whether a resolution guarantee holds true for a given partition. To this end, we first consider the case of inclusions that are more conductive than the background. The analogous results for less conductive inclusions are summarized in Section 2.4.3. We use the following notations:

$$\begin{aligned} \sigma_{B\min} &:= \sigma_0 - \epsilon, \\ \sigma_{B\max} &:= \sigma_0 + \epsilon, \\ \sigma_{D\min} &:= \sigma_0 + c, \\ z_{\min} &:= z_0 - \gamma(1, 1, \ldots, 1), \\ z_{\max} &:= z_0 + \gamma(1, 1, \ldots, 1). \end{aligned}$$

2.4.1 Verification of resolution guarantees

To verify whether a resolution guarantee holds true in a given setting, we will apply the following monotonicity-based inclusion detection method. In the following we denote the set of eigenvalues of a symmetric square matrix A by $\mathrm{eig}(A)$ and we write

$A_1 \geq A_2$ (or $A_2 \leq A_1$) if the difference $A_1 - A_2$ of two symmetric square matrices is positive semidefinite, i.e., if $A_1 - A_2$ possesses only non-negative eigenvalues.

Algorithm 2.4.2. *Mark each resolution element ω_s for which*

$$R(\tau_s, z_{max}) + \delta \mathrm{Id} \geq R_\delta, \tag{2.9}$$

where

$$\tau_s := \sigma_{B\min} \chi_{\Omega \setminus \omega_s} + \sigma_{D\min} \chi_{\omega_s}, \quad s \in \{1, 2, \ldots, N\}. \tag{2.10}$$

Then the reconstruction D_R is given by the union of the marked resolution elements.

Theorem 2.4.3. *The reconstruction of Algorithm 2.4.2 fulfills the resolution guarantee if*

$$\mu < -2\delta \leq 0 \tag{2.11}$$

with

$$\mu := \max_{s=1}^{N} \left(\min \left(\mathrm{eig} \left(R(\tau_s, z_{\max}) - R(\sigma_{B\max}, z_{\min}) \right) \right) \right). \tag{2.12}$$

Proof. First let $\omega_s \subseteq D$. Then $\tau_s \leq \sigma$ and $z_{\max} \geq z$. Theorem 2.3.1 implies that

$$R(\sigma, z) \leq R(\tau_s, z_{\max}).$$

Hence, $R(\tau_s, z_{\max}) + \delta \mathrm{Id} \geq R_\delta$ so that ω_s will be marked by Algorithm 2.4.2. This shows that part (i) of the resolution guarantee is satisfied.

To show part (ii) of the resolution guarantee, assume that $D = \emptyset$ and $D_R \neq \emptyset$. Then there must be an index $s \in \{1, 2, \ldots, N\}$ with

$$R(\tau_s, z_{\max}) + \delta \mathrm{Id} \geq R_\delta.$$

Using Theorem 2.3.1 we obtain

$$\begin{aligned} -2\delta \mathrm{Id} &\leq R(\tau_s, z_{\max}) - (\delta \mathrm{Id} + R_\delta) \\ &\leq R(\tau_s, z_{\max}) - R(\sigma, z) \\ &\leq R(\tau_s, z_{\max}) - R(\sigma_{B\max}, z_{\min}) \end{aligned}$$

and thus $\mu \geq -2\delta$. □

Theorem 2.4.3 gives a rigorous yet conceptually simple criterion to check whether a given resolution guarantee is valid or not. Given a partition $(\omega_s)_{s=1}^N$ and bounds on the background and contact impedance error, we obtain μ from calculating $R(\tau_s, z_{\max})$ and $R(\sigma_{B\max}, z_{\min})$ by solving the partial differential equations of the complete electrode model. If this yields a negative value for μ, the resolution guarantee holds true up to a measurement error of $\delta < -\mu/2$.

2.4.2 Fast linearized verification of resolution guarantees

Checking the criterion in Theorem 2.4.3 for a partition with N elements requires the solution of $N+1$ forward problems. A less accurate but considerably faster test can be obtained by replacing the monotonicity tests in Algorithm 2.4.2

$$R(\tau_s, z_{\max}) + \delta \mathrm{Id} \geq R_\delta,$$

with their linearized approximations

$$R(\sigma_{B\min}, z_{\max}) + \lambda R'(\sigma_{B\min}, z_{\max})(\chi_{\omega_s}) + \delta \mathrm{Id} \geq R_\delta, \tag{2.13}$$

where $\lambda \in \mathbb{R}$ is a suitably chosen contrast level (as defined in Algorithm 2.4.5 or 2.4.9),

$$R'\left(\sigma_{B\min}, z_{\max}\right)(\chi_{\omega_s}) = -\left(\int_{\omega_s} \nabla u_i \cdot \nabla u_j \,\mathrm{d}x\right)_{i,j=1}^{L-1}, \tag{2.14}$$

where u_i and u_j are the corresponding solutions (inner potentials) of the CEM introduced in Section 2.2 with interior conductivity $\sigma_{B\min}$ and contact impedances $z_{\max}$. One can interpret R' as the Fréchet derivative of the measurements with respect to the interior conductivity distribution, cf., e.g., Lionheart [Lio04] or Lechleiter and Rieder [LR08], but we will not require this in the following.

Remark 2.4.4. The matrix $R'\left(\sigma_{B\min}, z_{\max}\right)(\chi_{\omega_s})$ can be expressed in terms of the sensitivity matrix $\mathcal{S}$ that is frequently being used in FEM-based EIT solvers (cf., e.g., [CHS13] for a recent work in the context of inclusion detection).

Let $(q_r)_{r=1}^p$ be the elements of a FEM discretization of the considered domain Ω. The sensitivity matrix $\mathcal{S} \in \mathbb{R}^{(L-1)^2 \times p}$ is given by

$$\mathcal{S} = \begin{pmatrix} \mathcal{S}_1 \\ \vdots \\ \mathcal{S}_{L-1} \end{pmatrix} \tag{2.15}$$

with

$$\mathcal{S}_j = \left(\mathcal{S}_j^{[i,r]}\right) = \left(-\int_{q_r} \nabla u_i \cdot \nabla u_j \,\mathrm{d}x\right) \in \mathbb{R}^{(L-1)\times p}. \tag{2.16}$$

If each element ω_s in the resolution partition is a union of elements q_r of the FEM-discretization, then the entries of R' can be obtained from summing up the corresponding entries of $\mathcal{S}$ as follows:

$$R'\left(\sigma_{B\min}, z_{\max}\right)(\chi_{\omega_s}) = \left(\sum_{r:\ q_r \subseteq \omega_s} \mathcal{S}_j^{[i,r]}\right)_{i,j=1}^{L-1}. \tag{2.17}$$

To choose the parameter λ, we require the additional knowledge of a global bound $\sigma_{\max} \in \mathbb{R}$ with

$$\sigma(x) \leq \sigma_{\max} \quad \text{for all } x \in \Omega. \tag{2.18}$$

Algorithm 2.4.5. *Mark each resolution element ω_s for which*

$$T_s + \delta \mathrm{Id} \geq R_\delta, \tag{2.19}$$

where

$$T_s := R(\sigma_{B\min}, z_{\max}) + \lambda R'(\sigma_{B\min}, z_{\max})(\chi_{\omega_s}) \tag{2.20}$$

and

$$\lambda := (c+\epsilon)\frac{\sigma_{B\min}}{\sigma_{\max}}, \quad s \in \{1, 2, \ldots, N\}. \tag{2.21}$$

Then the reconstruction D_R is given by the union of the marked resolution elements.

Theorem 2.4.6. *The reconstruction of Algorithm 2.4.5 fulfills the resolution guarantee if*

$$\mu < -2\delta \leq 0 \tag{2.22}$$

with

$$\mu := \max_{s=1}^{N}(\min(\mathrm{eig}(T_s - R(\sigma_{B\max}, z_{\min})))). \tag{2.23}$$

Proof. First let $\omega_s \subseteq D$. Given a vector $w \in \mathbb{R}^{L-1}$, let u_w be the inner potential in a body Ω with interior conductivity $\sigma_{B\min}$ and contact impedances $z_{\max}$ that results from driving currents of $w_1, w_2, \ldots, w_{L-1}$ through the electrodes $E_1, E_2, \ldots, E_{L-1}$, respectively. (Note that this implies a current flux of $-\sum_{l=1}^{L-1} w_l$ through the grounded L-th electrode.)

Theorem 2.3.2 yields that

$$\begin{aligned} &w^T(R(\sigma_{B\min}, z_{\max}) - R(\sigma, z_{\max}))w \\ &\geq \int_\Omega \frac{\sigma_{B\min}}{\sigma}(\sigma - \sigma_{B\min})|\nabla u_w|^2 \mathrm{d}x, \end{aligned}$$

and since $\omega_s \subseteq D$ implies $\sigma - \sigma_{B\min} \geq (c+\epsilon)\chi_{\omega_s}$, it follows that

$$R(\sigma_{B\min}, z_{\max}) - R(\sigma, z_{\max}) \geq -\lambda R'(\sigma_{B\min}, z_{\max})(\chi_{\omega_s}).$$

Hence, we obtain from Theorem 2.3.1 that

$$\begin{aligned} &T_s + \delta \mathrm{Id} \\ &= R(\sigma_{B\min}, z_{\max}) + \lambda R'(\sigma_{B\min}, z_{\max})(\chi_{\omega_s}) + \delta \mathrm{Id} \\ &\geq R(\sigma, z_{\max}) + \delta \mathrm{Id} \geq R(\sigma, z) + \delta \mathrm{Id} \\ &\geq R_\delta. \end{aligned}$$

Hence, ω_s will be marked, which shows that part (i) of the resolution guarantee is satisfied.

The proof of part (ii) of the resolution guarantee is completely analogous to the proof of part (ii) in Theorem 2.4.3. □

2.4.3 Verification for less conductive inclusions

The theory and the results are almost the same in the case that we consider inclusions that are less conductive than the background. In that case we set

$$\sigma_{D\max} := \sigma_0 - c < \sigma_{B\min} \tag{2.24}$$

and consider the following Algorithms 2.4.7 and 2.4.9.

Algorithm 2.4.7. *Mark each resolution element ω_s for which*

$$R(\tau_s, z_{\min}) - \delta \mathrm{Id} \leq R_\delta, \tag{2.25}$$

where

$$\tau_s := \sigma_{B\max}\chi_{\Omega\setminus\omega_s} + \sigma_{D\max}\chi_{\omega_s}, \quad s \in \{1, 2, \ldots, N\}.$$

Then the reconstruction D_R is given by the union of the marked resolution elements.

Theorem 2.4.8. *The reconstruction of Algorithm 2.4.7 fulfills the resolution guarantee if*

$$\mu > 2\delta \geq 0 \tag{2.26}$$

with

$$\mu := \min_{s=1}^{N} \left(\max\left(\mathrm{eig}\left(R(\tau_s, z_{\min}) - R(\sigma_{B\min}, z_{\max})\right)\right)\right).$$

Proof. The proof of part (i) of the resolution guarantee is analogous to the proof of part (i) in Theorem 2.4.3.

To show part (ii) of the resolution guarantee, assume that $D = \emptyset$ and $D_R \neq \emptyset$. Then there must be an index $s \in \{1, 2, \ldots, N\}$ with

$$R(\tau_s, z_{\min}) - \delta \mathrm{Id} \leq R_\delta \leq R(\sigma, z) + \delta \mathrm{Id}.$$

Using Theorem 2.3.1, we obtain

$$R(\tau_s, z_{\min}) - 2\delta \mathrm{Id} \leq R(\sigma_{B\min}, z_{\max}),$$

and thus $\mu \leq 2\delta$. □

Algorithm 2.4.9. *Mark each resolution element ω_s for which*

$$T_s - \delta \mathrm{Id} \leq R_\delta, \tag{2.27}$$

where

$$T_s := R(\sigma_{B\max}, z_{\min}) + R'(\sigma_{B\max}, z_{\min})(\lambda\chi_{\omega_s}), \tag{2.28}$$

$$\lambda := -(c + \epsilon), \quad s \in \{1, 2, \ldots, N\}. \tag{2.29}$$

Then the reconstruction D_R is given by the union of the marked resolution elements.

Theorem 2.4.10. *The reconstruction of Algorithm 2.4.9 fulfills the resolution guarantee if*

$$\mu > 2\delta \geq 0 \tag{2.30}$$

with

$$\mu := \min_{s=1}^{N} \left(\max \left(\operatorname{eig} \left(T_s - R(\sigma_{B\min}, z_{\max}) \right) \right) \right). \tag{2.31}$$

Proof. First let $\omega_s \subseteq D$. Given a vector $w \in \mathbb{R}^{L-1}$, let u_w be the inner potential in a body Ω with interior conductivity $\sigma_{B\max}$ and contact impedances $z_{\min}$ that results from driving a current of w_j through the j-th electrode, respectively. As in the proof of Theorem 2.4.6, by applying the Theorems 2.3.1 and 2.3.2, we obtain

$$w^T \left(R(\sigma_{B\max}, z_{\min}) - \delta \mathrm{Id} - R_\delta \right) w \leq \lambda \int_D |\nabla u_w|^2 \, \mathrm{d}x.$$

This yields

$$T_s - \delta \mathrm{Id} \leq R_\delta.$$

Hence, ω_s will be marked, which shows that part (i) of the resolution guarantee is satisfied.

The proof of part (ii) of the resolution guarantee is completely analogous to the proof of part (ii) in Theorem 2.4.8. □

2.5 Numerical results

The numerical results in this section are generated with MATLAB® and the commercial FEM-software COMSOL®.

In all examples we use the measurement setup explained in Figure 2.1. Conductivities and contact impedances are given in Siemens/meter (S/m) and Ohm-square meter (Ωm^2), respectively. The unit of length is meter (m). Currents and voltages are measured in milliampere ($m\mathrm{A}$) and millivolt ($m\mathrm{V}$), respectively.

2.5.1 Results for academic examples

We consider two measurement setups (see Figure 2.3 and 2.4). For both settings, we assume that the background conductivity is approximately $\sigma_0 = 1$ and the contact impedances are approximately $z_0 = (1, 1, \ldots, 1) \in \mathbb{R}^L$. The inclusions conductivity contrast is assumed to be $c = 10$.

The results for Figure 2.3 using our non-linearized verification procedure in Theorem 2.4.3 are presented in Table 2.1. Table 2.2 shows the results for Figure 2.3 obtained from the linearized verification procedure in Theorem 2.4.6 under the additional assumption that $\sigma_{D\max} = 15$ is an upper bound on the inclusion contrast.

The desired resolution shown in the second measurement setup in Figure 2.4 is particularly ambitious. Using the non-linearized verification method, it is not possible to guarantee the shown resolution. Under the additional assumption $\sigma_{D\max} = 12$ on the upper bound of the inclusion contrast, the resolution can be guaranteed using the linearized validation method up to the errors given in Table 2.3.

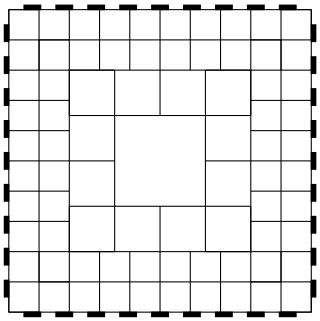

Figure 2.3: $\Omega = [-1,1]^2$ and 36 electrodes are covering 50% of the boundary. The first electrode E_1 is the lowermost one on the right boundary edge and the electrodes are numbered counter-clockwise. © 2015 IEEE

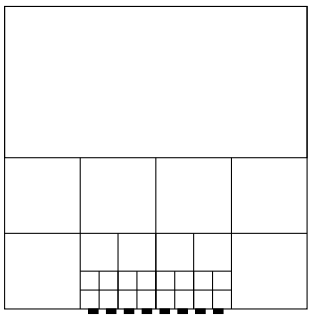

Figure 2.4: $\Omega = [-1,1]^2$ and 8 electrodes are covering 25% of the lower boundary edge. The electrodes are numbered from the left to the right. © 2015 IEEE

Table 2.1: RG validation for Figure 2.3 (non-linearized). © 2015 IEEE

background error ϵ:	contact imped. error γ:	abs. meas. noise δ:
0%	0%	0.13
0.25%	0%	0.11
0%	0.25%	0.10
0.25%	0.25%	0.088

Table 2.2: RG validation for Figure 2.3 (linearized). © 2015 IEEE

background error ϵ:	contact imped. error γ:	abs. meas. noise δ:
0%	0%	0.051
0.25%	0%	0.035
0%	0.25%	0.025
0.25%	0.25%	0.013

Table 2.3: RG validation for Figure 2.4 (linearized). © 2015 IEEE

background error ϵ:	contact imped. error γ:	abs. meas. noise δ:
0%	0%	0.026
0.05%	0%	0.022
0%	0.05%	0.0036
0.05%	0.05%	0.0022

2.5.2 Results using physiologically relevant parameters

The following setting is motivated by the idea of detecting hemorrhages inside fatty tissue. The resolution partition and the electrodes are concentrated to the lower half of a circle-shaped subject Ω. We used physiological parameter values based on the overview about electric properties of tissue [MPH06]. We assume that the background conductivity is approximately $\sigma_0 = 0.03$. The inclusion minimal conductivity contrast is $c = 0.43 - 0.03 = 0.4$ and the upper bound of the inclusion conductivity is $\sigma_{D\max} = 0.7$.

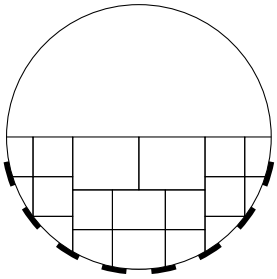

Figure 2.5: Ω is a disk with diameter of 0.05 and 8 electrodes are covering 47% of the lower half of the boundary. The electrodes are numbered from the left to the right. The resolution partition covers the lower half of the disk. © 2015 IEEE

Since realistic values for contact impedances are typically (or can be modeled to be) much smaller than 1 (cf. [VKV$^+$02]), we assume the contact impedance on each

electrode to be approximately 0.01.

The results for Figure 2.5 using our non-linearized verification procedure in Theorem 2.4.3 are presented in Table 2.4. Table 2.5 shows the results for Figure 2.5 obtained from the linearized verification procedure in Theorem 2.4.6.

Table 2.4: RG validation for Figure 2.5 (non-linearized). © 2015 IEEE

background error ϵ:	contact imped. error γ:	abs. meas. noise δ:
0%	0%	4.4
5%	0%	0.7
0%	5%	4.1
5%	5%	0.6

Table 2.5: RG validation for Figure 2.5 (linearized). © 2015 IEEE

background error ϵ:	contact imped. error γ:	abs. meas. noise δ:
0%	0%	1.8
1%	0%	0.7
0%	1%	1.8
1%	1%	0.7

2.5.3 Reconstruction guarantees in a region of interest

Our results can be extended to the case where certain areas should be excluded from the region of interest, e.g., if their background range is known to be violated. As an example, we will add to the setting in Section 2.5.2 an area ω_I consisting of bone and blood beside fat with a conductivity range of $(0.01, 0.7)$, cf. [MPH06].

The theory in 2.4.1 can be extended as follows. Let $\sigma_{I\min}, \sigma_{I\max} \in \mathbb{R}_+$ with

$$\sigma(x) \in (\sigma_{I\min}, \sigma_{I\max}) \quad \text{for all } x \in \omega_I$$

be the bounds for the conductivity in the area that is to be excluded from the region of interest. We apply Algorithm 2.4.2 with the following changes: τ_s in (2.10) is replaced by

$$\tau_s := \sigma_{B\min}\chi_{\Omega\setminus(\omega_s\cup\omega_I)} + \sigma_{D\min}\chi_{\omega_s} + \sigma_{I\min}\chi_{\omega_I} \tag{2.32}$$

and $\sigma_{B\max}$ in (2.12) (in Theorem 2.4.3) is replaced by

$$\sigma_{B\max}\chi_{\Omega\setminus\omega_I} + \sigma_{I\max}\chi_{\omega_I}. \tag{2.33}$$

Then analogously to the result in Theorem 2.4.3, we obtain a reconstruction guarantee where every element covered by the inclusion will be correctly marked and no element will be marked if there is no anomaly outside of ω_I.

We tested this variant on the setting shown in Figure 2.6, where ω_I is assumed to consist of bone and blood beside fat with a conductivity range of $(0.01, 0.7)$. The results are presented in Table 2.6.

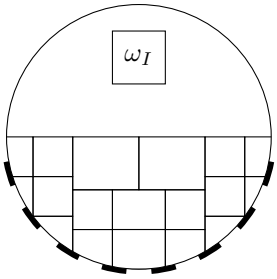

Figure 2.6: Ω is a disk with diameter of 0.05 and 8 electrodes are covering 47% of the lower half of the boundary. The electrodes are numbered from the left to the right. The resolution partition covers the lower half of the disk. The area ω_I allows the presence of bone and blood beside fat. © 2015 IEEE

Table 2.6: RG (extended version) validation for Figure 2.6. © 2015 IEEE

background error ϵ:	contact imped. error γ:	abs. meas. noise δ:
0%	0%	2.6
5%	0%	0.3
0%	5%	2.4
5%	5%	0.2

2.6 Conclusion and discussion

We have introduced a rigorous concept of resolution for anomaly detection and showed that it is principally possible to rigorously guarantee a certain resolution even for settings that include both, systematic modeling (background and contact impedance) errors and general (e.g., measurement) errors.

We have derived a constructive method to evaluate the amount of errors up to which a given desired resolution can be guaranteed. We have also derived a linearized variant of our method that allows fast validation of resolution guarantees (while still yielding rigorous results). In that context let us stress that somewhat surprisingly

the linearized variant does not seem to be always inferior to the non-linearized variant as the last example in Subsection 2.5.1 shows.

Our results may be used to determine whether a desired resolution can be achieved and to quantify the required measurement accuracy. Moreover, our results could be the basis of optimization strategies regarding the resolution, the driving patterns or the number and the positions of the electrodes.

It would be interesting to extend our approach to explicitly address other systematic errors, e.g., including the shape of the imaging domain and the position as well as the shape of the electrodes.

We believe that further investigation and experimental justification of the concept of resolution guarantees could help improving the reliability of EIT-based anomaly detection.

Chapter 3

Combining frequency-difference and ultrasound-modulated EIT

Up to some modifications the Sections 3.1 - 3.5 are the Sections 1-5 of the paper [HEU15] that has been submitted to the journal Inverse Problems.
© IOP. Unauthorized reproduction is prohibited.

3.1 Introduction

In the previous chapter we have shown that some kind of resolution guarantees (for anomaly detection) are principally possible for electrical impedance tomography (EIT) settings that include both systematic modeling and random measurement (or further) errors. In accordance with the numerical results in Section 2.5 this shows that reliable reconstructions of conductivity anomalies are principally possible for fairly small modeling and measurement errors. Nevertheless, the following considerations have to be taken into account. The measurements are very insensitive to changes in the conductivity values away from the electrodes. They do, however, strongly depend on the measurement geometry, i.e., the position of the electrodes and the shape of the imaging domain. In most applications it is not feasible to precisely measure the geometry, and electrodes are frequently placed by hand. Hence, such modeling or geometry errors present a major challenge for practical EIT applications.

In this chapter we propose a new measurement setup for anomaly detection and describe a reconstruction method that is completely unaffected by geometrical modeling errors, as it does not require the knowledge of the position of the electrodes or the shape of the imaging domain.

The main idea of our new technique is to combine ultrasound-modulated EIT measurements with frequency-difference EIT measurements. We focus an ultrasound wave on a small region inside the imaging domain to alter the conductivity in the focusing region. The resulting effect on the EIT measurements is then compared to the effect of a change in the electric current frequency. This comparison shows whether the focusing region lies inside a conductivity anomaly or not.

To decide whether the focusing region lies inside an anomaly, our method utilizes only the two sets of EIT measurements (with ultrasound-modulation and after the frequency change) and the ratio of the background conductivity before and after the frequency change. The latter can be estimated from comparing EIT measurements before and after the frequency change, as it is done in weighted frequency-difference EIT (see the references below). The method can be implemented using simple monotonicity tests, similar as in the Chapters 1 and 2.

The method does not use any forward simulations or explicitly known special solutions, that would depend on the geometry of the setup. Hence, it does not require any knowledge of the position of the electrodes or the shape of the imaging domain, and is hence completely unaffected by modeling errors.

We give a complete proof that our method correctly detects whether the focusing region lies inside an inclusion or not for the case that measurements are modeled by the *continuum model* (CM), in which the measurements are given by the Neumann-to-Dirichlet operator. For the case of measurements on a finite number of electrodes modeled by the *shunt model* (SM), we prove that the method correctly identifies the case where the focusing region lies inside the anomaly. We also give a physical justification (in the spirit of [HSW10]) that regions outside the anomaly will be identified correctly if enough electrodes are used for the measurements.

Let us now comment on related works and the origins of our approach. Our new method is based on a monotonicity-based comparison of weighted frequency-difference EIT (fdEIT) and ultrasound-modulated EIT (UMEIT) measurements. Monotonicity-based comparisons were first considered as heuristic inclusion detection methods. They were implemented and numerically tested by Tamburrino and Rubinacci [TR02, Tam06]. Recently, they were rigorously justified [HU] (the published version of Chapter 1) using the concept of localized potentials [Geb08]. Weighted fdEIT has been introduced in order to improve the reconstruction stability with respect to modeling errors in settings where no reference (anomaly-free) data is available, see [SLZ$^+$08, HS09, HSW10]. The hybrid tomography technique UMEIT was introduced in [ABC$^+$08]. When the measurement geometry is known, UMEIT allows to measure the interior electrical energy of the subject by altering the conductivity with a focused ultrasound wave (cf. the related idea of Impedance-Acoustic Tomography [GS08], where interior energy data is obtained from measuring expansion effects caused by electrical heating). Knowledge of this additional interior energy information eliminates the major cause of ill-posedness in the reconstruction process, which could greatly increase image resolution.

At this point, it has to be noted that the idea of using focused ultrasound waves in EIT yet has to be experimentally validated. The results in this chapter are derived under the idealistic assumption of a perfectly focused ultrasound wave that changes the conductivity in a well-defined ball-shaped region. Of course, in reality, such a perfect focus cannot be realized and the ultrasound wave will also affect the conductivity outside the focusing region.

The chapter is organized as follows. In Section 3.2 we introduce the general setting of complex conductivity EIT and ultrasound-modulated EIT for the continuous case, where boundary data is modeled by the CM. Then we develop a monotonicity relation for the complex conductivity EIT. Using this relation and the concept of localized potentials (see Chapter 1), we derive an anomaly detection result that makes use of a comparison of measurements at non-zero frequency and ultrasound-modulated DC measurements. In Section 3.3 we derive the corresponding result for a more realistic electrode measurement setting, where the boundary data is modeled with the SM. In Section 3.4 we numerically test the anomaly reconstruction method of Section 3.3 for two- and three-dimensional settings. Finally, in Section 3.5 we conclude the chapter with a discussion on its main results.

3.2 Continuous boundary data

3.2.1 The setting

We start by describing the general setting of complex conductivity EIT and ultrasound-modulated EIT with continuous boundary data. We consider a bounded imaging domain $\Omega \subset \mathbb{R}^n$, $n \geq 2$, with piecewise smooth boundary. For $x \in \Omega$, let

$$\gamma_\omega(x) = \sigma_\omega(x) + \mathrm{i}\omega\epsilon_\omega(x)$$

denote the complex admittivity of the imaging subject at frequency $\omega \geq 0$. We assume that

$$\Re(\gamma_\omega) = \sigma_\omega \in L^\infty_+(\Omega;\mathbb{R}) \quad \text{and} \quad \Im(\gamma_\omega) = \omega\epsilon_\omega \in L^\infty(\Omega;\mathbb{R}),$$

where $\Re(\cdot)$ and $\Im(\cdot)$ denote the real and imaginary part, the subscript "+" indicates functions with positive (essential) infima, and throughout this chapter all function spaces consist of complex-valued functions if not stated otherwise.

Complex EIT measurements consist of applying time-harmonic currents to the surface of the imaging domain and measuring the resulting electric surface potential. In the CM (see, e.g., [CIN99]), these measurements are described by the Neumann-to-Dirichlet operator

$$\Lambda(\gamma_\omega):\ L^2_\diamond(\partial\Omega) \to L^2_\diamond(\partial\Omega), \quad g \mapsto u^{(g)}_{\gamma_\omega}|_{\partial\Omega},$$

where $u^{(g)}_{\gamma_\omega} \in H^1_\diamond(\Omega)$ is the unique solution of

$$\nabla\cdot\left(\gamma_\omega\nabla u^{(g)}_{\gamma_\omega}\right) = 0 \text{ in } \Omega \quad \text{and} \quad \gamma_\omega\partial_\nu u^{(g)}_{\gamma_\omega}|_{\partial\Omega} = g. \tag{3.1}$$

Here, the subspaces of $L^2(\partial\Omega)$- and $H^1(\Omega)$-functions with vanishing integral mean on $\partial\Omega$ are denoted by $L^2_\diamond(\partial\Omega)$ and $H^1_\diamond(\Omega)$, respectively. ν is the outer normal on $\partial\Omega$.

The existence of an unique solution is a consequence of the Lax-Milgram theorem. Furthermore, it is well known that $\Lambda(\gamma_\omega)$ is a well-defined, linear and compact operator.

The idea of ultrasound-modulated EIT is to focus an ultrasound wave on a small part $B \subseteq \Omega$ in order to change the density of the material and thus its conductivity in B, cf. [ABC+08]. A simple, very idealistic model is that the focused ultrasound wave changes the conductivity from γ_ω to $\gamma_\omega(1+\alpha\chi_B)$, where $\alpha > 0$ depends on the strength of the ultrasound wave and χ_B is the characteristic function of B. Hence, ultrasound-modulated EIT measurements can be modeled as

$$\Lambda(\gamma_\omega(1 + \alpha\chi_B)).$$

In this chapter we will compare measurements at a non-zero frequency $\Lambda(\gamma_\omega)$, $\omega > 0$, with ultrasound-modulated DC measurements $\Lambda(\gamma_0(1 + \alpha\chi_B))$ in order to detect whether the ultrasound-modulated part B lies inside a conductivity anomaly or not.

3.2.2 Monotonicity results for the continuum model

We will compare measurements in the sense of operator definiteness. Given a bounded operator $A:\ L^2_\diamond(\partial\Omega) \to L^2_\diamond(\partial\Omega)$, we define its self-adjoint part by

$$\Re(A) := \frac{1}{2}(A + A^*),$$

where $A^*:\ L^2_\diamond(\partial\Omega) \to L^2_\diamond(\partial\Omega)$ is the adjoint of A, i.e.,

$$\int_{\partial\Omega} \overline{g}(Ah)\,\mathrm{d}s = \int_{\partial\Omega} \overline{(A^*g)}h\,\mathrm{d}s \quad \text{for all } g, h \in L^2_\diamond(\partial\Omega).$$

Obviously, $\Re(A)$ is self-adjoint.

For two self-adjoint bounded operators $A, B:\ L^2_\diamond(\partial\Omega) \to L^2_\diamond(\partial\Omega)$, we write $A \leq B$ if $B - A$ is positive semidefinite, i.e.,

$$\int_{\partial\Omega} \overline{g}(B - A)g\,\mathrm{d}s \geq 0 \quad \text{for all } g \in L^2_\diamond(\partial\Omega).$$

For compact operators, this is equivalent to the fact that all eigenvalues of $B - A$ are non-negative.

Note that the Neumann-to-Dirichlet operator $\Lambda(\gamma_\omega)$ satisfies

$$\int_{\partial\Omega} \overline{g}\Lambda(\gamma_\omega)h\,\mathrm{d}s = \int_{\partial\Omega} \overline{g}u^{(h)}_{\gamma_\omega}|_{\partial\Omega}\,\mathrm{d}s = \int_\Omega \overline{\gamma_\omega \nabla u^{(g)}_{\gamma_\omega}} \cdot \nabla u^{(h)}_{\gamma_\omega}\,\mathrm{d}x$$

and

$$\int_{\partial\Omega} g\Lambda(\gamma_\omega)h\,\mathrm{d}s = \int_\Omega \gamma_\omega \nabla u^{(g)}_{\gamma_\omega} \cdot \nabla u^{(h)}_{\gamma_\omega}\,\mathrm{d}x = \int_{\partial\Omega} h\Lambda(\gamma_\omega)g\,\mathrm{d}s.$$

In that sense, $\Lambda(\gamma_\omega)$ is symmetric but generally (for complex γ_ω) not self-adjoint.

In Chapter 1 we have seen that for the case of continuous boundary measurements and real-valued conductivity functions $\sigma_1, \sigma_2 \in L^\infty_+(\Omega;\mathbb{R})$ it holds that

$$\begin{aligned}&\int_\Omega \frac{\sigma_2}{\sigma_1}(\sigma_1-\sigma_2)\left|\nabla u^{(g)}_{\sigma_2}\right|^2 \mathrm{d}x \\ &\quad\leq \int_{\partial\Omega} g\,(\Lambda(\sigma_2)-\Lambda(\sigma_1))\,g\,\mathrm{d}s \leq \int_\Omega (\sigma_1-\sigma_2)\left|\nabla u^{(g)}_{\sigma_2}\right|^2 \mathrm{d}x,\end{aligned} \tag{3.2}$$

where $u^{(g)}_{\sigma_2}$ solves the EIT equation (3.1) with conductivity σ_2 and boundary currents given by g. Hence, we obtain the monotonicity relation

$$\sigma_1 \leq \sigma_2 \quad \text{implies that} \quad \Lambda(\sigma_1) \geq \Lambda(\sigma_2),$$

so that an imaging domain with larger conductivity leads to smaller measurements in the sense of operator definiteness. The monotonicity relation (3.2) goes back to Ikehata, Kang, Seo, and Sheen [KSS97, Ike98]. It is the basis of many results on inclusion detection in EIT, cf. [Kir05, IIN$^+$07, HS09, HS10, HSW10, Har13] and [HU] (presented in Chapter 1).

The following lemma extends the relation (3.2) to complex-valued conductivities (see also [Kir05, HS09, HSW10] for similar results).

Lemma 3.2.1. *Let $\gamma_1, \gamma_2 \in L^\infty_+(\Omega;\mathbb{R}) + \mathrm{i}L^\infty(\Omega;\mathbb{R})$, $g \in L^2_\diamond(\partial\Omega)$, and $u^{(g)}_{\gamma_1}, u^{(g)}_{\gamma_2} \in H^1_\diamond(\Omega)$ be the corresponding solutions of* (3.1)*. Then*

$$\begin{aligned}&\int_\Omega \left(\frac{\Re(\gamma_2)}{\Re(\gamma_1)}\Re(\gamma_1-\gamma_2) - \frac{\Im(\gamma_2)^2}{\Re(\gamma_1)}\right)\left|\nabla u^{(g)}_{\gamma_2}\right|^2 \mathrm{d}x \\ &\quad\leq \int_{\partial\Omega} \overline{g}\,\Re\left(\Lambda(\gamma_2)-\Lambda(\gamma_1)\right) g\,\mathrm{d}s \leq \int_\Omega \left(\Re(\gamma_1-\gamma_2) + \frac{\Im(\gamma_1)^2}{\Re(\gamma_1)}\right)\left|\nabla u^{(g)}_{\gamma_2}\right|^2 \mathrm{d}x.\end{aligned}$$

The proof of Lemma 3.2.1 is postponed to the end of this section.

3.2.3 Detecting inclusions in the continuous case

We assume that the imaging domain consists of a homogeneous background medium with one or several conductivity anomalies (inclusions) D. For simplicity, we will present our result for the case that the anomalies possess a constant admittivity and that the conductivity σ_ω and the permittivity ϵ_ω do not change with frequency. More precisely, we assume that $D \subset \Omega$ is a closed set with connected complement

and that γ_0 and γ_ω are given by

$$\gamma_0(x) = \begin{cases} \gamma_0^{(\Omega)} = \sigma_\Omega & \text{for } x \in \Omega \setminus D, \\ \gamma_0^{(D)} = \sigma_D & \text{for } x \in D, \end{cases} \tag{3.3}$$

$$\gamma_\omega(x) = \begin{cases} \gamma_\omega^{(\Omega)} = \sigma_\Omega + \mathrm{i}\omega\epsilon_\Omega & \text{for } x \in \Omega \setminus D, \\ \gamma_\omega^{(D)} = \sigma_D + \mathrm{i}\omega\epsilon_D & \text{for } x \in D, \end{cases} \tag{3.4}$$

with constants $\sigma_\Omega, \sigma_D, \epsilon_\Omega, \epsilon_D > 0$. We also assume that the anomaly fulfills

$$\epsilon_D\sigma_\Omega - \epsilon_\Omega\sigma_D \neq 0, \tag{3.5}$$

which is the contrast condition required to detect inclusion in weighted fdEIT, cf. [HS09, Remark 2.3]. Our results can be formulated under more general conditions as long as the background conductivities are constant, see Remark 3.2.5 below.

The ratio of the background conductivities is denoted by

$$\alpha := \frac{\gamma_\omega^{(\Omega)}}{\gamma_0^{(\Omega)}} = 1 + \mathrm{i}\omega\frac{\epsilon_\Omega}{\sigma_\Omega}. \tag{3.6}$$

We show that the anomaly D can be detected from comparing (ratio-weighted) EIT measurements at a non-zero frequency $\omega > 0$ with ultrasound-modulated DC measurements, i.e., we can detect D from the knowledge of $\Lambda(\gamma_\omega)$, $\Lambda(\gamma_0(1+\alpha\chi_B))$ and the background ratio α. Note that the background ratio α could also be estimated by additionally taking un-modulated DC measurements $\Lambda(\gamma_0)$ and comparing them with $\Lambda(\gamma_\omega)$ in the same way as in weighted fdEIT, cf. [SLZ+08, HS09, HSW10].

Theorem 3.2.2. *Let $c := \epsilon_D\sigma_\Omega - \epsilon_\Omega\sigma_D \neq 0$. For sufficiently small $\beta > 0$ and every open set $B \subseteq \Omega$, it holds that*

$$B \subseteq D \quad \textit{if and only if} \quad \Re\left(\alpha\Lambda(\gamma_\omega)\right) \begin{cases} \leq \Lambda((1+\beta\chi_B)\gamma_0) & \textit{if } c > 0, \\ \geq \Lambda((1-\beta\chi_B)\gamma_0) & \textit{if } c < 0. \end{cases} \tag{3.7}$$

The constant $\beta > 0$ is sufficiently small if

$$\beta \leq \begin{cases} \frac{\epsilon_\Omega}{\sigma_\Omega}C' & \textit{if } c > 0, \\ -\frac{\epsilon_D}{\sigma_D}C & \textit{if } c < 0, \end{cases}$$

where

$$C := \omega^2\frac{c}{\sigma_D\sigma_\Omega + \omega^2\epsilon_D\epsilon_\Omega} \quad \textit{and} \quad C' := \omega^2\frac{\sigma_\Omega}{\sigma_D}\cdot\frac{c}{\sigma_\Omega^2 + \omega^2\epsilon_\Omega^2}.$$

Theorem 3.2.2 shows that, for sufficiently small modulation strengths, the ultrasound-modulated DC measurements are larger ($c > 0$) or smaller ($c < 0$) than (the self-adjoint part of ratio-weighted) measurements taken at a non-zero frequency if and only if the focusing region lies inside the unknown inclusion D. The term larger and smaller are to be understood in the sense of operator definiteness.

3.2.4 Proof of the main results for the continuum model

Our proof of Theorem 3.2.2 relies on the monotonicity relation for complex conductivity EIT in Lemma 3.2.1 and the concept of localized potentials developed by Harrach in [Geb08]. To prove Lemma 3.2.1 we will first show the following auxiliary result that will also be useful for the case of electrode measurements.

Lemma 3.2.3. *Let* $\gamma_1, \gamma_2 \in L^\infty_+(\Omega;\mathbb{R}) + \mathrm{i}L^\infty(\Omega;\mathbb{R})$, $g \in L^2_\diamond(\partial\Omega)$, *and* $u_1, u_2 \in H^1(\Omega)$ *fulfill*

$$\begin{aligned}\int_\Omega \gamma_1 |\nabla u_1|^2 \,\mathrm{d}x &= \int_\Omega \gamma_2 \nabla u_2 \cdot \overline{\nabla u_1} \,\mathrm{d}x,\\ \int_\Omega \gamma_2 |\nabla u_2|^2 \,\mathrm{d}x &= \int_\Omega \gamma_1 \nabla u_1 \cdot \overline{\nabla u_2} \,\mathrm{d}x.\end{aligned}$$

Then

$$\begin{aligned}&\int_\Omega \left(\frac{\Re(\gamma_2)}{\Re(\gamma_1)} \Re(\gamma_1 - \gamma_2) - \frac{\Im(\gamma_2)^2}{\Re(\gamma_1)} \right) |\nabla u_2|^2 \,\mathrm{d}x\\ &\quad\leq \int_\Omega \Re(\gamma_2)|\nabla u_2|^2 \,\mathrm{d}x - \int_\Omega \Re(\gamma_1)|\nabla u_1|^2 \,\mathrm{d}x\\ &\quad\leq \int_\Omega \left(\Re(\gamma_1 - \gamma_2) + \frac{\Im(\gamma_1)^2}{\Re(\gamma_1)} \right) |\nabla u_2|^2 \,\mathrm{d}x.\end{aligned}$$

Proof. Since

$$\begin{aligned}0 &\leq \int_\Omega \Re(\gamma_1) \left| \nabla u_1 - \frac{\gamma_2}{\Re(\gamma_1)} \nabla u_2 \right|^2 \mathrm{d}x\\ &= \Re\left(\int_\Omega \gamma_1 |\nabla u_1|^2 \,\mathrm{d}x - 2\int_\Omega \gamma_2 \nabla u_2 \cdot \overline{\nabla u_1} \,\mathrm{d}x \right) + \int_\Omega \frac{|\gamma_2|^2}{\Re(\gamma_1)} |\nabla u_2|^2 \,\mathrm{d}x\\ &= -\int_\Omega \Re(\gamma_1)|\nabla u_1|^2 \,\mathrm{d}x + \int_\Omega \frac{|\gamma_2|^2}{\Re(\gamma_1)} |\nabla u_2|^2 \,\mathrm{d}x\\ &= \int_\Omega \Re(\gamma_2)|\nabla u_2|^2 \,\mathrm{d}x - \int_\Omega \Re(\gamma_1)|\nabla u_1|^2 \,\mathrm{d}x + \int_\Omega \left(\frac{|\gamma_2|^2}{\Re(\gamma_1)} - \Re(\gamma_2) \right) |\nabla u_2|^2 \,\mathrm{d}x,\end{aligned}$$

the first inequality follows from

$$\frac{|\gamma_2|^2}{\Re(\gamma_1)} - \Re(\gamma_2) = \frac{\Re(\gamma_2)^2 + \Im(\gamma_2)^2}{\Re(\gamma_1)} - \Re(\gamma_2) = \frac{\Re(\gamma_2)}{\Re(\gamma_1)} \Re(\gamma_2 - \gamma_1) + \frac{\Im(\gamma_2)^2}{\Re(\gamma_1)}.$$

Likewise, we obtain

$$\begin{aligned}
0 &\leq \int_\Omega \Re(\gamma_1)\left|\nabla u_1 - \frac{\overline{\gamma_1}}{\Re(\gamma_1)}\nabla u_2\right|^2 \mathrm{d}x \\
&= \int_\Omega \Re(\gamma_1)|\nabla u_1|^2\,\mathrm{d}x - 2\Re\left(\int_\Omega \overline{\gamma_1}\nabla u_2 \cdot \overline{\nabla u_1}\,\mathrm{d}x\right) + \int_\Omega \frac{|\gamma_1|^2}{\Re(\gamma_1)}|\nabla u_2|^2\,\mathrm{d}x \\
&= \int_\Omega \Re(\gamma_1)|\nabla u_1|^2\,\mathrm{d}x - \int_\Omega \Re(\gamma_2)|\nabla u_2|^2\,\mathrm{d}x + \int_\Omega \left(\frac{|\gamma_1|^2}{\Re(\gamma_1)} - \Re(\gamma_2)\right)|\nabla u_2|^2\,\mathrm{d}x
\end{aligned}$$

so that the second inequality follows from

$$\frac{|\gamma_1|^2}{\Re(\gamma_1)} - \Re(\gamma_2) = \Re(\gamma_1 - \gamma_2) + \frac{\Im(\gamma_1)^2}{\Re(\gamma_1)}.$$

□

We also require the following elementary computation.

Lemma 3.2.4. *Let $\gamma_0, \gamma_\omega : \Omega \to \mathbb{C}$, $\tilde{\beta} \in \mathbb{R}$ and $\alpha \in \mathbb{C}$ be given by* (3.3),(3.4) *and* (3.6). *Then,*

$$\begin{aligned}
\frac{\Re(\gamma_0)}{\Re(\gamma_\omega/\alpha)}\Re(\gamma_\omega/\alpha - \gamma_0) &= \begin{cases} 0 & \text{in } \Omega \setminus D, \\ \frac{\epsilon_\Omega \sigma_D}{\sigma_\Omega} C & \text{in } D, \end{cases} \\
\Re(\gamma_\omega/\alpha - \gamma_0) + \frac{\Im(\gamma_\omega/\alpha)^2}{\Re(\gamma_\omega/\alpha)} &= \begin{cases} 0 & \text{in } \Omega \setminus D, \\ \epsilon_D C & \text{in } D, \end{cases} \\
\Re(\gamma_\omega/\alpha - (1+\tilde{\beta}\chi_B)\gamma_0) &= \begin{cases} -\tilde{\beta}\sigma_\Omega \chi_B & \text{in } \Omega \setminus D, \\ \sigma_D\left(\frac{\epsilon_\Omega}{\sigma_\Omega} C' - \tilde{\beta}\chi_B\right) & \text{in } D, \end{cases} \\
\Re(\gamma_\omega/\alpha - (1+\tilde{\beta}\chi_B)\gamma_0) + \frac{\Im(\gamma_\omega/\alpha)^2}{\Re(\gamma_\omega/\alpha)} &= \begin{cases} -\tilde{\beta}\sigma_\Omega \chi_B & \text{in } \Omega \setminus D, \\ \epsilon_D C - \tilde{\beta}\sigma_D \chi_B & \text{in } D, \end{cases}
\end{aligned}$$

where

$$C := \omega^2 \frac{\epsilon_D \sigma_\Omega - \epsilon_\Omega \sigma_D}{\sigma_D \sigma_\Omega + \omega^2 \epsilon_D \epsilon_\Omega} \quad \text{and} \quad C' := \omega^2 \frac{\sigma_\Omega}{\sigma_D} \cdot \frac{\epsilon_D \sigma_\Omega - \epsilon_\Omega \sigma_D}{\sigma_\Omega^2 + \omega^2 \epsilon_\Omega^2}.$$

Proof. Let

$$\gamma_0 = \begin{cases} \gamma_0^{(\Omega)} = \sigma_\Omega & \text{in } \Omega \setminus D, \\ \gamma_0^{(D)} = \sigma_D & \text{in } D, \end{cases} \qquad \gamma_\omega = \begin{cases} \gamma_\omega^{(\Omega)} = \sigma_\Omega + \mathrm{i}\omega\epsilon_\Omega & \text{in } \Omega \setminus D, \\ \gamma_\omega^{(D)} = \sigma_D + \mathrm{i}\omega\epsilon_D & \text{in } D, \end{cases}$$

with real-valued constants $\sigma_\Omega, \sigma_D, \epsilon_\Omega, \epsilon_D > 0$ and let

$$\alpha = \gamma_\omega^{(\Omega)}/\gamma_0^{(\Omega)} = 1 + \mathrm{i}\omega\frac{\epsilon_\Omega}{\sigma_\Omega} \in \mathbb{C}.$$

Then, by the definition of α,

$$\gamma_\omega/\alpha - \gamma_0 = 0 \quad \text{in } \Omega \setminus D \quad \text{and} \quad \Im(\gamma_\omega/\alpha) = 0 \quad \text{in } \Omega \setminus D$$

so that

$$\begin{aligned}
\frac{\Re(\gamma_0)}{\Re(\gamma_\omega/\alpha)}\Re(\gamma_\omega/\alpha - \gamma_0) &= 0 && \text{in } \Omega \setminus D,\\
\Re(\gamma_\omega/\alpha - \gamma_0) + \frac{\Im(\gamma_\omega/\alpha)^2}{\Re(\gamma_\omega/\alpha)} &= 0 && \text{in } \Omega \setminus D,\\
\Re(\gamma_\omega/\alpha - (1+\tilde\beta\chi_B)\gamma_0) &= -\tilde\beta\sigma_\Omega\chi_B && \text{in } \Omega \setminus D,\\
\Re(\gamma_\omega/\alpha - (1+\tilde\beta\chi_B)\gamma_0) + \frac{\Im(\gamma_\omega/\alpha)^2}{\Re(\gamma_\omega/\alpha)} &= -\tilde\beta\sigma_\Omega\chi_B && \text{in } \Omega \setminus D.
\end{aligned}$$

In D we have that

$$\begin{aligned}
\Re(\gamma_0) &= \sigma_D,\\
\Re(\gamma_\omega/\alpha) &= \Re\left(\gamma_\omega^{(D)}\frac{\gamma_0^{(\Omega)}}{\gamma_\omega^{(\Omega)}}\right) = \sigma_\Omega\Re\left(\frac{\sigma_D + \mathrm{i}\omega\epsilon_D}{\sigma_\Omega + \mathrm{i}\omega\epsilon_\Omega}\right) = \sigma_\Omega\frac{\sigma_D\sigma_\Omega + \omega^2\epsilon_D\epsilon_\Omega}{\sigma_\Omega^2 + \omega^2\epsilon_\Omega^2},\\
\Im(\gamma_\omega/\alpha) &= \Im\left(\gamma_\omega^{(D)}\frac{\gamma_0^{(\Omega)}}{\gamma_\omega^{(\Omega)}}\right) = \sigma_\Omega\Im\left(\frac{\sigma_D + \mathrm{i}\omega\epsilon_D}{\sigma_\Omega + \mathrm{i}\omega\epsilon_\Omega}\right) = \omega\sigma_\Omega\frac{\epsilon_D\sigma_\Omega - \epsilon_\Omega\sigma_D}{\sigma_\Omega^2 + \omega^2\epsilon_\Omega^2}.
\end{aligned}$$

Hence, in D

$$\Re(\gamma_\omega/\alpha - \gamma_0) = \sigma_\Omega\frac{\sigma_D\sigma_\Omega + \omega^2\epsilon_D\epsilon_\Omega}{\sigma_\Omega^2 + \omega^2\epsilon_\Omega^2} - \sigma_D = \omega^2\epsilon_\Omega\frac{\epsilon_D\sigma_\Omega - \sigma_D\epsilon_\Omega}{\sigma_\Omega^2 + \omega^2\epsilon_\Omega^2}$$

and

$$\Re(\gamma_\omega/\alpha - (1+\tilde\beta\chi_B)\gamma_0) = \sigma_D\left(\frac{\epsilon_\Omega}{\sigma_\Omega}\omega^2\frac{\sigma_\Omega}{\sigma_D}\frac{\epsilon_D\sigma_\Omega - \epsilon_\Omega\sigma_D}{\sigma_\Omega^2 + \omega^2\epsilon_\Omega^2} - \tilde\beta\chi_B\right)$$

so that

$$\begin{aligned}
\frac{\Re(\gamma_0)}{\Re(\gamma_\omega/\alpha)}\Re(\gamma_\omega/\alpha - \gamma_0) &= \omega^2\sigma_D\epsilon_\Omega\frac{\epsilon_D\sigma_\Omega - \epsilon_\Omega\sigma_D}{\sigma_\Omega(\sigma_D\sigma_\Omega + \omega^2\epsilon_D\epsilon_\Omega)} = \frac{\epsilon_\Omega\sigma_D}{\sigma_\Omega}C,\\
\Re(\gamma_\omega/\alpha - (1+\tilde\beta\chi_B)\gamma_0) &= \sigma_D\left(\frac{\epsilon_\Omega}{\sigma_\Omega}C' - \tilde\beta\chi_B\right).
\end{aligned}$$

The last part of the assertion follows from

$$\begin{aligned}
&\Re(\gamma_\omega/\alpha - \gamma_0) + \frac{\Im(\gamma_\omega/\alpha)^2}{\Re(\gamma_\omega/\alpha)}\\
&= \omega^2\epsilon_\Omega\frac{\epsilon_D\sigma_\Omega - \epsilon_\Omega\sigma_D}{\sigma_\Omega^2 + \omega^2\epsilon_\Omega^2} + \omega^2\sigma_\Omega\frac{(\epsilon_D\sigma_\Omega - \epsilon_\Omega\sigma_D)^2}{(\sigma_\Omega^2 + \omega^2\epsilon_\Omega^2)(\sigma_D\sigma_\Omega + \omega^2\epsilon_D\epsilon_\Omega)}\\
&= \omega^2\frac{\epsilon_D\sigma_\Omega - \epsilon_\Omega\sigma_D}{\sigma_\Omega^2 + \omega^2\epsilon_\Omega^2}\left(\epsilon_\Omega + \sigma_\Omega\frac{\epsilon_D\sigma_\Omega - \epsilon_\Omega\sigma_D}{\sigma_D\sigma_\Omega + \omega^2\epsilon_D\epsilon_\Omega}\right)\\
&= \omega^2\frac{\epsilon_D\sigma_\Omega - \epsilon_\Omega\sigma_D}{\sigma_\Omega^2 + \omega^2\epsilon_\Omega^2}\,\frac{\omega^2\epsilon_D\epsilon_\Omega^2 + \epsilon_D\sigma_\Omega^2}{\sigma_D\sigma_\Omega + \omega^2\epsilon_D\epsilon_\Omega} = \omega^2\epsilon_D\frac{\epsilon_D\sigma_\Omega - \epsilon_\Omega\sigma_D}{\sigma_D\sigma_\Omega + \omega^2\epsilon_D\epsilon_\Omega} = \epsilon_D C
\end{aligned}$$

that also yields

$$\Re(\gamma_\omega/\alpha - (1+\tilde{\beta}\chi_B)\gamma_0) + \frac{\Im(\gamma_\omega/\alpha)^2}{\Re(\gamma_\omega/\alpha)} = \epsilon_D C - \tilde{\beta}\sigma_D\chi_B.$$

□

Now we are ready to prove Lemma 3.2.1 and Theorem 3.2.2.

Proof of lemma 3.2.1. Using

$$\begin{aligned}
\int_{\partial\Omega} \overline{g}\Lambda(\gamma_1)g\,\mathrm{d}s &= \int_{\partial\Omega} \overline{g}u^{(g)}_{\gamma_1}|_{\partial\Omega}\,\mathrm{d}s = \int_\Omega \overline{\gamma_1}\left|\nabla u^{(g)}_{\gamma_1}\right|^2\,\mathrm{d}x = \int_\Omega \overline{\gamma_2\nabla u^{(g)}_{\gamma_2}}\cdot\nabla u^{(g)}_{\gamma_1}\,\mathrm{d}x,\\
\int_{\partial\Omega} \overline{g}\Lambda(\gamma_2)g\,\mathrm{d}s &= \int_{\partial\Omega} \overline{g}u^{(g)}_{\gamma_2}|_{\partial\Omega}\,\mathrm{d}s = \int_\Omega \overline{\gamma_2}\left|\nabla u^{(g)}_{\gamma_2}\right|^2\,\mathrm{d}x = \int_\Omega \overline{\gamma_1\nabla u^{(g)}_{\gamma_1}}\cdot\nabla u^{(g)}_{\gamma_2}\,\mathrm{d}x,
\end{aligned}$$

the assertion immediately follows from Lemma 3.2.3.

□

Proof of Theorem 3.2.2. Let $\tilde{\beta} := \beta$ if $c > 0$ and $\tilde{\beta} := -\beta$ if $c < 0$. We apply Lemma 3.2.1 with $\gamma_1 := \gamma_\omega/\alpha$ and $\gamma_2 := \gamma_0$, and obtain

$$\begin{aligned}
&\int_\Omega \frac{\Re(\gamma_0)}{\Re(\gamma_\omega/\alpha)}\Re(\gamma_\omega/\alpha - \gamma_0)\left|\nabla u^{(g)}_{\gamma_0}\right|^2\,\mathrm{d}x\\
&\quad\leq \int_{\partial\Omega} \overline{g}\left(\Lambda(\gamma_0) - \Re\left(\Lambda(\gamma_\omega/\alpha)\right)\right)g\,\mathrm{d}s\\
&\quad\leq \int_\Omega \left(\Re(\gamma_\omega/\alpha - \gamma_0) + \frac{\Im(\gamma_\omega/\alpha)^2}{\Re(\gamma_\omega/\alpha)}\right)\left|\nabla u^{(g)}_{\gamma_0}\right|^2\,\mathrm{d}x.
\end{aligned}$$

Using the elementary computation in Lemma 3.2.4 it follows that

$$\begin{aligned}
\frac{\epsilon_\Omega\sigma_D}{\sigma_\Omega}C\int_D \left|\nabla u^{(g)}_{\gamma_0}\right|^2\,\mathrm{d}x &\leq \int_{\partial\Omega} \overline{g}\left(\Lambda(\gamma_0) - \Re\left(\alpha\Lambda(\gamma_\omega)\right)\right)g\,\mathrm{d}s\\
&\leq \epsilon_D C\int_D \left|\nabla u^{(g)}_{\gamma_0}\right|^2\,\mathrm{d}x. \qquad (3.8)
\end{aligned}$$

We also apply Lemma 3.2.1 with $\gamma_1 := (1+\tilde{\beta}\chi_B)\gamma_0$ and $\gamma_2 := \gamma_0$, and obtain

$$\begin{aligned}
\int_B \frac{\tilde{\beta}}{1+\tilde{\beta}}\gamma_0\left|\nabla u^{(g)}_{\gamma_0}\right|^2\,\mathrm{d}x &\leq \int_{\partial\Omega} \overline{g}\left(\Lambda(\gamma_0) - \Lambda((1+\tilde{\beta}\chi_B)\gamma_0)\right)g\,\mathrm{d}s\\
&\leq \int_B \tilde{\beta}\gamma_0\left|\nabla u^{(g)}_{\gamma_0}\right|^2\,\mathrm{d}x. \qquad (3.9)
\end{aligned}$$

From this we obtain

$$\begin{aligned}
&\frac{\epsilon_\Omega \sigma_D}{\sigma_\Omega} C \int_D \left|\nabla u_{\gamma_0}^{(g)}\right|^2 \,\mathrm{d}x - \int_B \tilde{\beta}\gamma_0 \left|\nabla u_{\gamma_0}^{(g)}\right|^2 \,\mathrm{d}x \\
&\quad\leq \int_{\partial\Omega} \overline{g} \left(\Lambda((1+\tilde{\beta}\chi_B)\gamma_0) - \Re\left(\alpha\Lambda(\gamma_\omega)\right)\right) g \,\mathrm{d}s \qquad (3.10) \\
&\quad\leq \epsilon_D C \int_D \left|\nabla u_{\gamma_0}^{(g)}\right|^2 \,\mathrm{d}x - \int_B \frac{\tilde{\beta}}{1+\tilde{\beta}}\gamma_0 \left|\nabla u_{\gamma_0}^{(g)}\right|^2 \,\mathrm{d}x. \qquad (3.11)
\end{aligned}$$

Additionally, we apply Lemma 3.2.1 with $\gamma_1 := \gamma_\omega/\alpha$ and $\gamma_2 := (1+\tilde{\beta}\chi_B)\gamma_0$, and obtain

$$\begin{aligned}
&\int_\Omega \frac{\Re((1+\tilde{\beta}\chi_B)\gamma_0)}{\Re(\gamma_\omega/\alpha)} \Re(\gamma_\omega/\alpha - (1+\tilde{\beta}\chi_B)\gamma_0) \left|\nabla u_{\gamma_2}^{(g)}\right|^2 \,\mathrm{d}x \\
&\quad\leq \int_{\partial\Omega} \overline{g} \left(\Lambda((1+\tilde{\beta}\chi_B)\gamma_0) - \Re\left(\Lambda(\gamma_\omega/\alpha)\right)\right) g \,\mathrm{d}s \\
&\quad\leq \int_\Omega \left(\Re(\gamma_\omega/\alpha - (1+\tilde{\beta}\chi_B)\gamma_0) + \frac{\Im(\gamma_\omega/\alpha)^2}{\Re(\gamma_\omega/\alpha)}\right) \left|\nabla u_{\gamma_2}^{(g)}\right|^2 \,\mathrm{d}x.
\end{aligned}$$

For the case $B \subseteq D$, with Lemma 3.2.4 it follows

$$\begin{aligned}
&\int_D \frac{(1+\tilde{\beta}\chi_B)\gamma_0}{\Re(\gamma_\omega/\alpha)} \sigma_D \left(\frac{\epsilon_\Omega}{\sigma_\Omega} C' - \tilde{\beta}\chi_B\right) \left|\nabla u_{\gamma_2}^{(g)}\right|^2 \,\mathrm{d}x \\
&\quad\leq \int_{\partial\Omega} \overline{g} \left(\Lambda((1+\tilde{\beta}\chi_B)\gamma_0) - \Re\left(\alpha\Lambda(\gamma_\omega)\right)\right) g \,\mathrm{d}s \qquad (3.12) \\
&\quad\leq \int_D (\epsilon_D C - \tilde{\beta}\sigma_D\chi_B) \left|\nabla u_{\gamma_2}^{(g)}\right|^2 \,\mathrm{d}x. \qquad (3.13)
\end{aligned}$$

(a) We first show that

$$B \subseteq D \quad \text{implies} \quad \Re\left(\alpha\Lambda(\gamma_\omega)\right) \leq \Lambda((1+\tilde{\beta}\chi_B)\gamma_0) \quad \text{if} \quad c > 0$$

or

$$B \subseteq D \quad \text{implies} \quad \Re\left(\alpha\Lambda(\gamma_\omega)\right) \geq \Lambda((1+\tilde{\beta}\chi_B)\gamma_0) \quad \text{if} \quad c < 0.$$

If we consider the case where $c > 0$, then $B \subseteq D$, $\tilde{\beta} \leq \frac{\epsilon_\Omega}{\sigma_\Omega} C'$ and inequality (3.12) yield

$$\int_{\partial\Omega} \overline{g} \left(\Lambda((1+\tilde{\beta}\chi_B)\gamma_0) - \Re\left(\alpha\Lambda(\gamma_\omega)\right)\right) g \,\mathrm{d}s \geq 0$$

so that $\Re\left(\alpha\Lambda(\gamma_\omega)\right) \leq \Lambda((1+\tilde{\beta}\chi_B)\gamma_0)$.

If $c < 0$, then $B \subseteq D$, $\tilde{\beta} \geq \frac{\epsilon_D}{\sigma_D} C$ and inequality (3.13) yield

$$\int_{\partial\Omega} \overline{g} \left(\Lambda((1+\tilde{\beta}\chi_B)\gamma_0) - \Re\left(\alpha\Lambda(\gamma_\omega)\right) \right) g \, \mathrm{d}s \leq 0$$

so that $\Re\left(\alpha\Lambda(\gamma_\omega)\right) \geq \Lambda((1+\tilde{\beta}\chi_B)\gamma_0)$.

(b) To show that

$$\Re\left(\alpha\Lambda(\gamma_\omega)\right) \leq \Lambda((1+\tilde{\beta}\chi_B)\gamma_0) \quad \text{implies} \quad B \subseteq D \quad \text{if} \quad c > 0$$

or

$$\Re\left(\alpha\Lambda(\gamma_\omega)\right) \geq \Lambda((1+\tilde{\beta}\chi_B)\gamma_0) \quad \text{implies} \quad B \subseteq D \quad \text{if} \quad c < 0,$$

we apply the technique of localized potentials [Geb08, HU] (where [HU] is the paper version of Chapter 1). Let $B \not\subseteq D$ and $\tilde{\beta} > 0$ if $c > 0$ or $\tilde{\beta} < 0$ if $c < 0$. Then we can choose a smaller open subset $B' \subseteq B$ with $\overline{B'} \cap D = \emptyset$. Since $D \subset \Omega$ and $\Omega \setminus D$ is connected, we obtain from [HU, Theorem 3.6] (Theorem 1.3.6) a sequence of currents $(g_k)_{k\in\mathbb{N}} \subset L^2_\diamond(\partial\Omega)$ so that the solutions $(u^{(g_k)})_{k\in\mathbb{N}} \subset H^1_\diamond(\Omega)$ of

$$\Delta u^{(g_k)} = 0, \quad \partial_\nu u^{(g_k)}|_{\partial\Omega} = g_k$$

fulfill

$$\lim_{k\to\infty} \int_{B'} |\nabla u^{(g_k)}|^2 \, \mathrm{d}x = \infty \quad \text{and} \quad \lim_{k\to\infty} \int_{D} |\nabla u^{(g_k)}|^2 \, \mathrm{d}x = 0.$$

Since γ_0 is constant on $\Omega \setminus D$, [HU, Lemma 3.7] (Lemma 1.3.7) yields that also the corresponding solutions $(u_0^{(g_k)})_{k\in\mathbb{N}} \subset H^1_\diamond(\Omega)$ of (3.1) fulfill

$$\lim_{k\to\infty} \int_{B'} |\nabla u_0^{(g_k)}|^2 \, \mathrm{d}x = \infty \quad \text{and} \quad \lim_{k\to\infty} \int_{D} |\nabla u_0^{(g_k)}|^2 \, \mathrm{d}x = 0.$$

If $c > 0$, it follows from (3.11) that

$$\int_{\partial\Omega} \overline{g_k} \left(\Lambda((1+\tilde{\beta}\chi_B)\gamma_0) - \Re\left(\alpha\Lambda(\gamma_\omega)\right) \right) g_k \, \mathrm{d}s \to -\infty,$$

which shows that $\Re\left(\alpha\Lambda(\gamma_\omega)\right) \not\leq \Lambda((1+\tilde{\beta}\chi_B)\gamma_0)$.

If $c < 0$, it follows from (3.10) that

$$\int_{\partial\Omega} \overline{g_k} \left(\Lambda((1+\tilde{\beta}\chi_B)\gamma_0) - \Re\left(\alpha\Lambda(\gamma_\omega)\right) \right) g_k \, \mathrm{d}s \to \infty,$$

which shows that $\Re\left(\alpha\Lambda(\gamma_\omega)\right) \not\geq \Lambda((1+\tilde{\beta}\chi_B)\gamma_0)$.

□

Remark 3.2.5. The theory of Theorem 3.2.2 can be applied to more general complex admittivities. As before, let the imaging domain consists of a homogeneous background medium with an anomaly region D. Furthermore, let $\omega > 0$ be a fixed frequency, σ_Ω and $\epsilon_\Omega = \epsilon_\Omega(\omega)$ be real constants. Then we consider the complex admittivities (for $\omega = 0$ and fixed $\omega > 0$)

$$\gamma_0(x) = \begin{cases} \gamma_0^{(\Omega)}(x) \equiv \sigma_\Omega & \text{for } x \in \Omega \setminus D, \\ \gamma_0^{(D)}(x) = \hat{\sigma}_D(x) & \text{for } x \in D, \end{cases}$$

$$\gamma_\omega(x) = \begin{cases} \gamma_\omega^{(\Omega)}(x) \equiv \sigma_\Omega + \mathrm{i}\omega\epsilon_\Omega & \text{for } x \in \Omega \setminus D, \\ \gamma_\omega^{(D)}(x) = \hat{\sigma}_D(x) + \mathrm{i}\omega\hat{\epsilon}_D(x) & \text{for } x \in D. \end{cases}$$

When either

$$\frac{\epsilon_D}{\sigma_D} > \frac{\epsilon_\Omega}{\sigma_\Omega} \quad \text{with} \quad \sigma_D := \operatorname{ess\,sup}(\hat{\sigma}_D) \text{ and } \epsilon_D := \operatorname{ess\,inf}(\hat{\epsilon}_D) \tag{3.14}$$

or

$$\frac{\epsilon_D}{\sigma_D} < \frac{\epsilon_\Omega}{\sigma_\Omega} \quad \text{with} \quad \sigma_D := \operatorname{ess\,inf}(\hat{\sigma}_D) \text{ and } \epsilon_D := \operatorname{ess\,sup}(\hat{\epsilon}_D) \tag{3.15}$$

is fulfilled, Theorem 3.2.2 still holds. It can be easily checked that the inequalities in (3.12) and (3.13) still hold with (3.14) and (3.15), respectively. Even for complex admittivities with frequency depend $\Re(\gamma_\omega(x)) = \hat{\sigma}_D^\omega(x)$ as in [HS09], the general theory of Theorem 3.2.2 can be applied to this case.

3.3 Electrode measurements

3.3.1 The setting

In a realistic setting, the currents will be applied using a finite number of electrodes $\mathcal{E}_l \subset \partial\Omega$, $l = 1, \ldots, m$ (well-separated domains in $\partial\Omega$) that are attached to the surface of the imaging domain. We assume that the electrodes are perfectly conducting and that contact impedances are negligible (the SM, cf., e.g., [CIN99]). Driving a current $I_l \in \mathbb{C}$ through the l-th electrode, respectively, with $\sum_{l=1}^m I_l = 0$, the electric potential is given by the solution $u_{\gamma_\omega} \in H^1_{\mathcal{E}}(\Omega)$ of the variational formulation of the SM

$$\sum_{l=1}^m I_l v|_{\mathcal{E}_l} = \int_\Omega \gamma_\omega \nabla u_{\gamma_\omega} \cdot \nabla v \, \mathrm{d}x \quad \forall v \in H^1_{\mathcal{E}}(\Omega), \tag{3.16}$$

where $H^1_{\mathcal{E}}(\Omega)$ is the subspace of H^1-functions that are locally constant on each $\mathcal{E}_l$, $l = 1, \ldots, m$, and these constants sum up to zero. The existence of an unique solution is a consequence of the Lax-Milgram theorem. Typically, one describes the SM by the equations (3.17)-(3.20) below that are more suitable to show the physical interpretation but have to be understood in an appropriate weak sense, cf., e.g., [SCI92, Hyv04, SD13]. In this formulation, the inner potential u_{γ_ω} fulfill

$$\nabla \cdot (\gamma_\omega \nabla u_{\gamma_\omega}) = 0 \quad \text{in} \quad \Omega, \tag{3.17}$$

with boundary conditions

$$\int_{\mathcal{E}_l} \gamma_\omega \partial_\nu u_{\gamma_\omega} \, \mathrm{d}s = I_l \tag{3.18}$$

$$u_{\gamma_\omega}|_{\mathcal{E}_l} = \text{const.} \tag{3.19}$$

for all $l = 1, 2, \ldots, m$, and

$$\gamma_\omega \partial_\nu u_{\gamma_\omega} = 0 \quad \text{on} \quad \partial\Omega \setminus \bigcup_{l=1}^{m} \mathcal{E}_l, \tag{3.20}$$

where ν is the outer normal on the boundary of Ω. We assume that the voltage-current measurements are carried out in the following complete dipole-dipole configuration. Let (j_r, k_r), $r = 1, \ldots, N$, be a set of electrode pairs with $j_r \neq k_r$. For each of these pairs, $r = 1, \ldots, N$, a current of $I = 1$ and $I = -1$ is driven through the j_r-th and the k_r-th electrode, respectively. The other electrodes are kept insulating. The resulting electric potential inside the imaging domain is given by the solution $u_{\gamma_\omega}^{\langle r \rangle} \in H^1_{\mathcal{E}}(\Omega)$ of (3.16) with $I_l = \delta_{j_r l} - \delta_{k_r l}$.

While the current is driven through the r-th pair of electrodes, we measure the required voltage difference on all pairs of electrodes, i.e., between the j_s and the k_s electrode for all $s = 1, \ldots, N$. We collect these measurements in the matrix

$$R(\gamma_\omega) = \left(u_{\gamma_\omega}^{\langle r \rangle}|_{\mathcal{E}_{j_s}} - u_{\gamma_\omega}^{\langle r \rangle}|_{\mathcal{E}_{k_s}} \right)_{r,s=1,\ldots,N} \in \mathbb{C}^{N \times N}.$$

Let us comment on our use of the shunt electrode model. It seems to be widely accepted that the most accurate electrode model in EIT is the *complete electrode model*, cf., e.g., [CIN99], where not only the shunting effects but also contact impedances between the electrodes and the imaging domain are taken into account (see also Chapter 2). The effect of contact impedances is often neglected in the case that voltages are not measured on current driven electrodes. To setup our matrix R, we do however require that the same electrode pairs are used for measuring voltages and applying currents, and the three main diagonals in R correspond to measurements where voltages are measured on non-insulated electrodes.

Contact impedances can also be neglected in the case of DC difference measurements on point electrodes, see [HHH11]. Since our comparison of two different measurements is widely analogous to difference measurements, we believe that our use of the SM is justified for sufficiently small electrodes.

3.3.2 Monotonicity results for the shunt model

As in the continuous case, we will compare measurements in the sense of operator definiteness. We define the self-adjoint part of a matrix $A \in \mathbb{C}^{N\times N}$ by

$$\Re(A) := \frac{1}{2}(A + A^*),$$

where $A^* \in \mathbb{C}^{N\times N}$ is the adjoint (conjugate transpose) of A, i.e.,

$$(Ah)^* g = h^* A^* g \quad \text{for all } g, h \in \mathbb{C}^N.$$

Obviously, $\Re(A)$ is self-adjoint.

For two self-adjoint matrices $A, B \in \mathbb{C}^{N\times N}$, we write $A \leq B$ if $B - A$ is positive semidefinite, i.e.,

$$g^*(B - A)g \geq 0 \quad \forall g \in \mathbb{C}^N.$$

This is equivalent to the fact that all eigenvalues of $B - A$ are non-negative.

Note that the entries of the measurement matrix $R(\gamma_\omega)$ satisfy

$$\begin{aligned} u^{\langle r\rangle}_{\gamma_\omega}|_{\mathcal{E}_{j_s}} - u^{\langle r\rangle}_{\gamma_\omega}|_{\mathcal{E}_{k_s}} &= \sum_{l=1}^{m} \left(\delta_{j_s,l} - \delta_{k_s,l}\right) u^{\langle r\rangle}_{\gamma_\omega}|_{\mathcal{E}_{k_l}} \\ &= \int_\Omega \gamma_\omega \nabla u^{\langle s\rangle}_{\gamma_\omega} \cdot \nabla u^{\langle r\rangle}_{\gamma_\omega} \,\mathrm{d}x = u^{\langle s\rangle}_{\gamma_\omega}|_{\mathcal{E}_{j_r}} - u^{\langle s\rangle}_{\gamma_\omega}|_{\mathcal{E}_{k_r}}. \end{aligned}$$

Hence, $R(\gamma_\omega)$ is a symmetric, but generally (for complex γ_ω) not a self-adjoint matrix. This also implies that $\Re(R(\gamma_\omega))$ coincides with the matrix obtained by taking the real part of each voltage measurement

$$\Re(R(\gamma_\omega)) = \left(\Re(u^{\langle r\rangle}_{\gamma_\omega})|_{\mathcal{E}_{j_s}} - \Re(u^{\langle r\rangle}_{\gamma_\omega})|_{\mathcal{E}_{k_s}}\right)_{r,s=1,\dots,N} \in \mathbb{R}^{N\times N}.$$

The monotonicity estimate from the continuous case can be extended to the case of electrode measurements.

Lemma 3.3.1. *Let $\gamma_1, \gamma_2 \in L^\infty_+(\Omega;\mathbb{R}) + \mathrm{i}L^\infty(\Omega;\mathbb{R})$, $g = (g_r)_{r=1}^N \in \mathbb{C}^N$ and $u^{[g]}_{\gamma_\tau} \in H^1_{\mathcal{E}}(\Omega)$ ($\tau = 1, 2$) denote the solution of*

$$\sum_{l=1}^{m} \left(\sum_{r:\ j_r = l} g_r - \sum_{r:\ k_r = l} g_r \right) \overline{v|_{\mathcal{E}_l}} = \int_\Omega \gamma_\omega \nabla u_{\gamma_\omega} \cdot \overline{\nabla v} \,\mathrm{d}x \quad \forall v \in H^1_{\mathcal{E}}(\Omega). \tag{3.21}$$

Then

$$\begin{aligned} &\int_\Omega \left(\frac{\Re(\gamma_2)}{\Re(\gamma_1)} \Re(\gamma_1 - \gamma_2) - \frac{\Im(\gamma_2)^2}{\Re(\gamma_1)} \right) \left|\nabla u^{[g]}_{\gamma_2}\right|^2 \,\mathrm{d}x \\ &\quad \leq \ g^* \,\Re\left(R(\gamma_2) - R(\gamma_1)\right) g \leq \int_\Omega \left(\Re(\gamma_1 - \gamma_2) + \frac{\Im(\gamma_1)^2}{\Re(\gamma_1)} \right) \left|\nabla u^{[g]}_{\gamma_2}\right|^2 \,\mathrm{d}x. \end{aligned}$$

The proof of Lemma 3.3.1 is postponed to the end of this section.

3.3.3 Detecting inclusions from electrode measurements

We make the same assumptions as for the continuous case in Subsection 3.2.3. The inclusion (or anomaly) $D \subset \Omega$ is assumed to be a closed set with connected complement. γ_0 and γ_ω are assumed to be given by

$$\gamma_0(x) = \begin{cases} \gamma_0^{(\Omega)} = \sigma_\Omega & \text{for } x \in \Omega, \\ \gamma_0^{(D)} = \sigma_D & \text{for } x \in D, \end{cases}$$
$$\gamma_\omega(x) = \begin{cases} \gamma_\omega^{(\Omega)} = \sigma_\Omega + \mathrm{i}\omega\epsilon_\Omega & \text{for } x \in \Omega, \\ \gamma_\omega^{(D)} = \sigma_D + \mathrm{i}\omega\epsilon_D & \text{for } x \in D, \end{cases}$$

with constants $\sigma_\Omega, \sigma_D, \epsilon_\Omega, \epsilon_D > 0$. The anomaly is assumed to fulfill the contrast condition (3.5), i.e., $\epsilon_D\sigma_\Omega - \epsilon_\Omega\sigma_D \neq 0$. The parameter

$$\alpha := \frac{\gamma_\omega^{(\Omega)}}{\gamma_0^{(\Omega)}} = 1 + \mathrm{i}\omega\frac{\epsilon_\Omega}{\sigma_\Omega}$$

denotes the ratio of the background conductivities.

Remark 3.3.2. As in Section 3.2 (see Remark 3.2.5), the theory of this section can be applied to a more general class of complex conductivities.

Our results for continuous boundary data motivate to compare (for sufficiently small modulation strengths $\beta > 0$) the matrix of ultrasound-modulated DC measurements $R((1+\beta\chi_B)\gamma_0)$ with the (self-adjoint part of the ratio-weighted) matrix of measurements taken at a non-zero frequency $R(\gamma_\omega)$. This comparison (in the sense of matrix definiteness) should yield information about whether the focusing region B lies inside the unknown inclusion D. In the next subsection we will prove the following theorem.

Theorem 3.3.3. *Let $c := \epsilon_D\sigma_\Omega - \epsilon_\Omega\sigma_D \neq 0$. For sufficiently small $\beta > 0$ and every open set $B \subseteq \Omega$, it holds that*

$$B \subseteq D \quad \textit{implies that} \quad \Re\left(\alpha R(\gamma_\omega)\right) \begin{cases} \leq R((1+\beta\chi_B)\gamma_0) & \textit{if } c > 0, \\ \geq R((1-\beta\chi_B)\gamma_0) & \textit{if } c < 0. \end{cases} \tag{3.22}$$

The constant $\beta > 0$ is sufficiently small if

$$\beta \leq \begin{cases} \frac{\epsilon_\Omega}{\sigma_\Omega}C' & \textit{if } c > 0, \\ -\frac{\epsilon_D}{\sigma_D}C & \textit{if } c < 0, \end{cases}$$

where

$$C := \omega^2\frac{c}{\sigma_D\sigma_\Omega + \omega^2\epsilon_D\epsilon_\Omega} \quad \textit{and} \quad C' := \omega^2\frac{\sigma_\Omega}{\sigma_D}\cdot\frac{c}{\sigma_\Omega^2 + \omega^2\epsilon_\Omega^2}.$$

The converse of the implication (3.27) will generally not be true in the case of measurements with a finite number of electrodes. However, when we increase the number of electrodes used for the measurements, then we can expect that the measurement matrices $R(\gamma_\omega)$ and $R((1+\beta\chi_B)\gamma_0)$ more and more resemble their continuous counterparts, the Neumann-to-Dirichlet operators, cf. the works of Hakula, Hyvönen and Lechleiter [Hyv04, LHH08, Hyv09]. In fact, we can give the following intuitive justification in the spirit of [HSW10].

Remark 3.3.4. Let $B \not\subseteq D$ and $\beta > 0$. If there exists a current pattern $g = (g_r)_{r=1}^N \in \mathbb{C}^N$ such that the resulting DC potential

$$u_{\gamma_0}^{[g]} := \sum_{r=1}^N g_r u_{\gamma_0}^{\langle r\rangle}$$

possesses a very large energy in $B \setminus D$ and a very small energy in D, then

$$\Re\left(\alpha R(\gamma_\omega)\right) \not\leq R((1+\beta\chi_B)\gamma_0) \quad \text{if} \quad c > 0$$

or

$$\Re\left(\alpha R(\gamma_\omega)\right) \not\geq R((1-\beta\chi_B)\gamma_0) \quad \text{if} \quad c < 0.$$

3.3.4 Proof of the main results for electrode measurements

Proof of Lemma 3.3.1.

Let $g = (g_r)_{r=1}^N \in \mathbb{C}^N$. First note that for $\tau = 1, 2$, by linearity,

$$u_{\gamma_\tau}^{[g]} = \sum_{r=1}^N u_{\gamma_\tau}^{\langle r\rangle} g_r \quad \text{and} \quad \sum_{r=1}^N g_r \left(u_{\gamma_\tau}^{\langle r\rangle}|_{\mathcal{E}_{j_s}} - u_{\gamma_\tau}^{\langle r\rangle}|_{\mathcal{E}_{k_s}}\right) = u_{\gamma_\tau}^{[g]}|_{\mathcal{E}_{j_s}} - u_{\gamma_\tau}^{[g]}|_{\mathcal{E}_{k_s}}.$$

We thus obtain

$$\begin{aligned} g^* R(\gamma_1) g &= \sum_{s=1}^N \overline{g_s} \left(u_{\gamma_1}^{[g]}|_{\mathcal{E}_{j_s}} - u_{\gamma_1}^{[g]}|_{\mathcal{E}_{k_s}}\right) \\ &= \sum_{l=1}^m \left(\sum_{s:\ j_s=l} \overline{g_s} - \sum_{s:\ k_s=l} \overline{g_s} \right) u_{\gamma_1}^{[g]}|_{\mathcal{E}_l} \\ &= \int_\Omega \overline{\gamma_1 \nabla u_{\gamma_1}^{[g]}} \cdot \nabla u_{\gamma_1}^{[g]} \,\mathrm{d}x = \int_\Omega \overline{\gamma_1} \left|\nabla u_{\gamma_1}^{[g]}\right|^2 \mathrm{d}x \end{aligned}$$

or

$$= \int_\Omega \overline{\gamma_2 \nabla u_{\gamma_2}^{[g]}} \cdot \nabla u_{\gamma_1}^{[g]} \,\mathrm{d}x$$

and likewise

$$g^* R(\gamma_2) g = \int_\Omega \overline{\gamma_2} \left|\nabla u_{\gamma_2}^{[g]}\right|^2 \mathrm{d}x = \int_\Omega \overline{\gamma_1 \nabla u_{\gamma_1}^{[g]}} \cdot \nabla u_{\gamma_2}^{[g]} \mathrm{d}x.$$

Hence, the assertion follows from Lemma 3.2.3. □

Proof of Theorem 3.3.3 and justification of Remark 3.3.4. Let $\tilde{\beta} := \beta$ if $c > 0$ and $\tilde{\beta} := -\beta$ if $c < 0$. As in the proof of Theorem 3.2.2, we obtain (from Lemma 3.2.4 and 3.3.1 instead of Lemma 3.2.4 and 3.2.1)

$$\begin{aligned}
&\frac{\epsilon_\Omega \sigma_D}{\sigma_\Omega} C \int_D \left|\nabla u_{\gamma_0}^{[g]}\right|^2 \mathrm{d}x - \int_B \tilde{\beta}\gamma_0 \left|\nabla u_{\gamma_0}^{[g]}\right|^2 \mathrm{d}x \\
&\quad \leq \quad g^* \left(R((1+\tilde{\beta}\chi_B)\gamma_0) - \Re\left(\alpha R(\gamma_\omega)\right)\right) g \qquad (3.23) \\
&\quad \leq \quad \epsilon_D C \int_D \left|\nabla u_{\gamma_0}^{[g]}\right|^2 \mathrm{d}x - \int_B \frac{\tilde{\beta}}{1+\tilde{\beta}} \gamma_0 \left|\nabla u_{\gamma_0}^{[g]}\right|^2 \mathrm{d}x. \qquad (3.24)
\end{aligned}$$

For $B \subseteq D$, as in the proof of Theorem 3.2.2, with $\gamma_2 := (1+\tilde{\beta}\chi_B)\gamma_0$ we obtain

$$\begin{aligned}
&\int_D \frac{(1+\tilde{\beta}\chi_B)\gamma_0}{\Re(\gamma_\omega/\alpha)} \sigma_D \left(\frac{\epsilon_\Omega}{\sigma_\Omega} C' - \tilde{\beta}\chi_B \right) \left|\nabla u_{\gamma_2}^{[g]}\right|^2 \mathrm{d}x \\
&\quad \leq \quad g^* \left(R((1+\tilde{\beta}\chi_B)\gamma_0) - \Re\left(\alpha R(\gamma_\omega)\right)\right) g \qquad (3.25) \\
&\quad \leq \quad \int_D (\epsilon_D C - \tilde{\beta}\sigma_D \chi_B) \left|\nabla u_{\gamma_2}^{[g]}\right|^2 \mathrm{d}x. \qquad (3.26)
\end{aligned}$$

If we consider the case $c > 0$, then $B \subseteq D$, $\tilde{\beta} \leq \frac{\epsilon_\Omega}{\sigma_\Omega} C'$ and inequality (3.25) yield

$$g^* \left(R((1+\tilde{\beta}\chi_B)\gamma_0) - \Re\left(\alpha R(\gamma_\omega)\right)\right) g \geq 0$$

so that $\Re\left(\alpha R(\gamma_\omega)\right) \leq R((1+\tilde{\beta}\chi_B)\gamma_0)$.

If we consider the case $c < 0$, then $B \subseteq D$, $\tilde{\beta} \geq \frac{\epsilon_D}{\sigma_D} C$ and inequality (3.26) yield

$$g^* \left(R((1+\tilde{\beta}\chi_B)\gamma_0) - \Re\left(\alpha R(\gamma_\omega)\right)\right) g \leq 0$$

so that $\Re\left(\alpha R(\gamma_\omega)\right) \geq R((1+\tilde{\beta}\chi_B)\gamma_0)$. This proves Theorem 3.3.3.

To justify Remark 3.3.4 we assume that, $B \not\subseteq D$ and that there exists $g \in \mathbb{C}^N$ so that $\int_{B\setminus D} |\nabla u_{\gamma_0}^{[g]}|^2 \mathrm{d}x$ is very large and $\int_D |\nabla u_{\gamma_0}^{[g]}|^2 \mathrm{d}x$ is very small. Then, with (3.23) and (3.24) we obtain

$$g^* \left(R((1+\tilde{\beta}\chi_B)\gamma_0) - \Re\left(\alpha R(\gamma_\omega)\right)\right) g \begin{cases} \not\geq 0 & \text{if} \quad c > 0, \\ \not\leq 0 & \text{if} \quad c < 0. \end{cases}$$

□

3.4 Numerical results

In this section we numerically test the monotonicity relation of Theorem 3.3.3 (for the practically relevant electrode setting of Section 3.3.1). Moreover, we present shape reconstructions of conductivity anomalies based on Theorem 3.3.3 and motivated by Remark 3.3.4.

3.4.1 Basic notations and assumptions

We consider electrode settings as described in Section 3.3.1. Let the conductivities γ_0 (DC) and γ_ω (AC) inside the imaging subject Ω be as described in Subsection 3.3.3. Furthermore, let m denote the number of electrodes $\mathcal{E}_1, \mathcal{E}_2, ..., \mathcal{E}_m$ attached to $\partial\Omega$ and let $(j_r, k_r) = (r, r+1)$, $r = 1, ..., m-1$, and $(j_m, k_m) = (m, 1)$ describe the dipole-dipole configuration as in the notation of Section 3.3.1. Then, for a ball-shaped focused ultrasound region B, Theorem 3.3.3 states that

$$B \subseteq D \tag{3.27}$$

implies

$$\Re\left(\alpha R(\gamma_\omega)\right) \begin{cases} \leq R((1+\beta\chi_B)\gamma_0) & \text{if } c > 0, \\ \geq R((1-\beta\chi_B)\gamma_0) & \text{if } c < 0, \end{cases} \tag{3.28}$$

with properly chosen β and $c := \epsilon_D\sigma_\Omega - \epsilon_\Omega\sigma_D \neq 0$. Since the matrices on both sides of inequality (3.28) are self-adjoint (cf. Section 3.3.2), it suffices to consider the eigenvalues of the difference operator of these matrices for checking this inequality.

For all numerical results, according to the assumptions of Theorem 3.3.3, the parameter β is set to

$$\beta = \begin{cases} \frac{\epsilon_\Omega}{\sigma_\Omega} C' & \text{for } c > 0, \\ -\frac{\epsilon_D}{\sigma_D} C & \text{for } c < 0, \end{cases} \quad \text{up to the fourth decimal,}$$

where

$$C := \omega^2 \frac{c}{\sigma_D\sigma_\Omega + \omega^2\epsilon_D\epsilon_\Omega} \quad \text{and} \quad C' := \omega^2 \frac{\sigma_\Omega}{\sigma_D} \cdot \frac{c}{\sigma_\Omega^2 + \omega^2\epsilon_\Omega^2}.$$

The frequency ω is set to $2\pi \cdot 100$ (Hz). For all numerical tests, the unit of length is specified in cm while all other units are given by the standard units. For the numerical results, the finite element method (implemented with MATLAB® and the commercial FEM-software COMSOL®) was used to compute the solutions of the SM numerically.

3.4.2 Basic monotonicity tests

In this subsection we numerically verify the monotonicity relation of Theorem 3.3.3 for a two- as well as a three-dimensional toy setting. To this end, for a test ball

$B \subseteq D$, we check whether all eigenvalues $\lambda_1, \dots, \lambda_m$ of

$$R((1+\beta\chi_B)\gamma_0) - \Re\left(\alpha R(\gamma_\omega)\right) \quad \text{or} \quad \mathrm{R}((1-\beta\chi_B)\gamma_0) - \Re\left(\alpha R(\gamma_\omega)\right)$$

are non-negative (if $c > 0$) or non-positive (if $c < 0$), respectively. Moreover, we numerically check whether this is not the case for some test balls outside D. Let us remind that the latter will be the case if the electrode setting is sufficiently well-chosen in the sense of Remark 3.3.4.

In our numerical tests, we can only expect to determine the eigenvalues λ_i with a finite precision up to $\lambda_i^\delta \in (\lambda_i - \delta, \lambda_i + \delta)$ for some $\delta > 0$. To take this into account, for $i = 1, 2, \dots, m$, we test

$$\lambda_i \begin{cases} > -\delta & \text{if } c > 0, \\ < \delta & \text{if } c < 0. \end{cases} \tag{3.29}$$

To approximate an error bound δ, we calculate the eigenvalues

$$\lambda_1^{\delta_i}(s_i), \lambda_2^{\delta_i}(s_i), \dots, \lambda_m^{\delta_i}(s_i) \quad \text{with} \quad i \in \{1, 2\}$$

for two FEM discretizations with maximal edge size of the FEM elements given by s_1 and $s_2 = s_1/2$. Then we set

$$\delta_{\text{app}} := \max_{j=1,2,\dots,m} (|\lambda_j^{\delta_1}(s_1) - \lambda_j^{\delta_2}(s_2)|) \tag{3.30}$$

as an approximative error bound for the error of the eigenvalues $\lambda_i^{\delta_2}(s_2) \approx \lambda_i$.

In the following, we numerically check the monotonicity relation for a two- as well as for a three-dimensional toy setting.

Example 3.4.1. *We consider the setting illustrated in Figure 3.1. The imaging domain Ω is a circle with radius 10 centered at $(0,0)$ and a circular anomaly D with radius 1.5 is located at $(5,0)$. On the boundary $\partial\Omega$, there are 16 electrodes $\mathcal{E}_1, \mathcal{E}_2, \dots, \mathcal{E}_{16}$ attached. The admittivity γ_ω is set to*

$$\gamma_\omega = \begin{cases} 1 + \mathrm{i}\omega \cdot 1 & \text{in } \Omega \backslash D, \\ 1 + \mathrm{i}\omega \cdot 2 & \text{in } D, \end{cases}$$

while $\gamma_0 \equiv 1$ in Ω. We choose β such that

$$\beta = 0.9999 \leq \frac{\epsilon_\Omega}{\sigma_\Omega} C' = 0.9999\ldots \quad (c > 0).$$

For checking the monotonicity relation, five circular test regions B_1, B_2, B_3, B_4 and B_5, with radii 1.25, are centered at $(0,0), (5,0), (0,5), (-5,0)$ and $(0,-5)$, respectively. Table 3.1 shows the eigenvalues of $R((1+\beta\chi_{B_j})\gamma_0) - \Re\left(\alpha R(\gamma_\omega)\right)$ for $j = 1, \dots, 5$. Only the eigenvalues of B_2 fulfill (3.29). Provided that the approximative error bound δ_{app} is sufficiently large, the balls B_1, B_3, B_4 and B_5 cannot be located inside the anomaly D. Moreover, B_2 is correctly not excluded being a potential subset of the anomaly.

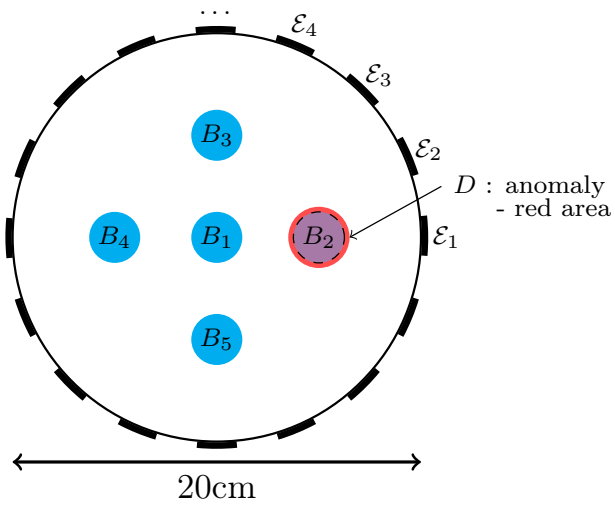

Figure 3.1: Ω is a two-dimensional circular domain with anomaly area D, 16 electrodes $\mathcal{E}_1, \ldots, \mathcal{E}_{16}$ are attached to $\partial\Omega$ and $B_1, \ldots, B_5$ are the five test balls showing the chosen focused ultrasound regions.

Example 3.4.2. *We consider the setting illustrated in Figure 3.2. The imaging domain Ω is a cylindrical domain with*

$$\Omega = \left\{(x_1, x_2, x_3) \in \mathbb{R}^3 \,:\, \|(x_1, x_2, 0)\| < 10,\ 0 < x_3 < 5\right\}$$

and a ball-shaped anomaly D with radius 1.5 is located at $(5, 0, 2.5)$. On the boundary $\partial\Omega$, there are 16 electrodes $\mathcal{E}_1, \mathcal{E}_2, \ldots, \mathcal{E}_{16}$ attached. The admittivity γ_ω is set to

$$\gamma_\omega = \begin{cases} 1 + \mathrm{i}\omega \cdot 1, & \text{in } \Omega\backslash D, \\ 2 + \mathrm{i}\omega \cdot 1, & \text{in } D, \end{cases}$$

while

$$\gamma_0 = \begin{cases} 1, & \text{in } \Omega\backslash D, \\ 2, & \text{in } D. \end{cases}$$

We choose β such that

$$\beta = 0.4999 \leq -\frac{\epsilon_D}{\sigma_D} C = 0.4999\cdots \quad (c < 0).$$

For checking the monotonicity relation, five test balls B_1, B_2, B_3, B_4 and B_5, with radii 1.25, are centered at $(0, 0, 2.5), (5, 0, 2.5), (0, 5, 2.5), (-5, 0, 2.5)$ and $(0, -5, 2.5)$, respectively. Table 3.2 shows the eigenvalues of $R((1 - \beta\chi_{B_j})\gamma_0) - \Re\left(\alpha R(\gamma_\omega)\right)$ for $j = 1, \ldots, 5$. Only the eigenvalues of B_2 fulfill (3.29). As in Example 3.4.1, provided that the approximative error bound δ_{app} is sufficiently large, the balls B_1, B_3, B_4 and B_5 cannot be located inside the anomaly D. Again, B_2 is correctly not excluded being a potential subset of the anomaly.

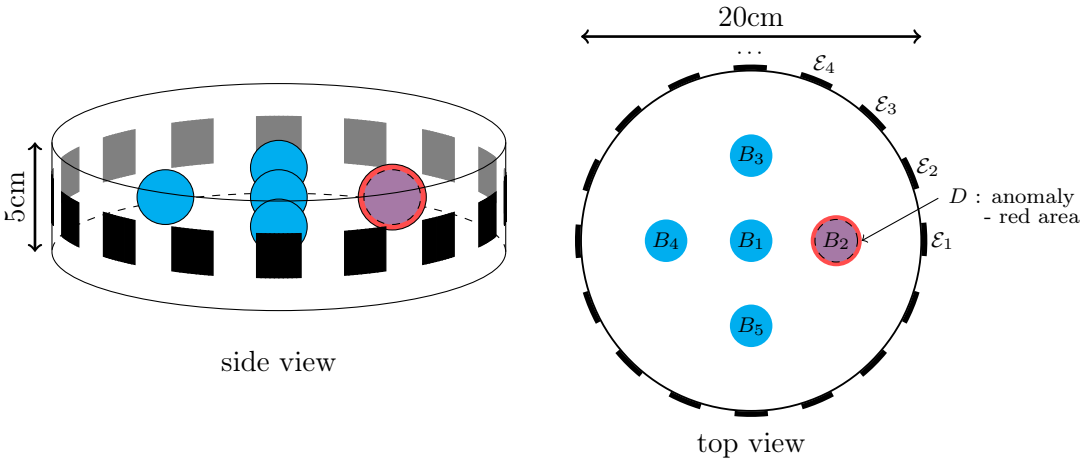

Figure 3.2: Ω is a three-dimensional cylindrical domain with anomaly area D, 16 electrodes $\mathcal{E}_1, \ldots, \mathcal{E}_{16}$ are attached to $\partial\Omega$ and $B_1, \ldots, B_5$ are the five test balls showing the chosen focused ultrasound regions.

B_1	B_2	B_3	B_4	B_5
-0.0024	-0.0000	-0.0098	-0.0105	-0.0098
-0.0024	-0.0000	-0.0097	-0.0104	-0.0097
-0.0000	-0.0000	-0.0003	-0.0004	-0.0003
-0.0000	-0.0000	-0.0002	-0.0003	-0.0002
-0.0000	-0.0000	-0.0000	-0.0000	-0.0000
-0.0000	-0.0000	-0.0000	-0.0000	-0.0000
-0.0000	-0.0000	-0.0000	-0.0000	-0.0000
-0.0000	-0.0000	-0.0000	-0.0000	-0.0000
-0.0000	0.0000	-0.0000	-0.0000	-0.0000
-0.0000	0.0000	-0.0000	0.0000	-0.0000
0.0000	0.0000	0.0000	0.0000	0.0000
0.0000	0.0000	0.0000	0.0000	0.0000
0.0003	0.0004	0.0005	0.0007	0.0005
0.0006	0.0005	0.0007	0.0009	0.0007
0.0142	0.0048	0.0146	0.0153	0.0146
0.0145	0.0049	0.0148	0.0155	0.0148

Table 3.1: This table presents the eigenvalues of $R((1 + \beta\chi_{B_j})\gamma_0) - \Re(\alpha R(\gamma_\omega))$, $j = 1, \ldots, 5$, for Example 3.4.1 with approximative error bound $\delta_{\text{app}} < 0.0024$.

B_1	B_2	B_3	B_4	B_5
-0.1639	-0.0800	-0.1667	-0.1723	-0.1668
-0.1621	-0.0785	-0.1642	-0.1696	-0.1642
-0.0052	-0.0054	-0.0065	-0.0079	-0.0065
-0.0034	-0.0041	-0.0045	-0.0060	-0.0045
-0.0001	-0.0003	-0.0002	-0.0003	-0.0002
-0.0000	-0.0001	-0.0000	-0.0001	-0.0000
-0.0000	-0.0000	-0.0000	-0.0000	-0.0000
-0.0000	-0.0000	-0.0000	-0.0000	-0.0000
-0.0000	-0.0000	-0.0000	0.0000	-0.0000
0.0000	-0.0000	0.0000	0.0000	0.0000
0.0000	-0.0000	0.0000	0.0000	0.0000
0.0000	-0.0000	0.0000	0.0001	0.0000
0.0001	-0.0000	0.0011	0.0019	0.0011
0.0001	0.0000	0.0017	0.0025	0.0017
0.0169	0.0000	0.0728	0.0788	0.0717
0.0173	0.0000	0.0749	0.0822	0.0753

Table 3.2: This table presents the eigenvalues of $R((1 - \beta\chi_{B_j})\gamma_0) - \Re(\alpha R(\gamma_\omega))$, $j = 1, \ldots, 5$, for Example 3.4.2 with approximative error bound $\delta_{\text{app}} < 0.0173$.

3.4.3 Shape reconstruction of conductivity anomalies

Based on Theorem 3.3.3, for a two-dimensional setting (Example 3.4.4) and a three-dimensional setting (Example 3.4.5), we present the reconstructions of an anomaly region $D = D_1 \cup D_2$ that consists of two separated inclusions D_1 and D_2 inside a subject Ω. In both settings the admittivity γ_ω is set to

$$\gamma_\omega = \begin{cases} 1 + \mathrm{i}\omega \cdot 2 & \text{in } \Omega \backslash D, \\ 1 + \mathrm{i}\omega \cdot 1 & \text{in } D, \end{cases}$$

while $\gamma_0 \equiv 1$ in Ω. Accordingly, we choose β such that

$$\beta = 0.4999 \leq -\frac{\epsilon_\Omega}{\sigma_\Omega} C' = 0.4999 \ldots \quad (c < 0).$$

For the shape reconstruction examples, we make the following simplifications. First of all, we consider only the FEM-discretized settings and neglect the discretization error itself. We take into account only a fairly small computational error δ_{cp} that arises from numerically computing the measurement data (for the FEM-discretized settings). Second, we test focused ultrasound regions only in appropriately large neighborhoods of the inclusions D_1 and D_2. These simplifications are used to reduce the otherwise enormous computational costs of solving the numerically relatively ill-conditioned SM. Let us refer to Remark 3.4.3 where we comment on these simplifications.

The implementation of the reconstruction method itself, based on Theorem 3.3.3, is quite simple. For a number of test balls B_j, $j = 1, 2, \ldots, N$, it is checked whether all eigenvalues $\lambda_1, \lambda_2, \ldots, \lambda_m$ of $R((1 - \beta\chi_{B_j})\gamma_0) - \Re(\alpha R(\gamma_\omega))$ fulfill the test criterion (3.29) introduced in the previous subsection that is

$$\lambda_i = \lambda_i(B_j) < \delta_{\text{cp}} \quad (\text{for } c < 0 \text{ and } \delta_{\text{cp}} \text{ instead of } \delta_{\text{app}}).$$

Then, the reconstruction is given by the union of all tested balls that fulfill this criterion. Provided that the constant δ_{cp} is well-chosen (see Remark 3.4.6), the method correctly identifies all test balls that are completely covered by the anomaly. Remark 3.3.4 motivates that the more electrodes are used (suitable positioned and sized), the less false positive test balls the method identifies.

Remark 3.4.3. In practice, testing the monotonicity criterion (3.28) requires only ultrasound-modulated DC and weighted AC measurements on the same geometry of interest probed for anomalies and does not require any numerical simulations. Moreover, for a rough localization of inclusions that are expected to be larger than a certain size, it suffices to test balls aligned to a coarse grid. Then one can check the monotonicity criterion for test balls that are aligned to a fine grid only in potentially relevant regions.

Example 3.4.4. *We consider the setting geometry illustrated in Figure 3.3. The imaging domain Ω is a circle with radius 10 centered at $(0, 0)$ and the anomaly is given by $D = D_1 \cup D_2$, where*

$$D_1 = \left\{x = (x_1, x_2) \in \mathbb{R}^2 \,:\, \|x - (-4, -5)\| \leq 2,\ x_2 \geq -5\right\},$$
$$D_2 = [1, 5] \times [4, 7].$$

On the boundary $\partial\Omega$, there are 16 electrodes $\mathcal{E}_1, \mathcal{E}_2, \ldots, \mathcal{E}_{16}$ attached. Figure 3.5 presents the reconstruction of the anomaly D.

Example 3.4.5. *We consider the setting geometry illustrated in Figure 3.4. The imaging domain is a cylindrical subject Ω with*

$$\Omega = \left\{(x_1, x_2, x_3) \in \mathbb{R}^3 \,:\, \|(x_1, x_2, 0)\| < 10,\ x_3 \in (0, 7)\right\}$$

and the anomaly is given by $D = D_1 \cup D_2$, where D_1 and D_2 are cuboids with

$$D_1 = [-6, -5] \times [-1, 1] \times [3, 4],$$
$$D_2 = [4, 5] \times [4, 5] \times [4, 5].$$

On the boundary $\partial\Omega$, there are 32 electrodes $\mathcal{E}_1, \mathcal{E}_2, \ldots, \mathcal{E}_{32}$ attached. Figure 3.6 presents the reconstruction of the anomaly D.

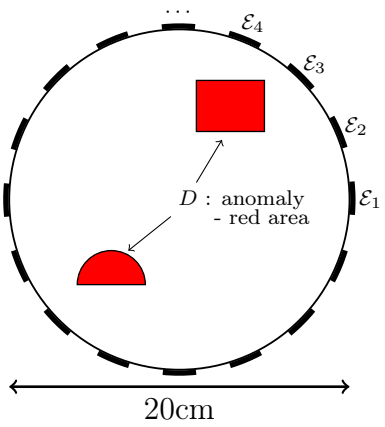

Figure 3.3: Ω is a two-dimensional circular domain with anomaly area D and 16 electrodes $\mathcal{E}_1, \ldots, \mathcal{E}_{16}$ are attached to $\partial\Omega$.

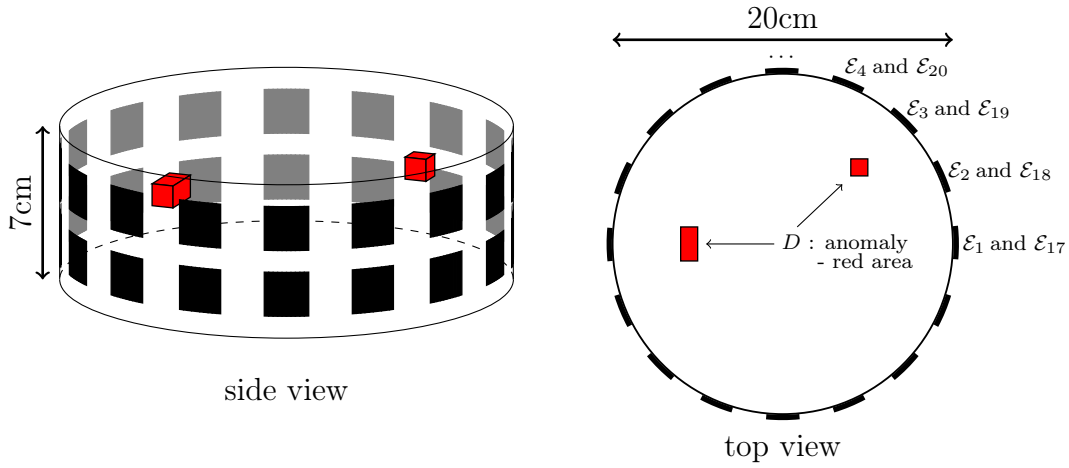

Figure 3.4: Ω is a three-dimensional cylindrical domain with anomaly area D and 32 electrodes $\mathcal{E}_1, \ldots, \mathcal{E}_{32}$ are attached to $\partial\Omega$. The first 16 and the last 16 electrodes are located in a lower circular and in an upper circular region, respectively.

Remark 3.4.6. To heuristically determine a value for δ_{cp}, we considered the values

$$\lambda^j_{\max} := \max\left(\operatorname{eig}\left(R((1-\beta\chi_{B_j})\gamma_0) - \Re\left(\alpha R(\gamma_\omega)\right)\right)\right) \tag{3.31}$$

for all tested balls B_j. Figure 3.7 shows that there is a noticeable gap between some values accumulating close to zero and the remaining values. For the reconstructions, we choose δ_{cp} to be a value that is located inside such a gap. The second row of Figure 3.7 shows two candidates. Since there is no new gap in the rightmost plot, the second candidate seems to be the better choice.

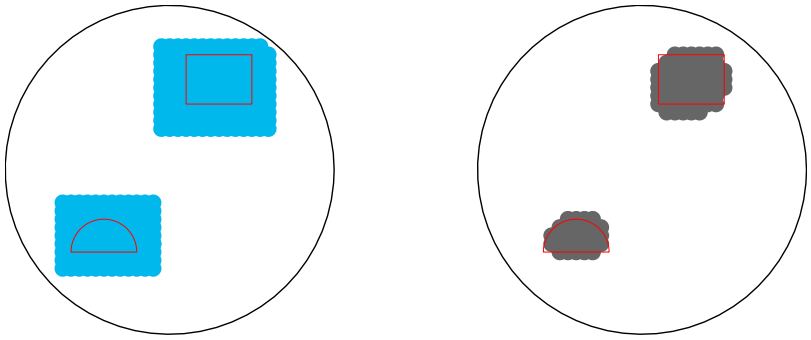

(a) Tested balls. **(b)** Reconstruction.

Figure 3.5: Results for the setting in Example 3.4.4 with $\delta_{\text{cp}} = 0.5 \cdot 10^{-7}$. The anomaly area D is framed in red.

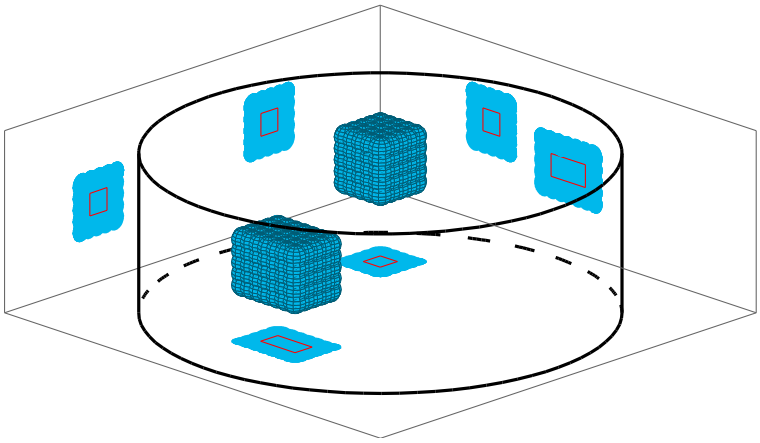

(a) Tested balls.

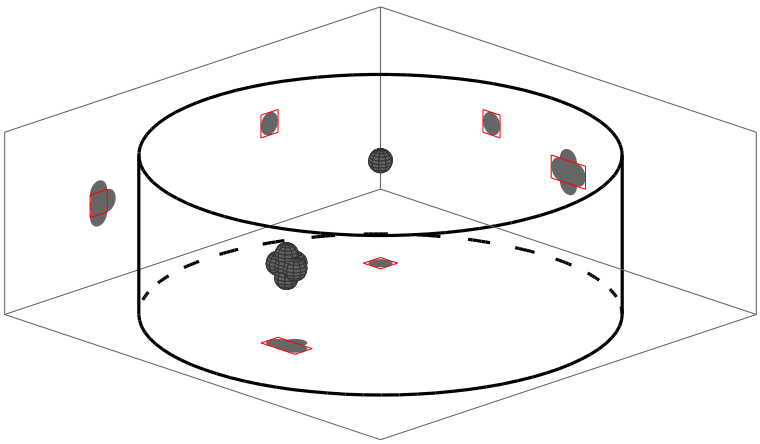

(b) Reconstruction.

Figure 3.6: Results for the setting in Example 3.4.5 with $\delta_{\text{cp}} = 0.5 \cdot 10^{-7}$. The anomaly area D is indicated in red on the projection planes.

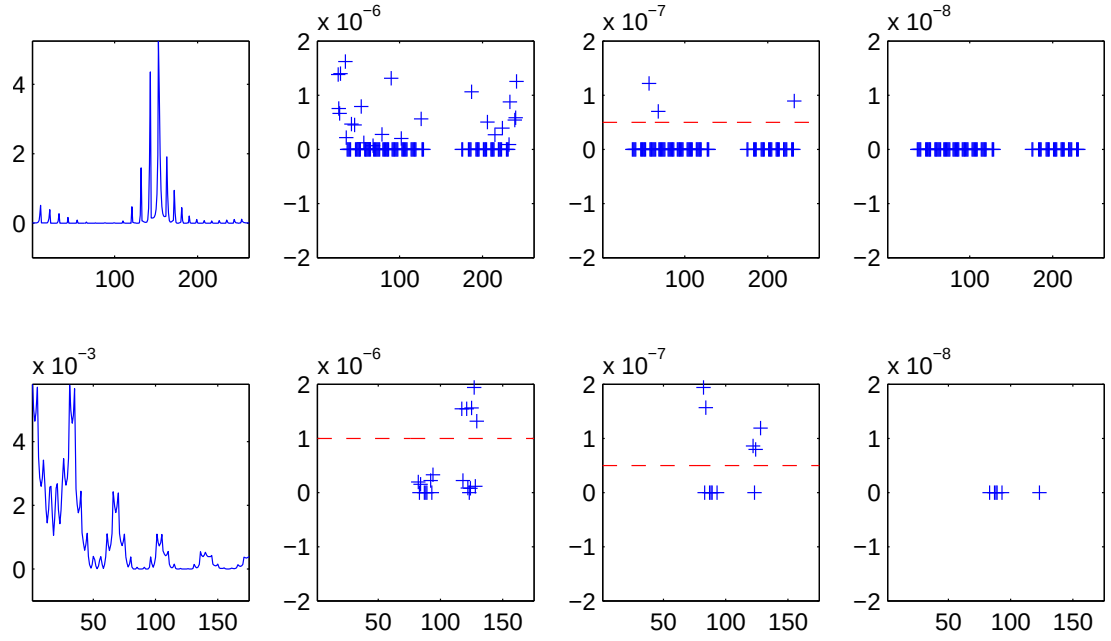

Figure 3.7: For Example 3.4.4 and Example 3.4.5, the upper and lower row respectively show the values $\lambda^j_{\max}$ for the tested balls B_j plotted against the indices j. The plots of the first column show the values $\lambda^j_{\max}$ for all test balls. In the remaining columns, the "+" markers mark the values $\lambda^j_{\max}$ inside ranges close to zero. The dashed red lines present candidates for error bounds δ_{cp}.

3.5 Conclusion and discussion

In this chapter we developed a new monotonicity-based anomaly detection method for EIT that does not require any reference simulations. Instead of using simulated reference measurements, the method is based on comparing weighted frequency-difference AC measurements and ultrasound-modulated DC measurements. To compare such measurements we generalized the concept of monotonicity-based testing for the complex conductivity EIT. For the CM, we showed that these monotonicity tests determine whether the focusing region of the ultrasound wave lies inside the inclusion or not. For the SM, we proved that our method correctly identifies the case where a focusing region lies inside the anomaly and with Remark 3.3.4 we justified that the method can be expected to work for a sufficiently large number of attached electrodes.

There are two main advantages of this method. First of all, no time consuming computations of reference simulations are required. Second, the method does not need a priory information on the imaging subjects shape or on the electrodes like position or shape. Especially, the second point is a great advantage. Conventional methods (that require the computation of reference data) highly suffer from imprecisely given setting parameters. Regarding the setting geometry, this effect is completely canceled out in the proposed method.

Our method requires that the complex conductivity is constant outside the anomaly region and fulfills a contrast condition. Furthermore, our method relies on an idealized model for the ultrasound-modulation, i.e., we assume that an ultrasound wave can be perfectly focused in a test ball such that it uniformly alters the conductivity in this test ball. In practical applications we cannot expect that the complex conductivity is perfectly constant outside the anomaly region and that the ultrasound wave can be perfectly focused. Concerning these challenges, we believe that the concept of worst-case testing, which is used in Chapter 2 (see [HU15a] for the paper version), might be helpful.

Chapter 4

Local uniqueness for an inverse boundary value problem with partial data

Up to minor changes, the Sections 4.1 - 4.3 and 4.5 are the Sections 1-4 of the paper [HU15b] that has been submitted to the Proceedings of the American Mathematical Society.

4.1 Introduction

Let $\Omega \subseteq \mathbb{R}^n$, $n \geq 3$, be a bounded Lipschitz domain with outer normal ν and $L^\infty_+(\Omega)$ denote the subset of $L^\infty(\Omega)$-functions with positive essential infima. We consider the question whether the potential $q \in L^\infty_+(\Omega)$ in the Schrödinger equation

$$-\Delta u + qu = 0 \quad \text{in} \quad \Omega \tag{4.1}$$

is uniquely determined by partial boundary data on a possibly arbitrarily small non-empty relatively open subset $\Gamma \subseteq \partial\Omega$.

For such a boundary subset $\Gamma \subseteq \partial\Omega$ and $q \in L^\infty_+(\Omega)$, the partial boundary data that we consider in this chapter are given by the *local Neumann-to-Dirichlet (NtD) operator*

$$\Lambda_\Gamma(q) \,:\, L^2(\Gamma) \to L^2(\Gamma), \quad g \mapsto u_q^{(g)}|_\Gamma, \tag{4.2}$$

where $u_q^{(g)} \in H^1(\Omega)$ is the unique solution of

$$-\Delta u_q^{(g)} + q u_q^{(g)} = 0 \text{ in } \Omega \qquad \text{with} \qquad \partial_\nu u_q^{(g)}|_{\partial\Omega} = \begin{cases} g, & \text{on } \Gamma, \\ 0, & \text{on } \partial\Omega \setminus \Gamma. \end{cases} \tag{4.3}$$

The existence of an unique solution is a consequence of the Lax-Milgram theorem. Furthermore, $\Lambda_\Gamma(q)$ is easily shown to be a compact self-adjoint linear operator.

In this chapter we will show the following local uniqueness result.

Theorem 4.1.1. *Let $q_1, q_2 \in L^\infty_+(\Omega)$ and $V \subseteq \mathbb{R}^n$ be an open connected set with $q_1 \geq q_2$ on $\Omega \cap V$ and $\Gamma := \partial\Omega \cap V \neq \emptyset$. Then*

$$q_1|_{\Omega\cap V} \not\equiv q_2|_{\Omega\cap V} \quad \textit{implies} \quad \Lambda_\Gamma(q_1) \neq \Lambda_\Gamma(q_2). \tag{4.4}$$

Moreover, in that case $\Lambda_\Gamma(q_2) - \Lambda_\Gamma(q_1)$ has a positive eigenvalue.

The *inverse potential problem* of the Schrödinger equation is closely related to the *inverse conductivity problem (Calderón Problem [Cal80, Cal06])*. For both problems, uniqueness from full boundary data on $\partial\Omega$ has been extensively studied in the last 30 years. To give a brief overview of prominent contributions, we list Kohn and Vogelius [KV84, KV85], Sylvester and Uhlmann [SU87], Nachman [Nac96], Astala and Päivärinta [AP06], Bukhgeim [BB08], Haberman and Tataru [HT$^+$13].

The uniqueness problem from partial boundary data has attracted growing attention over the last years. Typically, this problem is studied for data of type C_q^D or C_q^N on sets $\Gamma^D, \Gamma^N \subseteq \partial\Omega$, where

$$C_q^D := \left\{ (u|_{\Gamma^D}, \partial_\nu u|_{\Gamma^N}) \,:\, -\Delta u + qu = 0,\ \operatorname{supp}(u|_{\partial\Omega}) \subseteq \Gamma^D \right\},$$

$$C_q^N := \left\{ (u|_{\Gamma^D}, \partial_\nu u|_{\Gamma^N}) \,:\, -\Delta u + qu = 0,\ \operatorname{supp}(\partial_\nu u|_{\partial\Omega}) \subseteq \Gamma^N \right\}.$$

Obviously, for potentials $q \in L^\infty_+(\Omega)$, the question of uniqueness from data of type C_q^N with $\Gamma = \Gamma^D = \Gamma^N$ is equivalent to the question of uniqueness from the local NtD operator $\Lambda_\Gamma(q)$.

Hereafter, we list some recent results. Let us also refer to the overview of Kenig and Salo [KS14].

For dimension $n = 2$, Imanuvilov, Uhlmann and Yamamoto showed uniqueness from data of type C_q^D in [IUY10], where $\Gamma^D = \Gamma^N$ is an arbitrary open subset in $\partial\Omega$ and the potentials are in $\mathcal{C}^{2+\alpha}\left(\overline{\Omega}\right)$ for $\alpha > 0$.

For dimension $n \geq 3$, Kenig, Sjöstrand and Uhlmann proved uniqueness from data of type C_q^D for $q \in L^\infty(\Omega)$ in [KSU07], where Γ^D and Γ^N are open neighborhoods slightly larger than a front face and a back face of $\partial\Omega$, respectively. Nachman and Street presented a constructive proof of this result in [NS10]. In [Isa07] Isakov proved uniqueness from data of type C_q^D for $q \in L^\infty(\Omega)$, where $\Gamma^D = \Gamma^N$ and the remaining boundary part is contained in a plane or a sphere. In [KS12] Kenig and Salo presented a result that unifies and improves the approaches of [KSU07] and [Isa07]. In particular, they reduced the assumptions on the sets Γ^D, Γ^N and on a possibly remaining part, which is the case for $\Gamma^D = \Gamma^N \neq \partial\Omega$.

Theorem 4.1.1 is, to our knowledge, the first result that presents a uniqueness result for partial data on an arbitrary non-empty relatively open boundary part $\Gamma \subseteq \partial\Omega$ (with $\Gamma = \Gamma^D = \Gamma^N$) for dimension $n \geq 3$. Except the assumption that Ω has to be a Lipschitz domain, there are no further assumptions to the boundary required: neither to the boundary part Γ nor to the remaining boundary part.

This chapter is organized as follows. In Section 4.2 we prove Theorem 4.1.1. For that purpose, we present and combine a *monotonicity relation* for the local NtD operator (Lemma 4.2.1) and a new variant of the concept of *localized potentials* (Lemma 4.2.2, cf. [Geb08] for the initial concept). The approach of combining these two concepts has previously been used in [Har09, Har12, HU, HEU15] (where [HU] and [HEU15] are the paper versions of Chapter 1 and 3, respectively). Lemma 4.2.1 presents a monotonicity inequality that yields a lower bound for the change of the local NtD operator (in the sense of operator definiteness) caused by a change of the potential. This lower bound depends on the spatial change of the potential weighted by the solution of the Schrödinger equation corresponding to the initial potential. Lemma 4.2.2 shows the existence of so-called *localized potentials* and allows to control the lower bound of the monotonicity inequality in an appropriate way.[1] The proofs of Lemma 4.2.1 and 4.2.2 are given in Section 4.3 and 4.5, respectively. Section 4.4 presents some unique continuation properties that are needed to prove Lemma 4.2.2.

4.2 Proof of the main result

Let $q_1, q_2 \in L^\infty_+(\Omega)$, $V \subseteq \mathbb{R}^n$ be an open connected set and $\Gamma := \partial\Omega \cap V \neq \emptyset$.

To prove Theorem 4.1.1, we combine a monotonicity inequality for NtD operators (Lemma 4.2.1) and a result about the existence of localized potentials (Lemma 4.2.2).

Lemma 4.2.1. *Let $g \in L^2(\Gamma)$ and $u_1 := u_{q_1}^{(g)} \in H^1(\Omega)$ be the corresponding solution of (4.3). Then*

$$\langle g, (\Lambda_\Gamma(q_2) - \Lambda_\Gamma(q_1))\, g\rangle_{L^2(\Gamma)} \geq -\int_\Omega (q_2 - q_1){u_1}^2 \,\mathrm{d}x. \tag{4.5}$$

Lemma 4.2.1 is proven in Section 4.3.

Lemma 4.2.2. *Let $q_1 \gneq q_2$ on $\Omega \cap V$ (i.e., $q_1|_{\Omega\cap V} \geq q_2|_{\Omega\cap V}$ and $q_1|_{\Omega\cap V} \not\equiv q_2|_{\Omega\cap V}$). Then there exists a sequence $(g_m)_{m\in\mathbb{N}} \subset L^2(\Gamma)$ such that the corresponding solutions $(u_m)_{m\in\mathbb{N}} := \left(u_{q_1}^{(g_m)}\right)_{m\in\mathbb{N}} \subset H^1(\Omega)$ of (4.3) fulfill*

$$\lim_{m\to\infty} \int_{V\cap\Omega} (q_1 - q_2){u_m}^2 \,\mathrm{d}x = \infty \quad \text{and} \quad \lim_{m\to\infty} \int_{\Omega\setminus V} (q_1 - q_2){u_m}^2 \,\mathrm{d}x = 0. \tag{4.6}$$

Lemma 4.2.2 is proven in Section 4.5.

[1] Originally, the concept of localized potentials was used to locally control electrical potentials for the inverse conductivity problem. Since in this work it is used to locally weight the potentials of the Schrödinger equation, it seems appropriate to keep with the name "localized potentials".

Proof of Theorem 4.1.1. First we apply Lemma 4.2.2 and obtain a $g \in L^2(\Gamma)$ such that the corresponding solution $u := u_{q_1}^{(g)}$ of (4.3) fulfills

$$\int_{V\cap\Omega} (q_1 - q_2)u^2 \,\mathrm{d}x > 1 \quad \text{and} \quad \int_{\Omega\setminus V} (q_1 - q_2)u^2 \,\mathrm{d}x > -1.$$

Now we apply Lemma 4.2.1 and obtain

$$\begin{aligned}\langle g, (\Lambda_\Gamma(q_2) - \Lambda_\Gamma(q_1))\, g\rangle_{L^2(\Gamma)} &\geq -\int_\Omega (q_2 - q_1)u^2 \,\mathrm{d}x \\ &= \int_{V\cap\Omega} (q_1 - q_2)u^2 \,\mathrm{d}x + \int_{\Omega\setminus V} (q_1 - q_2)u^2 \,\mathrm{d}x \\ &> 1 - 1 = 0.\end{aligned}$$

This shows that $\Lambda_\Gamma(q_2) - \Lambda_\Gamma(q_1)$ is not negative semidefinite and thus has a positive eigenvalue. □

4.3 Monotonicity for Neumann-to-Dirichlet maps

Again, let $q_1, q_2 \in L^\infty_+(\Omega)$, $V \subseteq \mathbb{R}^n$ be an open connected set and $\Gamma := \partial\Omega \cap V \neq \emptyset$.

Here, we prove the monotonicity inequality of Lemma 4.2.1. In the context of the inverse conductivity problem, such monotonicity estimates are well-known, cf., e.g., Ikehata, Kang, Seo, and Sheen [KSS97, Ike98]) and the variants presented in the previous chapters.

Lemma 4.2.1 follows from [Har09, Lemma 4.1]. Since the proof is simple and short, we include it for the sake of completeness.

Proof of Lemma 4.2.1. Let $g \in L^2(\Gamma)$ and $u_i := u_{q_i}^{(g)} \in H^1(\Omega)$, $i \in \{1, 2\}$, be the corresponding solutions of (4.3). Then

$$b_i(u_i, w) := \int_\Omega \nabla u_i \nabla w + q_i u w \,\mathrm{d}x = \int_\Gamma g w|_\Gamma \,\mathrm{d}s =: l(w) \quad \forall w \in H^1(\Omega),\ i \in \{1, 2\}.$$

Using this we consider

$$\begin{aligned}&\langle g, (\Lambda_\Gamma(q_2) - \Lambda_\Gamma(q_1))\, g\rangle_{L^2(\Gamma)} \\ &\quad = l(u_2) - l(u_1) = b_2(u_2, u_2) - 2b_2(u_2, u_1) + b_1(u_1, u_1) \\ &\quad = -\int_\Omega (q_2 - q_1)u_1^2 - (\nabla(u_2 - u_1))^2 - q_2(u_1 - u_2)^2 \,\mathrm{d}x.\end{aligned}$$

Since $q_2 \geq 0$, the assertion follows. □

Remark 4.3.1. Additionally, an upper bound to the operator change can be derived, see, e.g., [Har09, Lemma 4.1] or cf. the proof of Lemma 1.3.1.

4.4 Unique continuation properties

Let $\Omega' \in \mathbb{R}^n$, $n \geq 3$, be a connected open set (e.g., $\Omega' = \Omega$) and $q \in L^\infty(\Omega')$. In this section we discuss unique continuation properties (UCP) for the Schrödinger equation

$$-\Delta u + qu = 0 \quad \text{on} \quad \Omega' \tag{4.7}$$

for a given solution space H. In particular, we prove Theorem 4.4.8, which shows unique continuation from sets of positive measure and plays a key role in the next section. Note that the assumption $n \geq 3$ is needed in the proof of Lemma 4.4.7

Below, we present definitions of three variants of UCP as they are typically formulated for second-order elliptic equations (cf., e.g., the work of Tataru and Koch [KT01]). Analog definitions are also common for partial differential inequalities.

Definition 4.4.1 (Weak UCP)**.** We say that an equation on Ω' has the weak unique continuation property (UCP) for H-solutions if the trivial solution $u \equiv 0$ is the only solution in H that vanishes identically on some non-empty open set $B \subseteq \Omega'$.

Definition 4.4.2. A function $u \in L^2_{\text{loc}}(\Omega')$ is said to have a zero of infinite order at $x_0 \in \Omega'$ if there exist $R_N \in \mathbb{R}_+$ and $C_N \in \mathbb{R}$ for all $N \in \mathbb{N}$ with

$$\int_{B_r(x_0)} u^2 \, \mathrm{d}x \leq C_N r^N \quad \text{for} \quad r \leq R_N. \tag{4.8}$$

Definition 4.4.3 (Strong UCP)**.** We say that an equation on Ω' has the strong unique continuation property (SUCP) for H-solutions if the trivial solution $u \equiv 0$ is the only solution in H that has a zero of infinite order.

Definition 4.4.4 (UCP from sets of positive measure)**.** We say that an equation on Ω' has the unique continuation property from sets of positive measure (UCP_+) for H-solutions if the trivial solution $u \equiv 0$ is the only solution in H that vanishes identically on some measurable set $E \subseteq \Omega'$ with positive measure.

Remark 4.4.5. (a) It is trivial that

$$\text{SUCP} \quad \text{implies} \quad \text{UCP}.$$

(b) It is well-known that $H^1(\Omega')$ solutions of equation (4.7) have the SUCP, see, e.g., the book of Hörmander [Hör94, Theorem 17.2.6]) or the overview on unique continuation properties for second order elliptic equations of Tataru and Koch in [KT01].

(c) To show that for equation (4.7)

$$\text{SUCP} \quad \text{implies} \quad \text{UCP}_+,$$

is not trivial, cf. the proof of Theorem 4.4.8, where Theorem 4.4.6 plays a key role.

Theorem 4.4.6. *Let $u \in H^1(\Omega')$ be a solution of (4.7) with $u|_E \equiv 0$, where $E \subseteq \Omega'$ is a measurable set of positive measure. Then u has a zero of infinite order at some point $x_0 \in E$.*

This has been shown in several articles for even more general settings (cf., e.g., the works of Regbaoui, de Figueiredo and Gossez, Hadi and Tsouli [Reg01, dFG92, HT01]). Since this result is essential for deriving the result on localized potentials (Lemma 4.2.2), we will give a compact proof (adapted for our special setting), which follows the proof of de Figueiredo and Gossez [dFG92].

Before we prove Theorem 4.4.6, we state and prove the following auxiliary lemma.

Lemma 4.4.7. *Let $u \in H^1(\Omega')$ be a solution of (4.7), let $B_r(x_0), B_{2r}(x_0) \subseteq \Omega'$ be two concentric balls for $x_0 \in \Omega'$ and let $r \in (0, 1]$. Then there exists a constant $c > 0$ (independent of r) such that*

$$\int_{B_r(x_0)} |\nabla u|^2 \,\mathrm{d}x \leq \frac{c}{r^2} \int_{B_{2r}(x_0)} u^2 \,\mathrm{d}x. \tag{4.9}$$

Proof. The solution u fulfills

$$\int_{\Omega'} \nabla u \nabla v + quv \,\mathrm{d}x = 0 \quad \text{for all } v \in \mathcal{D}(\Omega').$$

Let $\varphi \in \mathcal{D}(\Omega')$ with $\operatorname{supp} \varphi \subseteq \overline{B_{2r}(x_0)}$, $\varphi \leq 1$ and $\varphi|_{B_r(x_0)} \equiv 1$. It is well-known that there exists such a function that can be chosen to be rotationally symmetric, i.e., there exists a function h with $\varphi(x) := h(\|x - x_0\|)$. Let $\varphi_1(x) = h_1(\|x - x_0\|)$ be such functions (φ and h) for $r = 1$. Obviously, $|\nabla \varphi_1|$ is bounded by a constant $s > 0$. Hence, we can choose $\varphi(x) := h_1\left(\frac{1}{r}\|x - x_0\|\right)$ such that $|\nabla \varphi| \leq s/r$.

Since $\overline{\mathcal{D}(\Omega')} = H_0^1(\Omega')$, with $v = \varphi^2 u$ we obtain

$$\int_{\Omega'} \nabla u \cdot \left(2\varphi u \nabla \varphi + \varphi^2 \nabla u\right) + q\varphi^2 u^2 \,\mathrm{d}x = 0.$$

This yields

$$\int_{\Omega'} |\nabla u|^2 \varphi^2 \,\mathrm{d}x \leq -2 \int_{\Omega'} (\nabla u \cdot \nabla \varphi) \varphi u \,\mathrm{d}x + \|q\|_\infty \int_{\Omega'} \varphi^2 u^2 \,\mathrm{d}x.$$

From the Cauchy inequality it follows that

$$\begin{aligned} \int_{\Omega'} |\nabla u|^2 \varphi^2 \,\mathrm{d}x &\leq \epsilon \int_{\Omega'} |\nabla u|^2 \varphi^2 \,\mathrm{d}x + \frac{1}{\epsilon} \int_{\Omega'} |\nabla \varphi|^2 u^2 \,\mathrm{d}x + \|q\|_\infty \int_{\Omega'} \varphi^2 u^2 \,\mathrm{d}x \\ &\leq \epsilon \int_{\Omega'} |\nabla u|^2 \varphi^2 \,\mathrm{d}x + \frac{s^2}{\epsilon r^2} \int_{B_{2r}(x_0)} u^2 \,\mathrm{d}x + \|q\|_\infty \int_{B_{2r}(x_0)} u^2 \,\mathrm{d}x \end{aligned}$$

for any $\epsilon \in (0,1)$ and thus with $r \in (0,1]$ we obtain

$$\int_{B_r(x_0)} |\nabla u|^2 \,\mathrm{d}x \leq \frac{s^2/\epsilon + \|q\|_\infty}{1-\epsilon} \frac{1}{r^2} \int_{B_{2r}(x_0)} u^2 \,\mathrm{d}x.$$

□

Proof of Theorem 4.4.6. It is a well-known result of measure theory that almost every point x_0 of a Lebesgue measurable set $E \subseteq \mathbb{R}^n$ is a density point of E (see, e.g., [BR07]), i.e.,

$$\lim_{r \to 0} \frac{|E \cap B_r(x_0)|}{|B_r(x_0)|} = 1.$$

Since E is a set with positive measure, there exists such a density point x_0 of E. Hence, for all $\epsilon > 0$ there exists an $R = R(\epsilon)$ with

$$\frac{|B_r(x_0) \setminus E|}{|B_r(x_0)|} < \epsilon \quad \text{and} \quad B_r(x_0) \subseteq \Omega' \quad \text{for all } r \leq R. \tag{4.10}$$

W.l.o.g., we can assume that $0 < r \leq R \leq 1$. Note that $u|_E \equiv 0$. Then, by applying the Hölder inequality and the Sobolev inequality for $p^* = 2n/(n-2)$, we obtain

$$\begin{aligned}\int_{B_r(x_0)} u^2 \,\mathrm{d}x = \int_{B_r(x_0)\setminus E} u^2 \cdot 1 \,\mathrm{d}x &\leq \left(\left(\int_{B_r(x_0)\setminus E} |u|^{p^*} \,\mathrm{d}x \right)^{1/p^*} \right)^2 |B_r(x_0) \setminus E|^{2/n} \\ &\leq C_S^2 \int_{B_r(x_0)} u^2 + |\nabla u|^2 \,\mathrm{d}x |B_r(x_0) \setminus E|^{2/n},\end{aligned}$$

where $C_S > 0$ is a constant that comes from the Sobolev inequality.

Hence, with this, $C_B := |B_r(x_0)|/r^n$ (which does not dependent on r), (4.10) and Lemma 4.4.7 we can conclude

$$\int_{B_r(x_0)} u^2 \,\mathrm{d}x = C_S^2 C_B^{2/n} \epsilon^{2/n} r^2 \left(\int_{B_r(x_0)} u^2 \,\mathrm{d}x + \frac{c}{r^2} \int_{B_{2r}(x_0)} u^2 \,\mathrm{d}x \right)$$

and thus

$$\int_{B_r(x_0)} u^2 \,\mathrm{d}x \leq C \epsilon^{2/n} \int_{B_{2r}(x_0)} u^2 \,\mathrm{d}x, \tag{4.11}$$

where ϵ has to be small enough such that

$$\epsilon \leq \left(2 C_S^2 C_B^{2/n} \right)^{-n/2} \tag{4.12}$$

and thus (with $0 < r \leq 1$)

$$\frac{C_S^2 C_B^{2/n} c}{1 - C_S^2 C_B^{2/n} \epsilon^{2/n} r^2} \leq C := 2 C_S^2 C_B^{2/n} c.$$

Now we define

$$f(r) := \int_{B_r(x_0)} u^2 \, \mathrm{d}x$$

and choose a fixed $N \in \mathbb{N}$. In addition, we possibly have to choose a smaller bound for ϵ, i.e., $\epsilon > 0$ has to be sufficiently small such that inequality (4.12) as well as

$$C\epsilon^{2/n} \leq 2^{-N} \tag{4.13}$$

is fulfilled. As a consequence of this, $R = R(N) =: R_N$ depends on N.

From (4.11) and (4.13) it follows

$$f(r) \leq 2^{-N} f(2r).$$

By iteration we obtain

$$f(\rho) \leq 2^{-kN} f(2^k \rho) \quad \text{for } 2^{k-1}\rho \leq R_N. \tag{4.14}$$

For given r with $0 < r \leq R_N$, we can choose $k \in \mathbb{N}$ such that

$$2^{-k} R_N \leq r \leq 2^{-(k-1)} R_N.$$

With this and (4.14) we obtain

$$f(r) \leq 2^{-kN} f(2^k r) \leq 2^{-kN} f(2R_N).$$

Since $2^{-k} \leq r/R_N$, with $C_N := (1/R_N)^N f(2R_N)$ it follows that

$$\int_{B_r(x_0)} u^2 \, \mathrm{d}x = f(r) \leq C_N r^N \quad \text{for} \quad r \leq R_N.$$

□

Theorem 4.4.8 (Unique continuation from sets of positive measure)**.** *The trivial solution of*

$$-\Delta u + qu = 0 \tag{4.15}$$

is the only $H^1(\Omega')$-solution vanishing on a measurable set of positive measure.

Proof. Theorem 4.4.8 is the combination of the following two results (cf. the work of Regbaoui [Reg01, proof of Theorem 2.1]).

(a) $H^1(\Omega')$-solutions of (4.15) that vanish on a set of positive measure have zeros of infinite order, see Theorem 4.4.6.

(b) The trivial solution $u = 0$ is the only $H^1(\Omega')$-solution of (4.15) that has a zero of infinite order, see, e.g., the book of Hörmander [Hör94, Theorem 17.2.6].

□

4.5 Localized potentials

Again, let $q_1, q_2 \in L^\infty_+(\Omega)$, $V \subseteq \mathbb{R}^n$ be an open connected set and $\Gamma := \partial\Omega \cap V \neq \emptyset$. In addition, as assumed in Lemma 4.2.2, let $q_1 \gneq q_2$ on $\Omega \cap V$ (i.e., $q_1|_{\Omega\cap V} \geq q_2|_{\Omega\cap V}$ and $q_1|_{\Omega\cap V} \not\equiv q_2|_{\Omega\cap V}$).

Since the open set $V \cap \Omega$ is a countable union of closed balls and $q_1 \gneq q_2$ on $\Omega \cap V$, there exists a closed ball

$$B \subseteq V \cap \Omega \quad \text{where} \quad q_1 \gneq q_2 \tag{4.16}$$

and $V \setminus B$ is connected.

To prove Lemma 4.2.2, we introduce two operators in Definition 4.5.2 and present some properties of these operators and their adjoints in Lemma 4.5.3. In the proof of Lemma 4.5.3 the following theorem and Theorem 4.4.8 play key roles.

Theorem 4.5.1. *Let H_1, H_2 be Hilbert spaces, $L \in \mathcal{L}(H_1, H_2)$ and $h \in H_2$. Then*

$$h \in \mathcal{R}(L) \quad \textit{if and only if} \quad \exists C > 0 : |(h, g)_{H_2}| \leq C\|L^* g\|_{H_1} \quad \textit{for all } g \in H_2. \tag{4.17}$$

Proof. This is a well-known result from functional analysis (see, e.g., the book of Bourbarki [Bou03]). For Banach spaces, a proof is given in [FGS07, Lemma 3.4]. □

Definition 4.5.2 (Virtual measurement operators)**.** Let $B \subseteq V \cap \Omega$ be a non-empty closed ball with $q_1 \gneq q_2$ on B as in (4.16). The operators L_B and $L_{\Omega\setminus V}$ are defined by

$$L_B : L^2(B) \to L^2(\Gamma), \qquad f \mapsto v_B|_\Gamma, \tag{4.18}$$

$$L_{\Omega\setminus V} : L^2(\Omega \setminus V) \to L^2(\Gamma), \qquad h \mapsto v_{\Omega\setminus V}|_\Gamma, \tag{4.19}$$

where $v_B, v_{\Omega\setminus V} \in H^1(\Omega)$ are the unique solutions of

$$-\Delta v_B + q_1 v_B = |q_1 - q_2|^{1/2} f\chi_B \text{ in } \Omega \quad \text{with} \quad \partial_\nu v_B|_{\partial\Omega} = 0, \tag{4.20}$$

$$-\Delta v_{\Omega\setminus V} + q_1 v_{\Omega\setminus V} = |q_1 - q_2|^{1/2} h\chi_{\Omega\setminus V} \text{ in } \Omega \quad \text{with} \quad \partial_\nu v_{\Omega\setminus V}|_{\partial\Omega} = 0, \tag{4.21}$$

or equivalently

$$\int_\Omega \nabla v_B \cdot \nabla w + q_1 v_B w \,\mathrm{d}x = \int_B |q_1 - q_2|^{1/2} w f \,\mathrm{d}x \quad \text{for all } w \in H^1(\Omega), \tag{4.22}$$

$$\int_\Omega \nabla v_{\Omega\setminus V} \cdot \nabla w + q_1 v_{\Omega\setminus V} w \,\mathrm{d}x = \int_{\Omega\setminus V} |q_1 - q_2|^{1/2} w h \,\mathrm{d}x \quad \text{for all } w \in H^1(\Omega). \tag{4.23}$$

Lemma 4.5.3. *(a) The adjoint operators*

$$L_B^* : L^2(\Gamma) \to L^2(B) \quad \textit{and} \quad L_{\Omega\setminus V}^* : L^2(\Gamma) \to L^2(\Omega \setminus V) \tag{4.24}$$

fulfill

$$L_B^* g = \left(|q_1 - q_2|^{1/2} u\right)\big|_B \quad \text{and} \quad L_{\Omega\setminus V}^* g = \left(|q_1 - q_2|^{1/2} u\right)\big|_{\Omega\setminus V}, \tag{4.25}$$

where $u := u_{q_1}^{(g)} \in H^1(\Omega)$ *is the corresponding solution of* (4.3).

(b) The adjoint operator L_B^* *is injective and* $\overline{\mathcal{R}(L_B)} = L^2(\Gamma)$.

(c) $\mathcal{R}(L_B) \cap \mathcal{R}(L_{\Omega\setminus V}) = \{0\}$.

(d) $\mathcal{R}(L_B) \not\subseteq \mathcal{R}(L_{\Omega\setminus V})$.

(e) There exists no $C > 0$ *such that* $\|L_B^* g\| \leq C\|L_{\Omega\setminus V}^* g\|$ *for all* $g \in L^2(\Gamma)$.

Proof.

(a) For $f \in L^2(B)$, let $v_B^{(f)} \in H^1(\Omega)$ be the solution of

$$\int_\Omega \nabla v_B^{(f)} \cdot \nabla w + q_1 v_B^{(f)} w \,\mathrm{d}x = \int_B |q_1 - q_2|^{1/2} w f \,\mathrm{d}x \quad \text{for all } w \in H^1(\Omega).$$

Then, in particular,

$$L_B f = v_B^{(f)}|_\Gamma.$$

Furthermore, for $g \in L^2(\Gamma)$, let $u_{q_1}^{(g)}$ be the corresponding solution of (4.3). Then $u_{q_1}^{(g)}$ also solves the equivalent variational formulation

$$\int_\Omega \nabla w \cdot \nabla u_{q_1}^{(g)} + q_1 w u_{q_1}^{(g)} \,\mathrm{d}x = \int_\Gamma g w|_\Gamma \,\mathrm{d}s \quad \text{for all } w \in H^1(\Omega).$$

Hence, for arbitrary $f \in L^2(B)$ and $g \in L^2(\Gamma)$, it follows that

$$\begin{aligned}
\langle f, L_B^* g\rangle_{L^2(B)} = \langle L_B f, g\rangle_{L^2(\Gamma)} &= \int_\Gamma g v_B^{(f)}|_\Gamma \,\mathrm{d}s \\
&= \int_\Omega \nabla v_B^{(f)} \cdot \nabla u_{q_1}^{(g)} + q_1 v_B^{(f)} u_{q_1}^{(g)} \,\mathrm{d}x \\
&= \int_B |q_1 - q_2|^{1/2} u_{q_1}^{(g)} f \,\mathrm{d}x \\
&= \left\langle f, \left(|q_1 - q_2|^{1/2} u_{q_1}^{(g)}\right)|_B \right\rangle_{L^2(B)}.
\end{aligned}$$

This yields $L_B^* g = \left(|q_1 - q_2|^{1/2} u_{q_1}^{(g)}\right)\Big|_B$.

Analogously, it follows $L_{\Omega\setminus V}^* g = \left(|q_1 - q_2|^{1/2} u_{q_1}^{(g)}\right)\Big|_{\Omega\setminus V}$.

(b) First we prove the injectivity of L_B^*. Let $g \in L^2(\Gamma)$ with $L_B^* g = 0$ and $u := u_{q_1}^{(g)} \in H^1(\Omega)$ be the corresponding solution of (4.3). From (a) we obtain $L_B^* g = \left(|q_1 - q_2|^{1/2} u\right)|_B$. Since $q_1 - q_2 \gneq 0$ on B, there exists a set $E \subseteq B$ of positive measure such that $|q_1 - q_2|^{1/2} \neq 0$ on E. Hence, $\left(|q_1 - q_2|^{1/2} u\right)|_E \equiv 0$

implies $u|_E \equiv 0$. From Theorem 4.4.8 it follows that $u \equiv 0$ on Ω and thus $g = \partial_\nu u|_\Gamma = 0$. This shows the injectivity of L_B^* and thus $\overline{\mathcal{R}(L_B)} = \mathcal{N}(L_B^*)^\perp = L^2(\Gamma)$.

(c) Recall that B and $\Omega \setminus V$ are closed in Ω and that $V \setminus B$ is connected. Let

$$\phi = L_B f = L_{\Omega\setminus V} h \in \mathcal{R}(L_B) \cap \mathcal{R}(L_{\Omega\setminus V})$$

and $v_B, v_{\Omega\setminus V} \in H^1(\Omega)$ be the corresponding solutions of Definition 4.5.2. First we show that

$$v_B = v_{\Omega\setminus V} \quad \text{on} \quad \Omega \setminus \left(\overline{B} \cup \overline{\Omega \setminus V}\right) = (\Omega \cap V) \setminus B. \tag{4.26}$$

On $\Omega \cup V$ we define the continuations

$$q := \begin{cases} q_1, & \text{on } \Omega, \\ 1, & \text{on } V \setminus \Omega, \end{cases}$$

$$\tilde{v} := \begin{cases} v, & \text{on } \Omega, \\ 0, & \text{on } V \setminus \Omega \end{cases} \quad \text{and} \quad \tilde{v}_j := \begin{cases} \partial_{x_j} v, & \text{on } \Omega, \\ 0, & \text{on } V \setminus \Omega, \end{cases}$$

where $v := v_B - v_{\Omega\setminus V}$.

Obviously, $\tilde{v}, \tilde{v}_j \in L^2(\Omega \cup V)$. To verify that $\tilde{v} \in H^1(\Omega \cup V)$, it is left to show $\partial_{x_j} \tilde{v} = \tilde{v}_j$. This can be shown by using

$$v|_\Gamma = v_B|_\Gamma - v_{\Omega\setminus V}|_\Gamma = \phi - \phi = 0.$$

Let $\varphi \in \mathcal{D}(\Omega \cup V)$, then (using integration by parts)

$$\begin{aligned} \int_{\Omega\cup V} \tilde{v} \partial_{x_j} \varphi \,\mathrm{d}x &= \int_\Omega v \partial_{x_j} \varphi \,\mathrm{d}x \\ &= -\int_\Omega \varphi \partial_{x_j} v \,\mathrm{d}x + \int_{\partial\Omega} (\varphi v)|_\Gamma \nu_j \,\mathrm{d}s \\ &= -\int_\Omega v_j \varphi \,\mathrm{d}x = -\int_{\Omega\cup V} \tilde{v}_j \varphi \,\mathrm{d}x. \end{aligned}$$

Now we continue showing (4.26). Since $v = \tilde{v}|_\Omega$ fulfills

$$\begin{aligned} &\int_\Omega \nabla v \cdot \nabla w + q_1 v w \,\mathrm{d}x \\ &\qquad = \int_\Omega |q_1 - q_2|^{1/2} w (f\chi_B - h\chi_{\Omega\setminus V}) \,\mathrm{d}x \quad \text{for all } w \in H^1(\Omega), \end{aligned}$$

it holds

$$\int_{V\setminus B} \nabla \tilde{v} \cdot \nabla \varphi + q \tilde{v} \varphi \,\mathrm{d}x = 0 \quad \text{for all } \varphi \in \mathcal{D}(V \setminus B).$$

We obtain that $\tilde{v}$ (as a function in $H^1(V \setminus B)$) solves

$$-\Delta\tilde{v} + q\tilde{v} = 0 \quad \text{on} \quad V \setminus B$$

and vanishes on $V \setminus \Omega$. Since $V \setminus \Omega$ is a non-empty open set (V is open and has a non-empty intersection Γ with the Lipschitz domain Ω) and $V \setminus B$ is connected, Theorem 4.4.8 shows that $\tilde{v} \equiv 0$ on $V \setminus B$ and thus

$$v_B = v_{\Omega\setminus V} \quad \text{on} \quad (V \cap \Omega) \setminus B.$$

To finally show $\phi = 0$, we define

$$u := \begin{cases} v_B & \text{on } \Omega \setminus B, \\ v_{\Omega\setminus V} & \text{on } B. \end{cases}$$

We can partition test functions (in $\mathcal{D}(\Omega)$ and $H^1(\Omega)$) by using smooth partitions of unity. By this it can be shown that u is an $H^1(\Omega)$-function and the unique solution of

$$\begin{aligned} -\Delta u + q_1 u = 0 \quad &\text{on} \quad \Omega, \\ \partial_\nu u|_{\partial\Omega} = 0. & \end{aligned}$$

Hence, u has to be equal to the trivial solution and thus

$$\phi = v_B|_\Gamma = u|_\Gamma \equiv 0.$$

(d) The assertion simply follows from (b) and (c).

(e) Let us assume that there exists a constant $C > 0$ such that

$$\|L_B^* g\| \leq C\|L_{\Omega\setminus V}^* g\| \quad \text{for all } g \in L^2(\Gamma).$$

Then

$$\mathcal{R}(L_B) \subseteq \mathcal{R}(L_{\Omega\setminus V})$$

immediately follows from Theorem 4.5.1 and this is a contradiction to (d).

□

Proof of Lemma 4.2.2. The assertion follows from Lemma 4.5.3:

The trivial case is where $L_{\Omega\setminus V}^*$ is not injective. Then there exists an element $g \in L^2(\Gamma) \setminus \{0\}$ with $\|L_{\Omega\setminus V}^* g\| = 0$. By the injectivity of L_B^* we have $\|L_B^* g\| =: c_g \geq 0$. In this case we can set $g_m := mg$ for all $m \in \mathbb{N}$.

For the case where $L_{\Omega\setminus V}^*$ is injective, we derive a suitable sequence $(g_m)_{m\in\mathbb{N}} \subseteq L^2(\Gamma)$ as follows. Let $C_m = m^2$ for $m \in \mathbb{N}$. Lemma 4.5.3 (e) implies the existence of a sequence $(g'_m)_{m\in\mathbb{N}} \subseteq L^2(\Gamma)$ with

$$\|L_B^* g'_m\| > C_m\|L_{\Omega\setminus V}^* g'_m\| \quad \text{for all } m \in \mathbb{N}. \tag{4.27}$$

In particular, this implies $g'_m \neq 0$ for all $m \in \mathbb{N}$. Since $L^*_{\Omega\setminus V}$ is injective, we can set $g_m := \frac{g'_m}{m\|L^*_{\Omega\setminus V} g'_m\|}$. By multiplying (4.27) with $\frac{1}{m\|L^*_{\Omega\setminus V} g'_m\|}$, we obtain

$$\|L^*_B g_m\| > m \quad \text{for all } m \in \mathbb{N}.$$

Furthermore, it holds

$$\|L^*_{\Omega\setminus V} g_m\| = \frac{1}{m} \quad \text{for all } m \in \mathbb{N}.$$

For both cases, we obtain a sequence $(g_m)_{m\in\mathbb{N}}$ such that

$$\lim_{m\to\infty} \int_{V\cap\Omega} (q_1 - q_2) {u_m}^2 \,\mathrm{d}x = \lim_{m\to\infty} \|L^*_B g_m\|^2 = \infty,$$
$$\lim_{m\to\infty} \int_{\Omega\setminus V} (q_1 - q_2) {u_m}^2 \,\mathrm{d}x = \lim_{m\to\infty} \|L^*_{\Omega\setminus V} g_m\|^2 = 0,$$

where $u_m := u_{q_1}^{(g_m)} \in H^1(\Omega)$ is the corresponding solution of (4.3). □

Bibliography

[ABC+08] H. Ammari, E. Bonnetier, Y. Capdeboscq, M. Tanter, M. Fink, et al. Electrical impedance tomography by elastic deformation. *SIAM J. Appl. Math.*, 68(6):1557–1573, 2008.

[AGL11] A. Adler, R. Gaburro, and W. R. B. Lionheart. Electrical impedance tomography. In *Handbook of Mathematical Methods in Imaging*, pages 599–654. Springer, 2011.

[AP06] K. Astala and L. Päivärinta. Calderón's inverse conductivity problem in the plane. *Ann. of Math.*, pages 265–299, 2006.

[Bay06] R. H. Bayford. Bioimpedance tomography (electrical impedance tomography). *Annu. Rev. Biomed. Eng.*, 8:63–91, 2006.

[BB84] D. C. Barber and B. H. Brown. Applied potential tomography. *J. Phys. E: Sci. Instrum.*, 17(9):723–733, 1984.

[BB08] A. L. Bukhgeim and A. A. Bukhgeim. Recovering a potential from Cauchy data in the two-dimensional case. *J. Inverse Ill-Posed Probl.*, 16(1):19–33, 2008.

[BH00] M. Brühl and M. Hanke. Numerical implementation of two noniterative methods for locating inclusions by impedance tomography. *Inverse Problems*, 16(4):1029–1042, 2000.

[Bor02] L. Borcea. Electrical impedance tomography. *Inverse Problems*, 18(6):99–136, 2002.

[Bor03] L. Borcea. Addendum to 'Electrical impedance tomography'. *Inverse Problems*, 19(4):997–998, 2003.

[Bou03] N. Bourbaki. *Elements of mathematics: Topological vector spaces, Chapters 1-5*. Springer-Verlag, 2003.

[BR07] V. I. Bogachev and M. A. S. Ruas. *Measure theory*, volume 1. Springer, 2007.

[Bro03] B. H. Brown. Electrical impedance tomography (EIT): a review. *J Med Eng Technol.*, 27(3):97–108, 2003.

[Brü01] M. Brühl. Explicit characterization of inclusions in electrical impedance tomography. *SIAM J. Math. Anal.*, 32(6):1327–1341, 2001.

[BS+87] B. H. Brown, A. D. Seagar, et al. The Sheffield data collection system.

Clin. Phys. Physiol. Meas., 8:91, 1987.

[Cal80] A. P. Calderón. On an inverse boundary value problem. In W H Meyer and M A Raupp, editors, *Seminar on Numerical Analysis and its Application to Continuum Physics*, pages 65–73. Brasil. Math. Soc., Rio de Janeiro, 1980.

[Cal06] A. P. Calderón. On an inverse boundary value problem. *Comput. Appl. Math.*, 25(2–3):133–138, 2006.

[CHS13] M. K. Choi, B. Harrach, and J. K. Seo. Regularizing a linearized EIT reconstruction method using a sensitivity-based factorization method. *Inverse Problems Sci. Eng.*, pages 1–16, 2013.

[CIN99] M. Cheney, D. Isaacson, and J. C. Newell. Electrical impedance tomography. *SIAM review*, 41(1):85–101, 1999.

[CKI+07] M. H. Choi, T.-J. Kao, D. Isaacson, G. J. Saulnier, and J. C. Newell. A reconstruction algorithm for breast cancer imaging with electrical impedance tomography in mammography geometry. *IEEE Trans. Biomed. Eng.*, 54(4):700–710, 2007.

[dFG92] D. G. de Figueiredo and J.-P. Gossez. Strict monotonicity of eigenvalues and unique continuation. *Comm. Partial Differential Equations*, 17(1-2):339–346, 1992.

[FGS07] F. Frühauf, B. Gebauer, and O. Scherzer. Detecting interfaces in a parabolic-elliptic problem from surface measurements. *SIAM J. Numer. Anal.*, 45(2):810–836, 2007.

[FI89] A. Friedman and V. Isakov. On the uniqueness in the inverse conductivity problem with one measurement. *Indiana Univ. Math. J*, 38(3):563–579, 1989.

[Fri87] A. Friedman. Detection of mines by electric measurements. *SIAM J. Appl. Math.*, 47(1):201–212, 1987.

[Geb06] B. Gebauer. The factorization method for real elliptic problems. *Z. Anal. Anwend.*, 25(1):81–102, 2006.

[Geb08] B. Gebauer. Localized potentials in electrical impedance tomography. *Inverse Probl. Imaging*, 2(2):251–269, 2008.

[GH07] B. Gebauer and N. Hyvönen. Factorization method and irregular inclusions in electrical impedance tomography. *Inverse Problems*, 23(5):2159–2170, 2007.

[GH08] B. Gebauer and N. Hyvönen. Factorization method and inclusions of mixed type in an inverse elliptic boundary value problem. *Inverse Probl. Imaging*, 2(3):355–372, 2008.

[GIN87] D. G. Gisser, D. Isaacson, and J. C. Newell. Current topics in impedance

imaging. *Clin. Phys. Physiol. Meas.*, 8(4A):39, 1987.

[GIN90] D. G. Gisser, D. Isaacson, and J. C. Newell. Electric current computed tomography and eigenvalues. *SIAM J. Appl. Math.*, 50(6):1623–1634, 1990.

[GKI94] N. G. Gençer, M. Kuzuoglu, and Y. Z. Ider. Electrical impedance tomography using induced currents. *IEEE Trans. Med. Imag.*, 13(2):338–350, 1994.

[GM08] S. Grimnes and O. G. Martinsen. *Bioimpedance and Bioelectricity Basics, 2nd. ed.* Academic Press, Oxford, U.K., 2008.

[GS08] B. Gebauer and O. Scherzer. Impedance-acoustic tomography. *SIAM J. Appl. Math.*, 69:565–576, 2008.

[Had23] J. Hadamard. Lectures on the Cauchy problems in linear partial differential equations, 1923.

[Har09] B. Harrach. On uniqueness in diffuse optical tomography. *Inverse Problems*, 25(5):055010 (14pp), 2009.

[Har12] B. Harrach. Simultaneous determination of the diffusion and absorption coefficient from boundary data. *Inverse Probl. Imaging*, 6(4):663–679, 2012.

[Har13] B. Harrach. Recent progress on the factorization method for electrical impedance tomography. *Comput. Math. Methods Med.*, 2013:8 pages, 2013.

[HB03] M. Hanke and M. Brühl. Recent progress in electrical impedance tomography. *Inverse Problems*, 19(6):S65–S90, 2003.

[HEU15] B. Harrach, L. Eunjung, and M. Ullrich. Combining frequency-difference and ultrasound modulated EIT. *Inverse Problems*, 31(9):095003 (25pp), 2015. DOI: 10.1088/0266-5611/31/9/095003.

[HH09] H. Hakula and N. Hyvönen. On computation of test dipoles for factorization method. *BIT*, 49(1):75–91, 2009.

[HHH11] M. Hanke, B. Harrach, and N. Hyvönen. Justification of point electrode models in electrical impedance tomography. *Math. Models Methods Appl. Sci.*, 21(06):1395–1413, 2011.

[HHP07] N. Hyvonen, H. Hakula, and S. Pursiainen. Numerical implementation of the factorization method within the complete electrode model of electrical impedance tomography. *Inverse Probl. Imaging*, 1(2):299–317, 2007.

[HHP08] R. J. Halter, A. Hartov, and K. D. Paulsen. A broadband high-frequency electrical impedance tomography system for breast imaging. *IEEE Trans. Med. Imag.*, 55(2):650–659, 2008.

[Hol05] D. Holder. *Electrical Impedance Tomography: Methods, History and Applications*. IOP Publishing, Bristol, UK, 2005.

[Hör94] L. Hörmander. *The analysis of linear partial differential operators III*, volume 274. Springer, 1994.

[HS08] M. Hanke and B. Schappel. The factorization method for electrical impedance tomography in the half-space. *SIAM J. Appl. Math.*, 68(4):907–924, 2008.

[HS09] B. Harrach and J. K. Seo. Detecting inclusions in electrical impedance tomography without reference measurements. *SIAM J. Appl. Math.*, 69(6):1662–1681, 2009.

[HS10] B. Harrach and J. K. Seo. Exact shape-reconstruction by one-step linearization in electrical impedance tomography. *SIAM J. Appl. Math.*, 42(4):1505–1518, 2010.

[HSW10] B. Harrach, J. K. Seo, and E. J. Woo. Factorization method and its physical justification in frequency-difference electrical impedance tomography. *IEEE Trans. Med. Imag.*, 29(11):1918–1926, 2010.

[HT01] I. E. Hadi and N. Tsouli. Strong unique continuation of eigenfunctions for p-Laplacian operator. *Int. J. Math. Math. Sci.*, 25(3):213–216, 2001.

[HT+13] B. Haberman, D. Tataru, et al. Uniqueness in Calderón's problem with Lipschitz conductivities. *Duke Math. J.*, 162(3):497–516, 2013.

[HU] B. Harrach and M. Ullrich. Monotonicity-based shape reconstruction in electrical impedance tomography. *SIAM J. Math. Anal.*, 45(6):3382–3403. DOI: 10.1137/120886984.

[HU10] B. Harrach and M. Ullrich. Monotony based imaging in EIT. *AIP Conf. Proc.*, 1281:1975–1978, 2010.

[HU15a] B. Harrach and M. Ullrich. Resolution guarantees in electrical impedance tomography. *IEEE Trans. Med. Imag.*, 34(7):1513–1521, 2015. DOI: 10.1109/TMI.2015.2404133.

[HU15b] B. Harrach and M. Ullrich. Local uniqueness for an inverse boundary value problem with partial data. *submitted to Proc. Amer. Math. Soc.*, decision of acceptance is still open (as of April 2015).

[HW48] W. Hurewicz and H. Wallman. *Dimension theory*. Princeton university press, 1948.

[HW78] R. P. Henderson and J. G. Webster. An impedance camera for spatially specific measurements of the thorax. *IEEE Trans. Biomed. Eng.*, BME-25(3):250–254, 1978.

[Hyv04] N. Hyvönen. Complete electrode model of electrical impedance tomography: Approximation properties and characterization of inclusions. *SIAM*

J. Appl. Math., 64(3):902–931, 2004.

[Hyv09] N. Hyvönen. Approximating idealized boundary data of electric impedance tomography by electrode measurements. *Math. Models Methods Appl. Sci.*, 19(07):1185–1202, 2009.

[IIN+07] T. Ide, H. Isozaki, S. Nakata, S. Siltanen, and G. Uhlmann. Probing for electrical inclusions with complex spherical waves. *Comm. Pure Appl. Math.*, 60(10):1415–1442, 2007.

[IINS10] T. Ide, H. Isozaki, S. Nakata, and S. Siltanen. Local detection of three-dimensional inclusions in electrical impedance tomography. *Inverse Problems*, 26(3):035001, 17, 2010.

[Ike90] M. Ikehata. Inversion formulas for the linearized problem for an inverse boundary value problem in elastic prospection. *SIAM J. Appl. Math.*, 50(6):1635–1644, 1990.

[Ike98] M. Ikehata. Size estimation of inclusion. *J. Inverse Ill-Posed Probl.*, 6(2):127–140, 1998.

[Ike99] M. Ikehata. How to draw a picture of an unknown inclusion from boundary measurements. Two mathematical inversion algorithms. *J. Inverse Ill-Posed Probl.*, 7(3):255–271, 1999.

[Ike00] M. Ikehata. Reconstruction of the support function for inclusion from boundary measurements. *J. Inverse Ill-Posed Probl.*, 8(4):367–378, 2000.

[Ike02] M. Ikehata. A regularized extraction formula in the enclosure method. *Inverse Problems*, 18(2):435–440, 2002.

[Ike05] M. Ikehata. A new formulation of the probe method and related problems. *Inverse Problems*, 21(1):413–426, 2005.

[Ike07] M. Ikehata. Probe method and a Carleman function. *Inverse Problems*, 23(5):1871–1894, 2007.

[IS00] M. Ikehata and S. Siltanen. Numerical method for finding the convex hull of an inclusion in conductivity from boundary measurements. *Inverse Problems*, 16(4):1043–1052, 2000.

[IS04] M. Ikehata and S. Siltanen. Electrical impedance tomography and Mittag-Leffler's function. *Inverse Problems*, 20(4):1325–1348, 2004.

[Isa86] D. Isaacson. Distinguishability of conductivities by electric current computed tomography. *IEEE Trans. Med. Imag.*, 5(2):91–95, 1986.

[Isa07] V. Isakov. On uniqueness in the inverse conductivity problem with local data. *Inverse Probl. Imaging*, 1(1):95, 2007.

[IUY10] O. Imanuvilov, G. Uhlmann, and M. Yamamoto. The Calderón problem with partial data in two dimensions. *J. Amer. Math. Soc.*, 23(3):655–691,

2010.

[IUY11] O. Y. Imanuvilov, G. Uhlmann, and M. Yamamoto. Determination of second-order elliptic operators in two dimensions from partial Cauchy data. *Proc. Natl. Acad. Sci. USA*, 108(2):467–472, 2011.

[KG08] A. Kirsch and N. Grinberg. *The Factorization Method for Inverse Problems*, volume 36 of *Oxford Lecture Ser. Math. Appl.* Oxford Univ. Press, Oxford, U.K., 2008.

[Kir98] A. Kirsch. Characterization of the shape of a scattering obstacle using the spectral data of the far field operator. *Inverse Problems*, 14(6):1489–1512, 1998.

[Kir00] A. Kirsch. New characterizations of solutions in inverse scattering theory. *Appl. Anal.*, 76(3-4):319–350, 2000.

[Kir05] A. Kirsch. The factorization method for a class of inverse elliptic problems. *Math. Nachr.*, 278(3):258–277, 2005.

[KLO08] V. Kolehmainen, M. Lassas, and P. Ola. Electrical impedance tomography problem with inaccurately known boundary and contact impedances. *IEEE Trans. Med. Imag.*, 27(10):1404–1414, 2008.

[KS03] S. Kusiak and J. Sylvester. The scattering support. *Comm. Pure Appl. Math.*, 56(11):1525–1548, 2003.

[KS12] C. E. Kenig and M. Salo. The Calderón problem with partial data on manifolds and applications. *arXiv preprint arXiv:1211.1054*, 2012.

[KS14] C. E. Kenig and M. Salo. Recent progress in the Calderón problem with partial data. *Contemp. Math*, 615:193–222, 2014.

[KSS97] H. Kang, J. K. Seo, and D. Sheen. The inverse conductivity problem with one measurement: stability and estimation of size. *SIAM J. Math. Anal.*, 28(6):1389–1405, 1997.

[KSU07] C. E. Kenig, J. Sjöstrand, and G. Uhlmann. The Calderón problem with partial data. *Ann. of Math.*, pages 567–591, 2007.

[KT01] H. Koch and D. Tataru. Carleman estimates and unique continuation for second-order elliptic equations with nonsmooth coefficients. *Comm. Pure Appl. Math.*, 54(3):339–360, 2001.

[KV84] R. V. Kohn and M. Vogelius. Determining conductivity by boundary measurements. *Comm. Pure Appl. Math.*, 37(3):289–298, 1984.

[KV85] R. V. Kohn and M. Vogelius. Determining conductivity by boundary measurements II. Interior results. *Comm. Pure Appl. Math.*, 38(5):643–667, 1985.

[Lec06] A. Lechleiter. A regularization technique for the factorization method.

Inverse Problems, 22(5):1605–1625, 2006.

[LHH08] A. Lechleiter, N. Hyvönen, and H. Hakula. The factorization method applied to the complete electrode model of impedance tomography. *SIAM J. Appl. Math.*, 68(4):1097–1121, 2008.

[Lio04] W. R. B. Lionheart. EIT reconstruction algorithms: Pitfalls, challenges and recent developments. *Physiol. Meas.*, 25:125–142, 2004.

[LR08] A. Lechleiter and A. Rieder. Newton regularizations for impedance tomography: convergence by local injectivity. *Inverse Problems*, 24(6):065009, (18pp), 2008.

[MAF+10] F. S. Moura, J. C. C. Aya, A. T. Fleury, M. B. P. Amato, and R. G. Lima. Dynamic imaging in electrical impedance tomography of the human chest with online transition matrix identification. *IEEE Trans. Biomed. Eng.*, 57(2):422–431, 2010.

[MBSB96] P. Metherall, D. C. Barber, R. H. Smallwood, and B. H. Brown. Three-dimensional electrical impedance tomography. *Nature*, 380(6574):509–512, 1996.

[MPH06] D. Miklavčič, N. Pavšelj, and F. X. Hart. Electric properties of tissues. *Wiley Encyclopedia of Biomedical Engineering*, 2006.

[Nac96] A. I. Nachman. Global uniqueness for a two-dimensional inverse boundary value problem. *Ann. of Math. (2)*, 143(1):71–96, 1996.

[NGI88] J. C. Newell, D. G. Gisser, and D. Isaacson. An electric current tomograph. *IEEE Trans. Biomed. Eng.*, 35(10):828–833, 1988.

[NJTM12] D. T. Nguyen, C. Jin, A. Thiagalingam, and A. L. McEwan. A review on electrical impedance tomography for pulmonary perfusion imaging. *Physiol. Meas.*, 33(5):695–706, 2012.

[NKK11] A. Nissinen, V. Kolehmainen, and J. P. Kaipio. Compensation of modelling errors due to unknown domain boundary in electrical impedance tomography. *IEEE Trans. Med. Imag.*, 30(2):231–242, 2011.

[NPT07] A. I. Nachman, L. Päivärinta, and A. Teirilä. On imaging obstacles inside inhomogeneous media. *J. Funct. Anal.*, 252(2):490–516, 2007.

[NS10] A. Nachman and B. Street. Reconstruction in the Calderón problem with partial data. *Comm. Partial Differential Equations*, 35(2):375–390, 2010.

[PLP93] K. Paulson, W. R. B. Lionheart, and M. Pidcock. Optimal experiments in electrical impedance tomography. *IEEE Trans. Med. Imag.*, 12(4):681–686, 1993.

[Pot06] R. Potthast. A survey on sampling and probe methods for inverse problems. *Inverse Problems*, 22(2):R1–R47, 2006.

[Reg01] R. Regbaoui. Unique continuation from sets of positive measure. In *Carleman Estimates and Applications to Uniqueness and Control Theory*, pages 179–190. Springer, 2001.

[RSP+12] P. Rahmati, M. Soleimani, S. Pulletz, I. Frerichs, and A. Adler. Level-set-based reconstruction algorithm for EIT lung images: first clinical results. *Physiol. Meas.*, 33(5):739, 2012.

[RTV06] G. Rubinacci, A. Tamburrino, and S. Ventre. Regularization and numerical optimization of a fast eddy current imaging method. *IEEE Trans. Magn.*, 42(4):1179–1182, 2006.

[SB85] A. D. Seagar and R. H. T. Bates. Full-wave computed tomography. Part 4: Low-frequency electric current CT. *IEE Proceedings*, 132(7):455–466, 1985.

[Sch09] S. Schmitt. The factorization method for EIT in the case of mixed inclusions. *Inverse Problems*, 25(6):065012, 20, 2009.

[SCI92] E. Somersalo, M. Cheney, and D. Isaacson. Existence and uniqueness for electrode models for electric current computed tomography. *SIAM J. Appl. Math.*, 52(4):1023–1040, 1992.

[SD13] S. Staboulis and J. Dardé. Electrode modelling: The effect of contact impedance. *arXiv preprint arXiv:1312.4202*, 2013.

[SK11] S. Schmitt and A. Kirsch. A factorization scheme for determining conductivity contrasts in impedance tomography. *Inverse Problems*, 27(9):095005, 17, 2011.

[SLZ+08] J. K. Seo, J. Lee, H. Zribi, S. W. Kim, and E. J. Woo. Frequency-difference electrical impedance tomography (fdEIT): Algorithm development and feasibility study. *Physiol. Meas.*, 29:929–944, 2008.

[SU87] J. Sylvester and G. Uhlmann. A global uniqueness theorem for an inverse boundary value problem. *Ann. of Math.*, 125(2):153–169, 1987.

[SYB84] A. D. Seagar, T. S. Yeo, and R. H. T. Bates. Full-wave computed tomography. Part 2: Resolution limits. *IEE Proceedings*, 131(8):616–622, 1984.

[Tam06] A. Tamburrino. Monotonicity based imaging methods for elliptic and parabolic inverse problems. *J. Inverse Ill-Posed Probl.*, 14(6):633–642, 2006.

[TR02] A. Tamburrino and G. Rubinacci. A new non-iterative inversion method for electrical resistance tomography. *Inverse Problems*, 18(6):1809–1829, 2002.

[TVR10] A. Tamburrino, S. Ventre, and G. Rubinacci. Recent developments of a monotonicity imaging method for magnetic induction tomography in

the small skin-depth regime. *Inverse Problems*, 26(7):074016, 2010.

[Uhl08] G. Uhlmann. Commentary on Calderón's paper (29), on an inverse boundary value problem. In *Selected papers of Alberto P. Calderón*, pages 623–636. Amer. Math. Soc., Providence, RI: AMS, pp. 623-636, 2008.

[UW08] G. Uhlmann and J.-N. Wang. Reconstructing discontinuities using complex geometrical optics solutions. *SIAM J. Appl. Math.*, 68(4):1026–1044, 2008.

[VKV+02] T. Vilhunen, J. P. Kaipio, P. J. Vauhkonen, T. Savolainen, and M. Vauhkonen. Simultaneous reconstruction of electrode contact impedances and internal electrical properties: I. Theory. *Meas. Sci. Technol.*, 13(12):1848–1854, 2002.

[WFN85] A. Wexler, B. Fry, and M. R. Neuman. Impedance-computed tomography algorithm and system. *Appl Opt.*, 24(23):3985–3992, 1985.

[WR14] R. Winkler and A. Rieder. Resolution-controlled conductivity discretization in electrical impedance tomography. *SIAM J. Imag. Sci.*, 7(4):2048–2077, 2014.